STUDIES ON ELECTROCHEMICALLY PREPARED SOLAR SELECTIVE BLACK LAYERS

A THESIS

SUBMITTED TO THE

UNIVERSITY OF POONA

FOR THE DEGREE OF

DOCTOR OF PHILOSOPHY

(IN CHEMISTRY)

BY

H. S. POTDAR
M. Sc.

DIVISION OF PHYSICAL CHEMISTRY
NATIONAL CHEMICAL LABORATORY
POONA 411 008. (INDIA)

1984

कुपुत्रो जायेत क्वचिदपि कुमाता न भवति।

==========

DEDICATED

TO

MY MOTHER

==========

CERTIFICATE

This is to certify that the thesis entitled - 'Studies on Electrochemically Prepared Solar Selective Black Layers' describes the original work done by Shri H.S. Potdar under my supervision for the Degree of Doctor of Philosophy in Chemistry of the University of Poona, Pune.

[Dr. A.P.B. Sinha]
Research Guide

ACKNOWLEDGEMENT

I am deeply indebted to Dr. A.P.B. Sinha, FNA, Head, Physical Chemistry Division, for his invaluable and inspiring guidance during the course of this work.

I wish to express my sincere gratitude to Dr. S.K. Date, Dr. S.D. Sathaye and Dr. N.R. Pavaskar for their interest and stimulating discussions.

I thank Dr. C.I. Jose and his colleagues for extending their whole-hearted help in infra-red reflectance measurements.

I am also thankful to Dr. S. Badrinarayan, Dr. Mandale A.B. and Dr.(Mrs) Mitra, A. of the Special Instruments Laboratory, who have taken special pains to give me the maximum advantage of the facilities available.

Cooperation from my colleagues in many phases of this investigation is warmly acknowledged.

Finally, thanks are due to the Director, National Chemical Laboratory, Pune-8, for permitting me to submit this work in the form of a thesis.

[H. S. POTDAR]

Pune-8

May 1984

CONTENTS

.....

.....

CHAPTER – I

INTRODUCTION

CHAPTER I

INTRODUCTION

From the very beginning, human society has depended on energy in its various forms for achieving its objectives. Members of human society are energy consuming systems. Today per capita energy consumption has a definite relationship with the standard of living and, the stage of economic development of a country. For example, the per capita consumption of energy in the USA (11,128 kg of coal equivalent) is about 60 times more than in India (189 kg of coal equivalent).

Once man thought that fossil fuels would last forever. Deposits of coal and petroleum were being found faster than they could be used. But now, the position has changed completely. Experts calculate that our known reserves of all types of fuel including the atomic materials, will last for only a few hundred years at the present rate of consumption. Even if new supplies of fossil fuels are discovered along with more atomic materials it will be only delaying of the inevitable result. This is, because fossil fuels and atomic materials once used are gone forever.

Solar energy is the most obvious alternative energy source particularly in a sun-drenched land like India. The sun is a source of energy income, not energy capital like fossil fuels, for it is virtually inexhaustible. The average daily incidence of solar energy in

southern India is about 5kwh per square meter of horizontal surface. And this is the prime reason for interest in solar energy.

In sun, therefore we find a non-depleting energy source that is everlasting for all practical purposes. And now more and more scientists are working on how to convert this energy into useful form of energy so that man's energy need could be met.

1.1 Ways of Harnessing Solar Energy

A number of ways have been suggested to harness solar energy. The principle ones are given below:

(i) photovoltaic

(ii) photothermal

(iii) solar photoelectrolysis with semiconductor electrodes

In the first case, solar energy is used to provide electrical energy directly without the need of any intermediate steps. In the second approach i.e. photothermal conversion, solar energy is transformed in to the thermal energy of a working fluid. It is this second aspect which has been looked in the present work.

1.2 Types of Solar Thermal Systems

There are basically two types of solar thermal systems in operation depending upon the temperature. They are:

(i) Flat plate collector type system

(ii) Concentrating collector type system.

In the first, the thermal energy is collected at relatively low temperatures ($\leq 100^{o}C$) and used directly for applications such as water heating, space heating and for agricultural uses. The most common device for this purpose is the flat plate collector (Figure 1.1). It consists of an absorber panel with channels brazed on the backside for carrying thermal transfer fluid. The panel is well insulated below and from the sides with normal insulation and covered above with a transparent window to minimize the convection losses. The solar energy is allowed to pass through this window on a blackened absorber panel where it is absorbed. The temperature of the absorber panel increases. The thermal transfer fluid is allowed to flow through this channel and collected at the outlet of the collector at higher temperature. In the flat plate collector system both components of solar energy, i.e. normal or specular as well as diffused are used in conversion.

(ii) Concentrating type or focussing type collector - In the second kind of system, the energy is collected at higher temperature ($> 100^{o}C$) using mirrors for concentrating the solar rays. The thermal energy from such systems can be used to drive conventional steam turbines for the generation of electricity etc. This concept called concentratic type collector, usually employs a parabolic reflector to concentrate the solar energy on to a thermal transfer pipe fixed at the focus of the system. The pipe

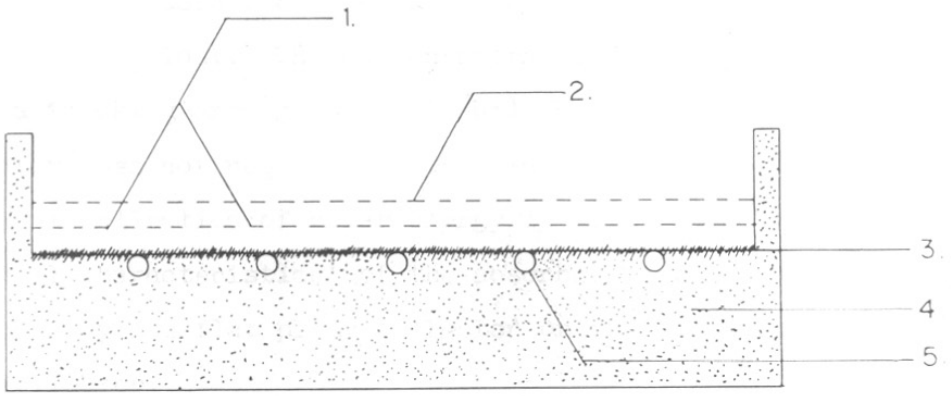

1) TRANSPARENT COVERS.

2) SOLAR RADIATION -(DIRECT + DIFFUSE.)

3) ABSORBING SURFACE.

4) INSULATION.

5) FLUID TUBE.

FIGURE 1·1. BASIC FLAT-PLATE SOLAR COLLECTOR.

is surrounded by an evacuated glass cylinder to reduce the convective losses. The typical cylindrical parabola is shown in Figure 1.2. In this concept only normal solar radiations are used for conversion, where as diffused radiations are lost. The concentrating type collector needs a tracking arrangement (15^{o}/hr), but the flat plate collector does not require any tracking mechanism. The efficient collection of solar energy is determined by the 'spectral characteristics' of the absorber panel in both cases namely the flat plate collector or the concentrating type collector.

1.3 The Use of Selective Coating

Selective coating, first proposed by Tabor [1] and Gier and Dunkle [2] is an important cost effective way to increase the efficiency of both types of collectors. This is achieved by

(i) maximizing absorption of solar energy, and

(ii) minimizing the losses from the absorber panel or surface i.e. conduction, convection and radiation.

We will assume that by proper engineering, the conduction and convection losses can be made negligible at the absorber panel but the radiation losses are the major losses with which we have to be concerned, since they are proportional to 4th power of the absolute temperature and they are independant of medium. The energy that we lose through reflection and reradiation will never be regained by any clever design and engineering used in subsequent

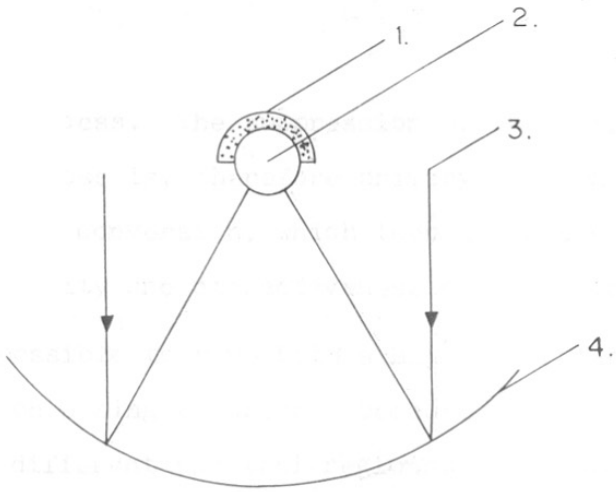

1) INSULATION.

2) RECEIVER.

3) DIRECT SOLAR RADIATION.

4) CYLINDRICAL PARABOLIC CONCENTRATOR.

FIG. 1·2 SCHEMATIC SECTION AND VIEW OF A CYLINDRICAL PARABOLIC CONCENTRATOR WITH RECEIVER INSULATED ON TOP PORTION.

stages of the process. The suppression of the reflection and reradiation loss is, therefore primary concern in the efficiency of the conversion, which then decides on the economic feasibility and attractiveness of the process.

It is possible to have both a high absorptance and low emittance on a single surface, because the two phenomena occur in different spectral regions. The solar energy is primarily confined to the wave length 0.3 to 2.5μm , whereas the energy emitted from a hot surface (100-400^{o}C) is generally above 2 μm.

Figure 1.3 shows that the solar energy incident outside the earth's atmosphere (AM0) and on the surface of the earth for air mass 2 (AM2) and for various concentration factors. The total radiated energy from a black body at three different temperatures is also shown. Note that there is not much overlap between the solar region and the radiative region. For a given value of flux concentration and the absorber temperature, the incident solar flux and the radiated thermal flux are equal at a wave length designated as the cut-off wave length ($\lambda_{cut-off}$). The spectral profile of an ideal selective absorber surface would have unity absorptance at all wave lengths shorter than the $\lambda_{cut-off}$, while have zero absorptance or emittance at all longer wave lengths i.e. > 2.5 μm. The spectral profile of the ideal selective absorber is a step function as shown in Figure 1.4.

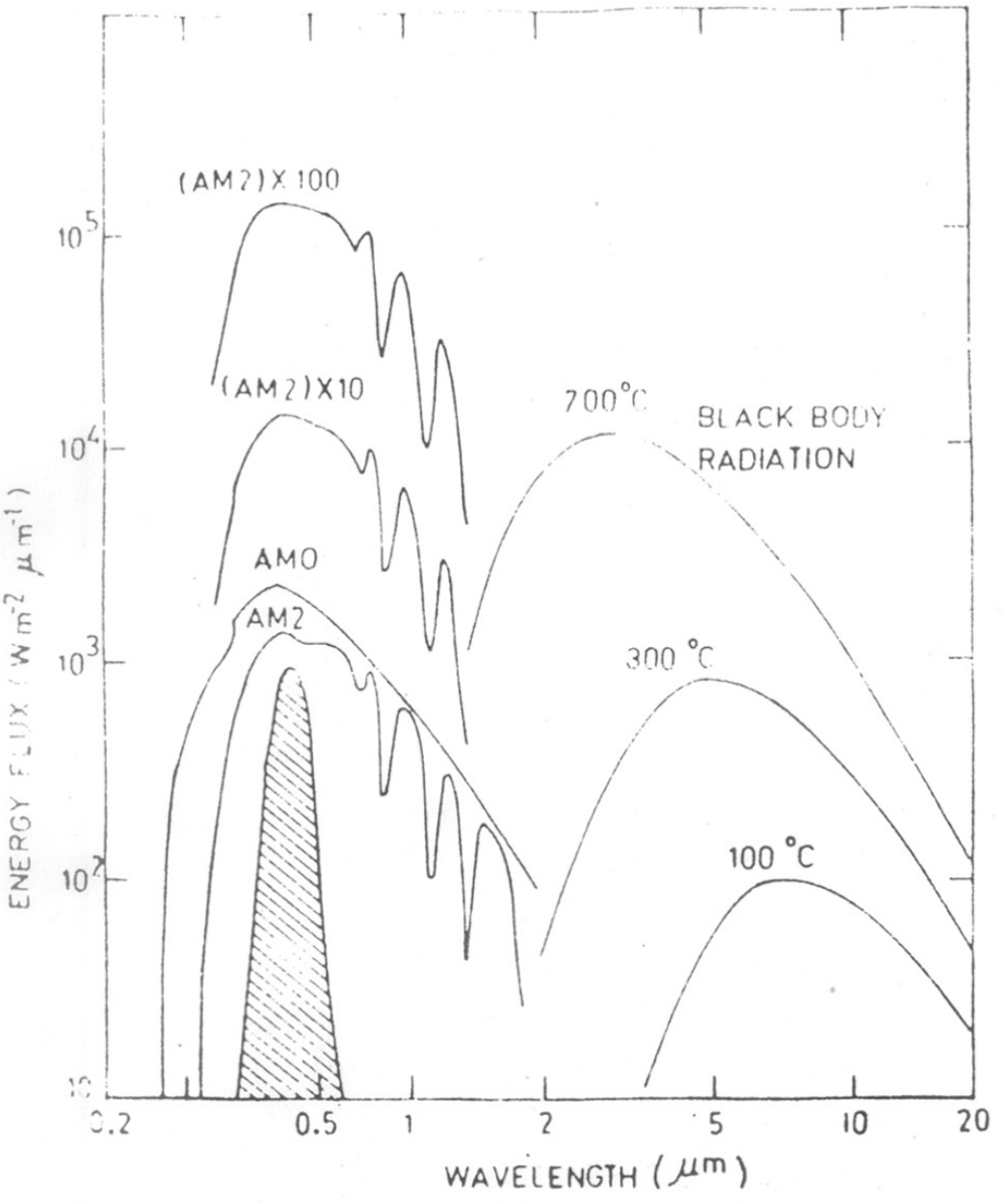

FIG. 1-3 SPECTRAL SOLAR FLUX IRRADIANCE FOR OUTSIDE THE EARTH'S ATMOSPHERE (AMO) AND ON THE SURFACE OF EARTH (AM2) CON--DITIONS FOR VARIOUS CONCENTRATION FACTORS COMPARED TO THE SPECTRAL FLUX RADIATED BY A BLACK BODY AT 100°C AND 700°C.

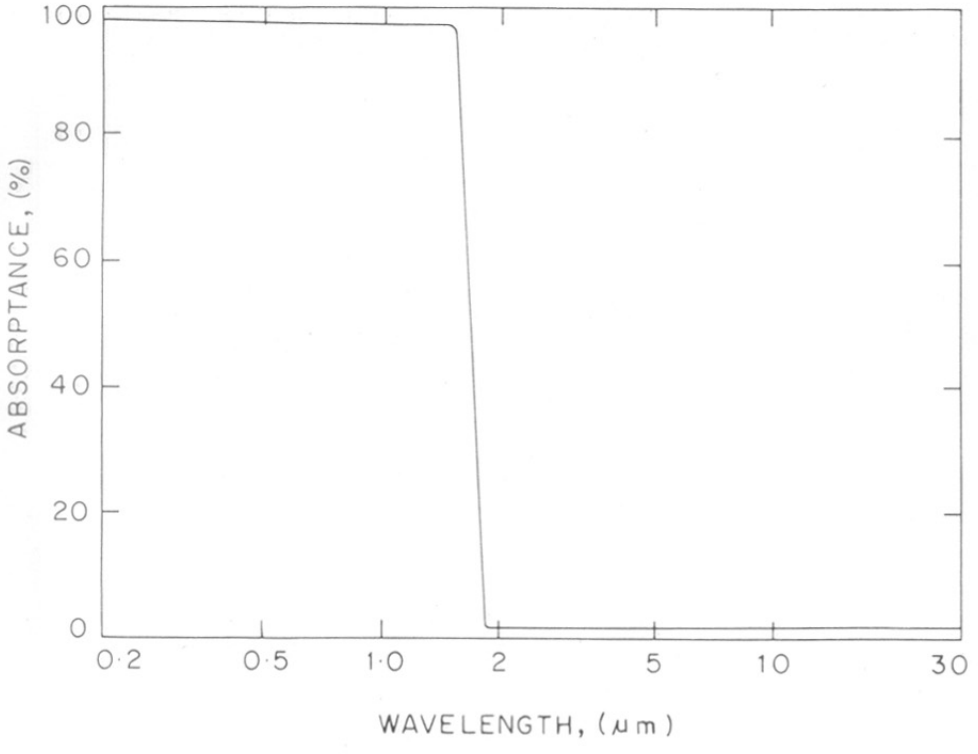

FIG. 1·4 THE SPECTRAL PROFILE OF AN IDEAL SELECTIVE ABSORBER.

In practice, no real surface meets these requirements perfectly, but attempts have been made to get as close to this as possible and to optimize solar collectors by developing selective absorbent surface with high absorption over the solar region and at the same time low emission in the thermal IR region. Excellent reviews and books are now available on this subject [3-14,17].

1.4 Absorptance (α) and Emittance (ϵ) of Selective Surface

The ability of a surface to absorb or emit is expressed by two main parameters, the integrated absorptance (α) and total hermispherical emittance (ϵ).

The total absorptance (α) is simply the function of available solar energy incident on the surface, that is absorbed. i.e.

$$\alpha = \frac{\text{absorbed energy flux}}{\text{incident energy flux}}$$

$$= \frac{\int_{0.3\mu m}^{2.5\mu m} A(\lambda)\, I(\lambda)\, d\lambda}{\int_{0.3\mu m}^{2.5\mu m} I(\lambda)\, d\lambda}$$

where $A(\lambda)$ is the spectral absorptance at particular wave length

$I(\lambda)$ = spectral solar irradiance

The hemispherical thermal emittance (ϵ) is defined as a ratio of the energy radiated by the absorber

surface to that radiated by a black body at the same temperature.

$$\epsilon = \frac{\text{Energy flux emitted/unit surface area at temperature T}}{\text{Energy flux emitted/unit black body area at the same temperature}}$$

$$\epsilon = \frac{\int_{2.5\mu m}^{\alpha\,\mu m} B(\lambda,T)\, W(\lambda,T)\, d\lambda}{\int_{2.5\mu m}^{\alpha\,\mu m} W(\lambda,T)\, d\lambda}$$

where

$B(\lambda,T)$ is the spectral emittance at temperature T

$W(\lambda,T)$ is the black body irradiance at the same temperature

For an opaque body

$$\rho(\lambda) + \alpha(\lambda) = 1$$

where $\rho(\lambda)$ is the function of incident solar flux that is reflected.

Making use of Kirchoff's law $\alpha(\lambda) = \epsilon(\lambda)$

$$\alpha(\lambda) = \epsilon(\lambda) = 1 - \rho(\lambda)$$

Therefore α and ϵ can thus be defined in terms of the experimental measured $\rho(\lambda)$ as follows:

$$\alpha = \frac{\int_{0.35\mu m}^{2.5\mu m} [1-\rho(\lambda)]\, I(\lambda)\, d\lambda}{\int_{0.35\mu m}^{2.5\mu m} I(\lambda)\, d\lambda}$$

$$\epsilon = \frac{\int_{2.5\mu m}^{\alpha\mu m} 1 - \rho(\lambda,T)\ W(\lambda,T)\ d\lambda}{\int_{2.5\mu m}^{\alpha\mu m} W(\lambda,T)\ d\lambda}$$

1.5 Figure of Merit for Selective Surface α/ϵ.

Real convertor surfaces can only approximate the ideal profile. The spectral selectivity of a surface is characterized by two integrals, the solar absorptance(α) and the thermal emittance (ϵ).

One would like to make α as close to unity as possible and ϵ to be as close to zero as possible.

The quotient α/ϵ is often cited as a figure of merit for a selective surface. For a given concentration, this α/ϵ ratio determines the highest attainable temperature by the collector and hence maximum Carnot efficiency of the conversion. It is important to know the values of α and ϵ separately, because for two surfaces with the same α/ϵ ratio, the one with higher α will produce the higher conversion efficiency under almost all conditions.

1.6 Basic Requirements of Selective Surfaces

The basic requirements of a practical selective surface for a collector are as follows:

(i) high absorptance (α) in the solar region i.e. $0.3\mu m - 2.5\mu m$.

(ii) low thermal emittance (ϵ) in the region $> 2.5\mu m$.

(iii) long term stability at desired operating temperature

(iv) stability against the atmospheric condition.

(v) applicability of the selective surface to given substrate materials

(vi) reproducibility

(vii) ease of large area fabrication

(viii) reasonable cost

1.7 Advantages of Selectivity

In order to evaluate the advantages of a solar selective absorber surface over a surface which acts as a black body, the conversion efficiencies of both must be compared. The conversion efficiency is the ratio of power extracted to the incident solar input. The thermoenergetic efficiencies i.e. the product of conversion efficiency and Carnot efficiency must also be compared incase the heat extracted is used in a thermodynamic cycle. And all these comparisons must be made under the same climatic conditions, taking into account the design of the collector. Further more it is necessary to compare not only the instantaneous efficiencies but also the integrated efficiencies over a day/week/year.

It is extremely difficult, if not impossible to draw general conclusions under all circumstances. A particular selective surface must be evaluated for each case taking into account the optical properties and the cost. Neverthless, one can determine approximately the

operation temperature and concentration factor ranges for which the use of a selective absorber allows a significant improvement in the performance.

A detailed study of the gain obtained by the use of a selective surface as a function of the incident flux, the concentration factor, the temperature of the absorber and for various collector designs has been carried out by Spitz et al. [15] According to them the convective and conductive thermal losses are prominent in the low temperature range and a reduction of the radiative thermal loss by using a selective surface, does not lead to any appreciable increase in the conversion efficiency. For this reason, a selective surface would not be of much use for temperatures less than 60°C.

On the other hand, in the medium temperature range between 60°C and 150°C, the spectral selectivity can increase the conversion efficiency significantly, even if convective and conductive losses represent still important part of the global thermal loss. The efficiency gain is appreciable for temperatures above 70°C particularly in the case of collectors operating under vacuum. These workers have also shown that efficiency of a one window selective collector is superior to that of a double window non-selective absorber collector.

For higher temperatures solar thermal conversion using focussing collectors, the thermal losses by convection and conduction can be neglected incomparison to the

radiative losses. A comparison of the conversion and thermoenergetic efficiencies of a selective surface ($\alpha \simeq 0.9$ and $\epsilon \approx 0.1$) with those of an absorber coating acting like black body ($\alpha \simeq 1$ and $\epsilon \simeq 1$) is shown in Figures 1.5 and 1.6. It reveals that in each case, selectivity leads to an increase in the efficiency. The gain obtained is appreciable for concentration factor lower than 100 and the absorber temperature less than 1000 K. Thus, for high temperature applications selectivity is inevitable.

1.8 Methods for Obtaining Spectral Selectivity

The required selective profile may be achieved in a number of ways. These can be grouped into the following six categories:

(a) Intrinsic selective material
(b) Absorber-reflector tandem
(c) Interfe-rence stacks
(d) Selectivity through textural effects
(e) Particulate coatings
(f) Coatings based on quantum size effects

Most of the coatings reported in the literature fall in two or more of the above mentioned categories. In the following sections, we review the individual group.

(a) Intrinsic selective material - As pointed out by Seraphin [16], theoretical considerations based on casualty such as dispersion relations do not rule out the spectral selectivity to be provided by one single material. A hypothetical semiconductor with 10^{20} cm^{-3} density of free carriers and reasonable effective masses could generate the

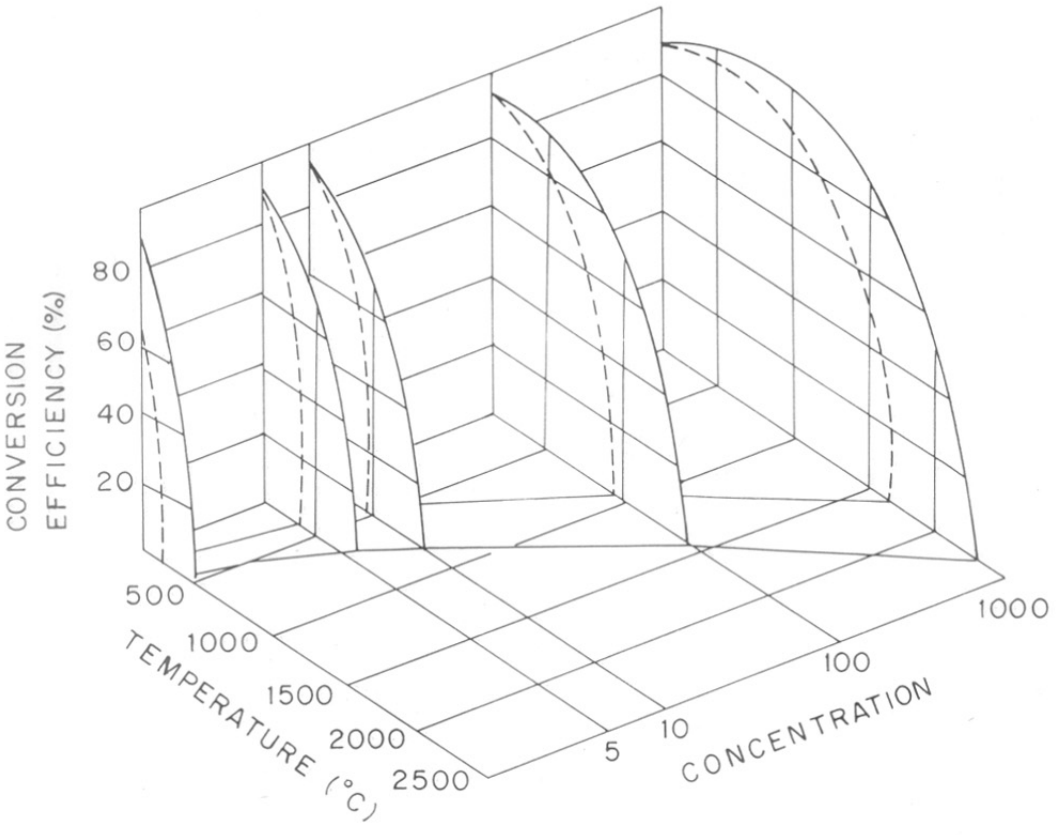

FIG. 1·5 CONVERTION EFFICIENCY OF A COLLECTOR EQUIPPED WITH SELECTIVE SURFACE $\alpha = 0.90$, $\varepsilon = 0.10$ (——) AND A BLACK BODY (----) AS A FUNCTION OF TEMPERATURE FOR DIFFERENT VALUES OF CONCENTRATION FACTOR.

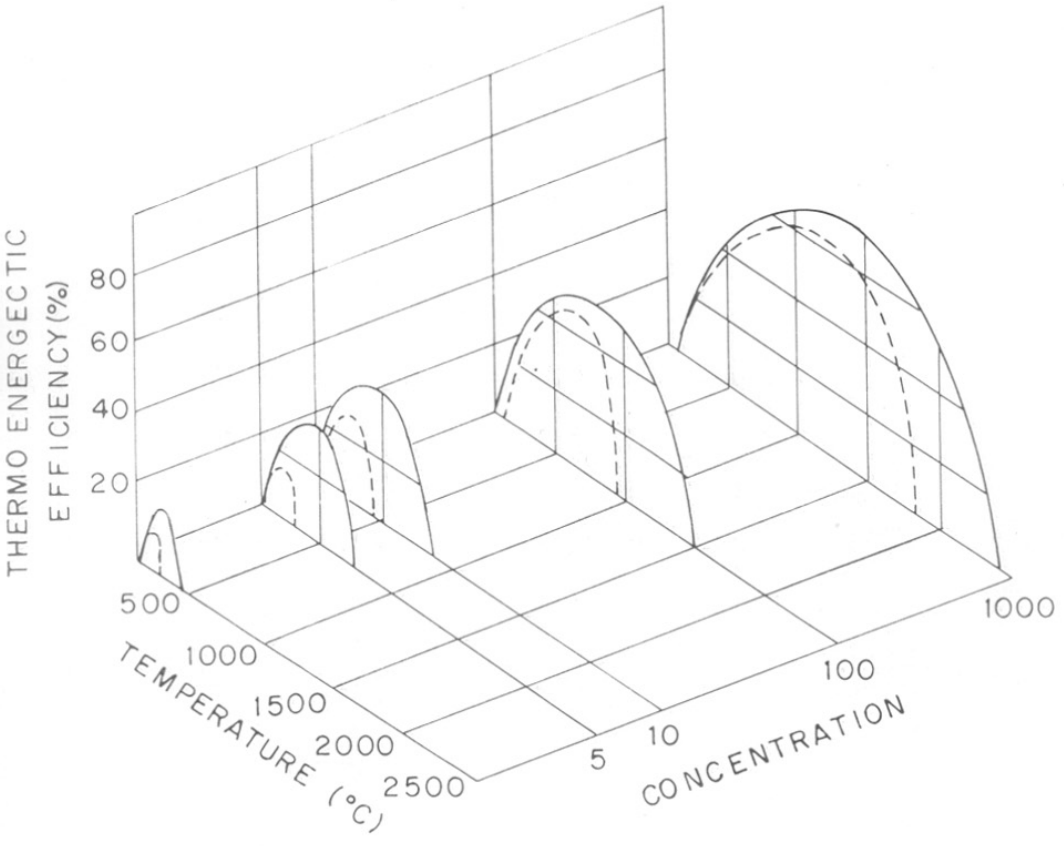

FIG. 1·6 THERMOENERGETIC EFFICIENCY OF A COLLECTOR EQUIPPED WITH A SELECTIVE ABSORBER (—) ($\alpha = 0{\cdot}90, \varepsilon = 0{\cdot}10$) AND OF A BLACK BODY (----) ABSORBER AS A FUNCTION OF TEMPERATUE FOR DIFFERENT VALUES OF CONCENTRATION FACTOR.

step function. However, a plasma edge near 2μm requires a level of doping that interferes with the intrinsic optical properties of the host and may even change its crystal structure.

The plasma-edge of most metals, on the other hand is located too far in to the ultraviolet to give a sufficient solar absorptance. The problem here is to tie down the number of free carriers and thereby move the plasma edge into the near infrared. This approach may work in the transition metals, for which the already low carrier density can be further reduced by partial charge transfer to neighbours of high electron affinity. A number of these transition metal compounds approximate the desired step function in their optical spectrum. The examples are some of the transition metal compounds like Hafnium carbide, Rhenium trioxide and divanadium penta-oxide [11]. The major drawback however is the location of λ_{cutoff} at wavelengths lying much earlier in the solar spectrum. The other examples are metallic tungston, MoO_3 doped Mo, dieuropium trioxide and lanthanum hexaboride.

(b) Absorber-reflector tandem - Since no single material has yet been synthesized with a spectral selectivity that is very close to that of an ideal photothermal convertor, use is made of two materials to achieve the desired optical property.

A thin layer of a material that absorbs solar

radiation but transparent in the infrared is deposited on a material having high infrared reflectance and thus low emittance. The absorption material is semiconductor having its absorption edge located at or near cutoff wavelength. For wavelength, shorter than the absorption edge, all the incident energy (except that reflected) is absorbed in this upper layer, where as for wavelengths longer than absorption edge, the upper thin layer would be transparent to the IR radiation and thus has the low emittance of the substrate underneath. The upper absorbent layer is usually a semiconductor having a energy gap between 0.5 eV and 1.26 eV [13]. The problem linked with the use of semiconductor is the considerable high reflectance of the semiconducting layer.

For air/material interface, the reflectance for the normal incidence is expressed as:

$$R = \frac{(1 - n)^2}{(1 + n)^2}$$

where R is the reflectance and
n is the refractive index of semiconductor.

Since most of the semiconductors, suitable as absorbers, have high refractive indices as is evident from the Mosse's relation [18]

$$n^4 E_g = 77$$

They will have high surface reflectance of 30-40% over the solar spectrum, thereby reducing the actual solar absorptance. Due to this reason all approaches based on the absorber-reflector tandem require additional process for the reduction of surface reflection. There are mainly two approaches tried for the lowering the reflectance. They are:

(a) antireflective coating
(b) use of textural effects

An optical material suitable as an antireflection coating should have a refractive index equal to the square root of the support semiconductor layer and its thickness should be one-quarter of the wavelength of light. [19] The main problem is that elaborate, expensive vacuum deposition technique is required for their fbrication, which makes fabrication of large areadifficult.

The use of structural or textural effects to minimize surface reflection is, therefore more useful. For example, the resulting microstructure of PbS coatings[20,21] prepared under poor vacuum conditions or by spray pyrolysis[22] resulted in a low reflectance coating. Microvoids produced in amorphous silicon [23] and Germanium [24] by post-chemical etching helped to reduce the surface reflections.

A number of techniques have been utilized so far, to obtain absorber-reflector tandems. These techniques and important tandems investigated are summarized in Table-1.1. Schematic diagram for absorber reflector tandem is shown in Figure 1.7.

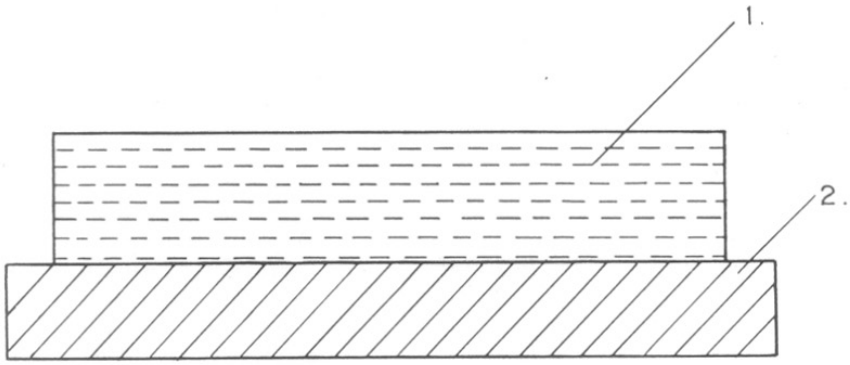

1) SELECTIVE-BLACK COATING

2) WHITE REFLECTOR

FIGURE 1·7 BASIC CONFIGURATION OF THE ABSORBER-REFLECTOR TANDEM.

(c) Interference stacks - Two basic approaches for producing interference coatings with low visible and high IR reflectance were first presented by Hass et al.[25] They utilized combinations of absorbing and non-absorbing layers to suppress the visible reflectance of an opaque metal underlayer, while leaving the high infrared reflectance of the metal unaltered.

This method depends not only on the optical properties of the individual layers, but also on the film thickness to wavelength ratio. At the visible wavelengths, where the optical thickness of the film is a sizable fraction of a wavelength, interference effects predominates. But for longer wavelengths the optical thicknesses are so small that the films are unable to affect the incident radiation.

In the first design, the metal film or substrate is first coated with a partially absorbing layer, which provides a substantial decrease in the visible reflectance. Next a non-absorbing layer is added to further lower the reflectance and increase the spectral bandwidth of the high absorption region.

A second design, which has been used extensively in recent coatings for solar energy absorbers consists of a sequence of opaque metal/dielectric/thin semitransparent metal/dielectric layer. This design increases the bandwidths of the high absorption region, and in addition,

allows the spectral location of this absorptance band to be shifted over an appreciable range by changing the thickness of the dielectric layers. Both of these designs offer sharp transitions between high absorptance and low emittance regions. There are many examples of the interference coatings which have been investigated as selective absorbers, e.g. Al_2O_3-Mo-Al_2O_3 (AMA),[26] NiS-ZnS,[27,28] Ag/Al_2O_3/Cr/Al_2O_3.[29]

The limitation with most multilayer coatings is that they are fairly expensive to fabricate as they require vacuum technology for their fabrication. Secondly, they are susceptible to corrosion and interdiffusion at high temperature, resulting in degradation of optical properties. Moreover, large area fabrication would be difficult. The reported AMA absorber, on the other hand, appears not to suffer from many of these problems. Some of interference stacks so far tried are summarized in Table 1.1.

(d) Selectivity through textural effects - With selective surfaces of this type use is made of the effect of the surface texture [13] on the optical properties of the surface. The coefficient of solar absorption is increased by multiple reflections between surface irregularities of suitable size and shape.

One approach tried was to produce microporosities, grooves or other textural faults on the surface of the metal. The microporosities act as black body cavities for

short wavelength solar radiation ($\lambda < 2\mu m$), whereas, for longer wavelengths ($\lambda > 2\mu m$), the surface appears smooth and highly reflecting in this region. A sand-blasted surface that has lost its polish fits into this category. There is a considerable range of surface structures that offer possibilities of second or multiple reflections. A simple 'V' groove on the plane surface gives this result for certain angle of incidence of solar rays. Figure 1.8 shows several examples of applications, depending on the opening angle of the 'V'. The best angle is achieved with a curved profile called a 'Gothic Vee', obtained by taking the crest of the groove as the centre of the curve of the opposite face. This construction ensures double reflection for all the rays.

A waveguide method of providing a selective surface has been proposed by Horwitz[30]. It employs an array of the deep holes in a metal. Light of wavelengths greater than the hole diameter will not resolve the hole and hence will see a reflecting surface. However, short wavelengths can resolve the holes and can propogate along them as in a microwaveguide. On the basis of an elementary theory, it has been predicted that such meshes should yield a ratio of 30:1 between the solar absorptance and thermal emittance at temperatures of about 200°C. A metallic layer pierced by laser, ion beams and electron beams with 10^8 holes per sq. cm, hole diameter of 1 μm and depth 10μm has been proposed by Wakeren.[31] The problem, however, lies

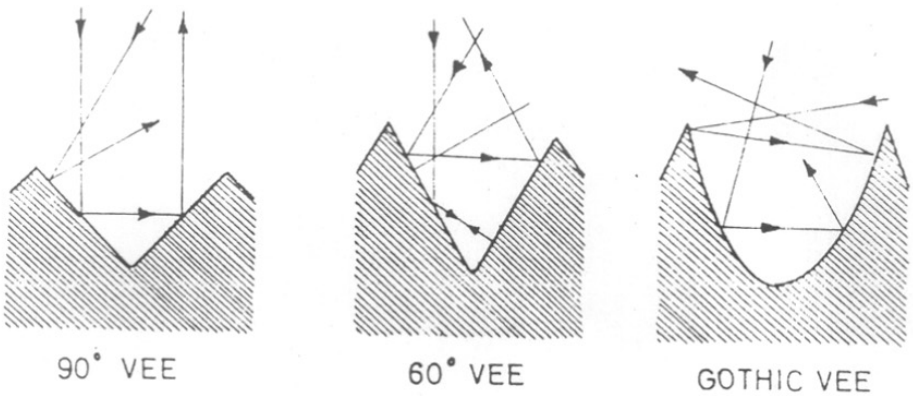

FIG. 1·8 REFLECTIVITY FROM ANY ANGLE OF INCIDENCE FOR DIFFERED 'V' GROOVE SURFACES OFFERING MULTIREFLEC--TION POSSIBILITY.

in the manufacture of such surfaces.

An interesting textural surface has been made by Cuomo et al. [32] Their approach consists in fabricating a surface with a microstructure similar in geometry to an acoustic anechoic surface. The surface consists of a dense forest of aligned needles whose diameters are of the order of visible wavelengths, the spacing between needles is several wavelengths. This surface would absorb with high efficiency, because of multiple reflections as the incident photons penetrate the needle maze. Since absorption is dominated by geometric factors, the surface of the structure can be made of a material which emits poorly in the infrared. Such a material would have an absorptance for the most wavelengths smaller than the needle spacing over a narrow incident cone about the needle direction. However, this high absorption cone, which will have high emissivity, will not greatly affect the total hemispherical emissivity because of its small solid angle. If the surface is made of a metal with low emissivity, the total hemispherical emissivity may not significantly increase above the normal emissivity of the metal. Such an absorber using tungston [32] single crystal whisker or dendrites grown on a variety of substrates was shown to have integrated absorptance of about 0.96 and hemispherical emittance at 550°C of 0.26. Rhenium[7] and Nickel [33] surfaces of similar microstructure have been sprayed by CVD technique and shown to have good solar selectivity.

A structural topology that meets the selectivity requirements may be created not only by the formation of dendrites but also by the microroughness of a surface made of a large number of crystallites formed by the random growth of numerous monocrystals. This disordered monocrystalline formation is obtained by high flux evaporation of a metal under vacuum. Such type of surfaces have been developed at ISPRA.[13] Potential methods of obtaining different types of surface microstructures have been presented by Pellagrini.[34] These methods are based on mechanisms such as liquid-solid transformations, depositions from vapour phase and chemical reactions in oxidising and corrosive environments.

(e) Particulate coatings - Composite metal/insulator films which are also referred to as cermet films are a well known class of selective absorbers when prepared in a very finely divided dielectric rich form.[35] The composite material strongly absorbs radiation over much or all of the range of solar spectrum but is transparent to longer wavelength radiation. When deposited on a highly reflecting metal mirror, the tandem forms a selective surface approximating the general desired absorptance characteristics.

Several methods have been employed to produce these composite films including electroplating and various forms of vapour deposition. Electroplated black-chrome - a composite of Cr-Cr oxide is one of the most widely used

selective surfaces. Electroplated coatings of black-chrome and other metals have the advantage of low cost. However, such coatings do not appear to be stable at temperatures above 300°C.

Optical measurements have shown that the Maxwell-Garnett theory can be applied in detail to metal-insulator composites, in cases where the metal particles are nearly spherical and are embedded in a non-crystalline matrix and where volume fraction of absorbing metal is small. More involved effective medium theories [39] are now available for dealing with the problem. Otherwise, the extinction coefficient is generally much broader than predicted by theory. This fact has two important implications. First, since the behaviour of the optical properties is quite similar for most metal insulator composite materials, the choice of constituents for the composite can be made largely on the basis of considerations of physical stability. Secondly, some basic conclusions can be drawn concerning the design of optimized composite film and performance capabilities of such films. These have been discussed in great detail by Cruighead et al.[35] Their calculations show that a composite film with an approximately graded composition deposited on a metal substrate forms an efficient selective absorber. Composite materials Ni/Al_2O_3, V/SiO_2, V/Al_2O_3, $Fe/Al2O3$ have been investigated. For example, the composite Ni/Al_2O_3 having spherical nickel particles with decreasing concentration in a matrix of amorphous Al_2O_3

produced a good selective surface with $\alpha = 0.94$ and $\epsilon = 0.10$. On the same principle, Gittleman,[36] has studied the dispersion of semiconducting grains in an insulator of low dielectric constant. He has shown that granular semiconductors (Si/Al_2O_3) are a type of materials that are capable of efficient absorption of solar energy (60% more efficient than silicon). Reflectivity measurements for granular films of germanium (35% by volume in Al_2O_3) on Al prepared by sputtering agree closely with the theory. To prepare such surfaces, some material problems have to be solved. The most important of which is to find an insulator that does not react with the semiconductor at high temperature.

One of the most attractive possibilities, particularly for lower temperature applications on large surface uses, is the formulation of spectrally selective paints. The basic approach to this problem is to suspend particles of the semiconductor in a suitable binder that has both high IR transparency and high temperature stability. The optical properties of the pigments, the particle sizes and their distributions and multiple scattering effects within the pigment-binder composite all interact to produce the final spectral properties. Extensive work in this direction has been carried out by Lin and Zimmer.[37] The major problem has been to find a suitable binder which will allow the intrinsic IR transparency of the pigments to dominate in order to produce low emittance. The various paint formulations investigated so far are listed in Table-1.1.

(f) Coatings based on quantum size effects- Quantum size effect occur in ultra thin films.[10] These effects can result in the high absorption of visible light while maintaining low emittance. The critical thicknes for the quantum size effect to be utilized in a metal must be nearly 20-30 A^{o} and for a degenerate semiconductor 100-500 A^{o} is necessary. The combination of a quantum size effect material and metallic substrate can make a selective absorber. This effect has been observed in vacuum deposited indium antimonide (InSb)[38] on silver and Al substrate.

1.9 Basic Principles

The physics of selective surfaces are governed by four physical laws:

(a) Stephan-Boltzman's law
(b) Kirchhoff's law
(c) Planck's law
(d) Wein's law

(a) Stephan-Boltzman's law

An ideal black surface is one which, when heated to a temperature T, emits thermal radiation q_r per unit area which is given by the expression

$$q_r = \sigma T^4 \qquad (1)$$

where σ = Stephan-Boltzmann constant and
T is the absolute temperature

q_r is termed as emissive power. No surface can emit more energy at temperature T than this amount. Most surfaces

emit less and hence eqn. (1) is written as

$$q_r = \epsilon \sigma T^4$$

where ϵ is less than unity and is termed as the thermal emissivity or emittance.

As every surface that emits is also an absorber, it receives radiation from its surrounding i.e. net radiation loss is written as follows:

$$q_r = \epsilon_e \sigma (T^4 - T_s^4)$$

where T_s is temperature of surroundings. ϵ_e is the effective emittance in the presence of surroundings.

(b) Kirchhoff's law -

Kirchhoff's law states that the monochromatic emittance and monochromatic absorptance are equal for radiation of any given wavelength λ, i.e.

$$\epsilon(\lambda) = \alpha(\lambda)$$

where $\alpha(\lambda)$ is the monochromatic absorptance at wavelength λ and $\epsilon(\lambda)$ is the monochromatic emittance.

For any surface, the sum of absorptance $\alpha(\lambda)$, transmittance $t(\lambda)$ and reflectance $r(\lambda)$ must be unity as per conservation of energy principle

$$\alpha(\lambda) + t(\lambda) + r(\lambda) = 1$$

Thus, for a non-transparent material

$$\alpha(\lambda) + r(\lambda) = 1$$

$$\alpha(\lambda) = 1 - r(\lambda)$$

$$\text{i.e.} \quad \alpha(\lambda) = \epsilon(\lambda) = 1 - r(\lambda)$$

This equation is useful as it allows $\epsilon(\lambda)$ or $\alpha(\lambda)$ to be determined by a reflection measurement. It is also important in computing interchange of radiation between surfaces.

(e) Planck's law -

The blackbody emission of eqn. (1) covers a wide range of wavelengths, the spectral distribution of the energy being governed by Planck's equation

$$q_\lambda = \frac{C_1 \lambda^{-5}}{e^{C_2/\lambda T} - 1}$$

where q_λ is the monochromatic emissive power at wavelength λ and C_1 and C_2 are constants.

If the body is not black then

$$q_\lambda = \epsilon_\lambda C_1 \lambda^{-5} / e^{C_2/\lambda T} - 1 \qquad (2)$$

(d) Wien's law -

The expression (2) has a peak value at λmax given by Wien's formula

$$\lambda_{max} = \frac{2898}{T}$$

where λ is in micrometers(μ) and T is in degrees Kelvin. About 25% of the emitted energy is at wavelength below λ_{max} and 75% above.

1.10 Present Work

The aim of the present work is to prepare selective surfaces useful for photothermal conversion by employing electrochemical methods and to characterize them. The materials studied in this thesis are copper-black on copper substrate by an anodic oxidation process and molybdenum-black on nickel plated copper substrate by a cathodic electrodeposition process. The results are presented in the following Chapters.

Chapter II describes the general set up used for the electrodeposition of the above mentioned selective-blacks. Details of optical, structural and thermal characterization of these coatings are also presented.

Chapter III describes the preparation of copper-black in detail and results on optical and thermal and structural characterization of these coatings are presented. Important conclusions drawn from this study are given at the end.

Chapter IV describes the preparation of molybdenum-black and results on optical, thermal and structural characterization of these coatings are presented. Important conclusions drawn from this study are given at the end.

In Chapter V, summary of the present work and scope for the further research is summarised.

TABLE 1.1

SUMMARY OF SELECTIVE SURFACES

Materials	Fabrication technique	Absorptance (α)	Emittance (ϵ)	Ref.
(a) INTRINSIC				
Eu_2O_3				4,5, 10
ReO_3				"
HfC	Sputtering	0.65	0.1(100)	"
V_2O_5				"
LaB_6				"
MoO_3 doped Mo				"
(b) METAL/SEMICONDUCTOR				
a-Si	CVD	0.77	0.1	40
a-Si	Sputtering & chemical etching	0.94	0.5	23
a-Ge	as above	0.94	0.55	24
$Si+Si_3N_4$	CVD + vac.evap.	0.76	0.07(500)	42,43
CuOx	Chem. conv.	0.91	0.16	44
	chemical etching	0.93	0.11	45
	spray pyrolysis	0.3	0.11(80)	47
	an-odization	0.98	0.2	46 (present work)
Cu_2O	Thermal oxidation	0.85		48
CoOx	Anodization	0.93	0.24	49,55
	Thermal oxidation	0.87	0.07(60)	50,51, 52

.....

Table 1.1 contd..

Materials	Fabrication technique	Absorptance (α)	Emittance (ϵ)	Ref.
	Electroplating	0.95	0.2	50,51, 52
	Spray pyrolysis	0.88	0.14	53,54
		0.8	0.075	114
		0.93	0.22(100)	111
	Cathodic electro-deposition	0.90	0.15	115
$CoO+Fe_2O_3$	Thermal oxidation	0.90	0.3(140)	52
ZnO	Chemical conv.	0.93	0.08	56
	Anodization	0.95	0.08	57,58
Wo_3	Sputtering	0.83	0.07	59
CoS	Electroplating	0.97	0.20	50,52
Cu_2S	Chemical conv.	0.79	0.2(200)	44
	Spray pyrolysis	0.89	0.25	60
PbS	Vac. evap.	0.98	0.2(240)	61,62, 63
	Spray pyrolysis	0.92	0.21	64
FeCx	Sputtering	0.80	0.02(150)	59
Te	Vac. evap.	0.95	-	65
Black nickel	Electroplating	0.95	0.18	3,68, 69
	Chemical conv.	0.94	0.15	67,68
NiS-PbS NiS-CdS	Spray pyrolysis			108
ZrB_2	CVD	0.67-0.77	0.06	110

.....

Table 1.1 contd...

Materials	Fabrication technique	Absorptance (α)	Emittance (ϵ)	Ref.
Oxides of S.S.	Thermal oxidation S.S.	0.85-0.90	0.10-0.20	97
Al-Ca	Anodization	0.8	0.06	116
Moly-black	Dip coating	0.84	0.2	113
Black enamel/SnO_2	Spray pyrolysis	0.92	0.15	24
(c) INTERFERENCE				
Al_2O_3/Mo/Al_2O_3	Vac. evap.	0.95	0.34(100)	26
Al/Ge/SiO	Vac. evap.	0.79	0.012(100)	87
Ni/Ge/SiO	Vac. evap.	0.88	0.035(100)	87
Cr/Ge/SiO	Vac. evap.	0.93	0.11(100)	87
Al/PbS/SiO	Vac. evap.	0.89	0.02(100)	87
Ni/PbS/SiO	Vac. evap.	0.93	0.043(100)	87
SiO/Cr/SiO	Vac. evap.	0.88	0.1	44
MgF_2/Mo/CeO_2/Mo	Vac. evap.	0.95	0.07	88
MgF_2/Mo/MgF_2/Mo	Vac. evap.	0.89	0.07	88
SiO_2/Mo/SiO_2/Mo	Vac. evap.	0.86	0.08	89
Ag/Al_2O_3	CVD	0.95	0.04	90
PbS/ZrO_2	Sputtering	0.82	0.02	92
Wo_2/Al_2O_3	Sputtering	0.93	0.09	59

.....

Table 1.1 contd...

Materials	Fabrication technique	Absorptance (α)	Emittance (ε)	Ref.
C/metal	Reactive sputtering	0.92	0.07	91
(d) COMPOSITES				
Al_2O_3/Ni	Vac. evap.	0.94	0.10(150)	72
	Electroplating	0.93	0.20	73,74
	Anodization	0.90	0.06(100)	100
Al_2O_3/Pt	Vac. evap.	0.94	0.07(150)	72
Al_2O_3/Au	Sputtering	0.95	0.025	72
Al_2O_3/Cu	Sputtering	0.90	0.045	80
Al_2O_3-CO	Electroplating	0.94	0.31	73,74
	Evaporation	0.95	0.1	101
Cr_2O_3/Cr	Sputtering	0.92	0.08	76
	Electroplating	0.95	0.07	76,77, 78
	Plasma spray	0.90	0.5(80)	44
	Ebonizing	0.90	0.50	79
SiO_2-Fe	Sputtering	0.90	0.03	80
MgO/Au	Sputtering	0.93	0.04	81
Cr_2O_3-MoO_2	Electroplating	0.96		82
CuO/Cu	Sputtering	0.94	0.04	83
CaF_2-Ge	Sputtering	0.72	0.10	84
Cr,Fe,Mo, SS,Ta,W silicides	Sputtering	0.85	0.02	85

.....

Table 1.1contd..

Materials	Fabrication technique	Absorptance (α)	Emittance (ϵ)	Ref.
Cr,Fe,Mo, Ni,Ta,W carbides	Sputtering	0.90	0.06	85,86
Cu/C	Sputtering	0.94	0.04(120)	104
Au/MgO	Reactive sputtering			105
Titanium nitrides & carbides	Sputtering			106
Ni/C	Reactive sputtering	0.80-090	0.028-0.045 (150)	107
Metal-C	Sputtering			109
W/WO_3	CVD	0.92	0.20	102
TiO_2	Anodization	0.93	0.23	103
Moly.black	Chemical conv.	0.88	0.2	112
	CVD	0.82	0.08	70
	Electroplating	0.85	0.11	71 (present work)
Black W	CVD	0.83	0.05	73
(e) TEXTURAL EFFECT				
W dendrite	CVD	0.99	0.26	32
Steel dendrite	CVD	0.89	0.47(260)	92
	Vac. evap.			
Ni dendrite	CVD	0.95	0.6(100)	33
	Vac. evap.	0.70	0.35	13

.....

Table 1.1 contd...

Materials	Fabrication technique	Absorptance (α)	Emittance (ϵ)	Ref.
Rhenium	CVD			57
Gold	Gas evap.	0.99	0.1(100)	93
Al-Cu alloy	Etching			98
Si-C alloy	Glow discharge	0.76		99
Paints				
PbS in PP	Spray	0.92	0.80	94
PbS in EPDM	Spray	0.91	0.68	94
CdTe in EPDM	Spray	0.88	0.80	37,41
Sb_2Se_3 in EPDM	Spray	0.79	0.56	37,41
Si in EPDM	Spray	0.79	0.56	37,41
Cu-CrOx in EPDM	Spray	0.92	0.36	37,41
FeMnCuOx in EPDM	Spray	0.90	0.27	37,41
FeMnCuOx in PP	Spray	0.95	0.90	37,41
FeMnCuOx in EP	Spray	0.92	0.36	37,41
FeMnCuOx in EP	Spray	0.92	0.36	37,41
CuCrMnOx in Silicone	Spray	0.92	0.68	94
COFeMnOx in silicone	Spray	0.91	0.60	94
CoFe oxide	Spray	0.87	0.63	94

.....

Table 1.1 contd...

Materials	Fabrication technique	Absorptance (α)	Emittance (ϵ)	Ref.
Soot in poly urethane	Spray	0.90	0.3(100)	95
C in SiO_2 colloid	Dip coating	0.91	0.06	96

Numbers mentioned in the brackets are temperatures at which emittance has been measured.

PP = polypropylene

EPDM= ethylene propylene diene material

EP = ethylene propylene

CHAPTER – II

EXPERIMENTAL

CHAPTER II

EXPERIMENTAL

Selective coatings reported in this thesis were prepared by using electrochemical deposition techniques i.e. by cathodic reduction or by anodic oxidation process. In this chapter, we describe the experimental details for the initial substrate preparation and the set up used for the preparation of films. Essential details of optical, structural and thermal measurements on these coatings are also presented. These results are discussed in subsequent chapters.

2.1 Substrate Preparation

The surface finishing of a substrate influences the optical and thermal properties of the final selective surface. The contaminants affect the adhesion and quality of the coating. It is, therefore, essential to thoroughly clean and polish the metal substrate before deposition. Copper, nickel plated copper, stainless steel and nickel plates of size (2 cm x 6 cm) were used as the substrate. The plates were initially polished with a fine emery paper. These substrate plates were then dipped in 15% hydrochloric acid (HCl) for a few minutes, washed with distilled water several times and finally rinsed with carbon tetrachloride (CCl_4). A careful cleaning of the substrate is found to be absolutely essential for obtaining uniform deposit.

2.2 Electrodeposition Set-up

The technique of electrodeposition is well-established and has been used for a number of processes. Excellent books and reviews[117] are now available on the art of the electrodeposition technique.

The schematic block diagram of the electro-deposition set-up used in the present work is shown in Figure 2.1. It consists of a corning container, containing the reaction bath insulated from the bottom as well as from the sides with normal insulating material. Two brass-electrode-holders were mounted on the bakelite sheet. One electrode holder is fixed and other can be moved through the groove in the bakelite sheet, so that distance between the two electrodes can be easily varied. The bath was electrically heated to different temperatures from 30°C to 90°C. The temperature is being recorded with the help of a thermometer, fixed on the bakelite sheet. The anode or cathode was used in the form of strip size (2 cm x 6 cm) after cleaning as described in section 2.1. Arrangements were also made for fitting metal plates to the electrode holder. The metal plates were held vertically in the reaction bath. A constant current source (0-1 Amp) was used for the deposition process. The voltage across the electrodes was measured by a volt-meter, connected across the electrodes. The reaction bath was stirred mildly during the deposition to obtain uniform coatings. The details of the bath and deposition conditions used for

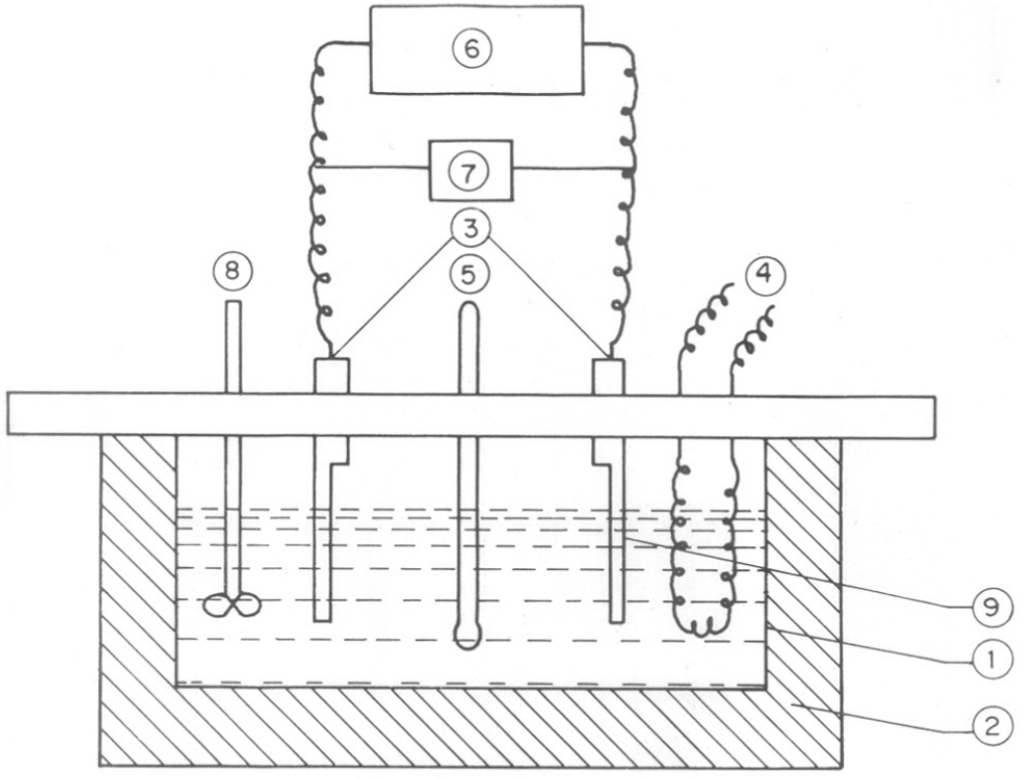

1) CORNING CONTAINER.

2) THERMAL INSULATION.

3) ELECTRODE HOLDER.

4) IMERSION HEATER.

5) THERMOMETER.

6) CONSTANT CURRENT SOURCE.

7) VOLTMETER.

8) STIRRER.

9) METAL ELECTRODES.

FIGURE 2·1 EXPERIMENTAL ARRANGEMENT FOR ELECTRO-DEPOSITION TECHNIQUE.

making selective surface are given in the respective chapters.

2.3 Normal Reflectance Measurements (0.4μm-0.8μm)

The reflectance measurements in the range 0.4μm-0.8μm were taken using a spectrophotometer[118] designed and fabricated in this laboratory. The main features of the apparatus are shown in Figures 2.2 and 2.3.

The spectrophotometer consists of a light source 1, a condensing lens 2, a polaroid 3, a collimeter 4, a prism 5, which is fixed over a rotating table moving over a graduated scale 6, a telescope 7, a focussing lens 8 and a sample holder 9, a photocell 10 and a graduated disc 11. A tungston lamp (10 V, 7.5 Amps) was used as a source of excitation. Both collimeter and the telescope were provided with adjustable slits (S1 and S2). The prism 5 could be rotated on the graduated base 6, so as to select the suitable monochromatic light. The sample holder 9, which is placed at the focuss of the second lens 8 is free to rotate around the vertical axis which coincides with the central shaft of the disc 11 and its position over the disc (not shown in Fig.) can be read out by a pointer. The photocell 10 placed very close to the sample holder can similarly be rotated around the sample axis, its position similarly can be recorded.

The intensity of light on the photocell (Philips 90 CV and 92 AV) was measured by a voltage reading with the help of microvoltmeter. The prism scale 6, was calibrated

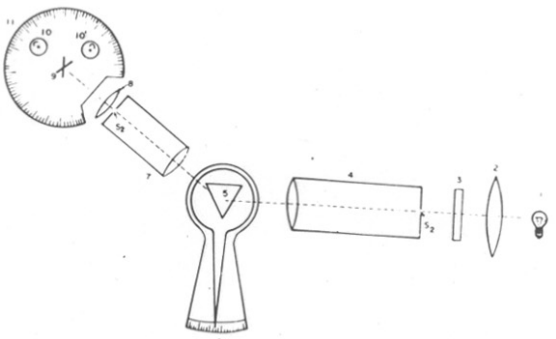

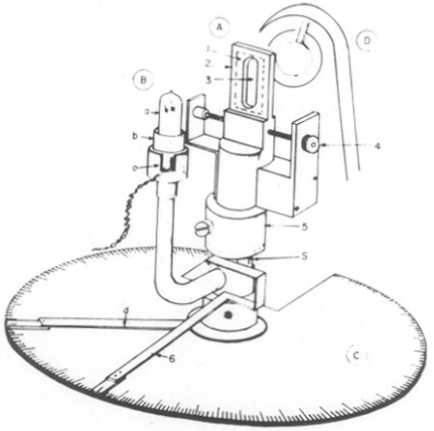

FIGURE 2·2 & 2·3. BLOCK DIAGRAM FOR THE SPECTROPHOTOMETER.

with respect to the wavelength by inserting suitable narrow band width filters in place of polaroids and measuring the maximum intensity of light through the telescope by adjusting the position on the scale 6. The accuracy of calibration was 50 A^{o}. Care was also taken to ensure that the same portion of the photocell was exposed at all angles of incidence. The entire assembly was enclosed in a dark case.

Measurement of reflectance - First the photocell was kept at zero position on the scale and the initial microvoltmeter reading was recorded. The reading thus obtained (Io) gave the intensity of the light at particular wavelength.

Then the sample was exposed to selected wavelength at an angle of incidence of 10^{o}. The reflected intensity (I_R) is again measured with the help of microvoltmeter by moving the photocell to proper position. The ratio I_R/I_o gave the reflectance of the sample at the selected wavelength. Same procedure was repeated for measuring the reflectance of the sample at different wavelengths. The values of absorptance obtained from these measurements at different wavelengths were used to determine the total absorptance (α) over the solar spectrum region.

2.3.1 Total reflectance measurement in the range (0.38 μm-0.76 μm)

Total reflectance (diffuse + specular) of these films was recorded as a function of wavelength in the region

0.38 μm - 0.76 μm with a pye-unicam spectrophotometer model UV/VIS SP8-100 using the reflectance attachment. Barium sulphate ($BaSO_4$) was used as a standard. The reflectance accessory consists of an integrating sphere conforming to C.I.E. recommendations, sample mounting discs and specular caps. It is used for measuring the total reflectance of a flat surface in 8°/total and 8°/ diffuse configurations. We carried out the total reflectance measurement on our samples for optimizing the deposition time to get high absorptance in this region without affecting the transparency in the IR region.

2.3.2 Normal reflectance measurement in the region (1 μm - 15 μm)

The reflectance in this region was recorded as a function of wavelength by a Perkin-Elmer double beam spectrophotometer model 221 using the reflectance attachment. Front coated standard aluminum mirrors were used as the standard, while carrying out the measurements. The values of absorptances obtained at different wavelengths from these measurements were used for the determination of total α and total ε by graphical method.

2.4 Solar Absorptance Measurement (α)

The D & S (Devices and Services Co., Texas) Alphatometer is a miniaturized pyranometer specially designed for measurements of solar absorption. The radiation detector is a black and white 32 junction thermopile. This calibration ensures nearly a constant response to the radiations in the solar wavelength (0.3 - 2.5 μm).

Solar absorptance measurement (α) - The instrument used is shown in Figure 2.4. First the board was faced towards the sun and tilted so that incidence angle was 25°. This was indicated by the end of the shadow on the sun-angle indicator, which is fixed on the mounting board. The distance between the detector surface and the sample surface was kept equal to 2.5 cms. The detector was rotated with the knob so that the sensing surface was parallel to the sample and facing the sun. The voltage reading (V_r) was recorded when it became steady. RD1 Scaling Digital Voltmeter was used as a voltage reading device. This voltage is proportional to the incident radiation falling on the sample. Then detector was rotated through 180°, so that the sensing surface was parallel to the sample and facing it. The voltage reading (V_r) obtained is proportional to the solar radiation reflected by the sample. The reflectance (ρ) was then determined by the ratio

$$\rho = \frac{V_r}{V_i}$$

Solar absorptance (α) was then determined using the relation

$$\alpha = 1 - \rho$$

We measured solar absorptance (α) by this method on the sample for which deposition time was optimised.

2.5 Emissivity Measurements

The D & S emissometer (Fig. 2.5) is a special type of instrument for measuring the emittance. The detector of the device is heated to 180°F, so that the sample does not

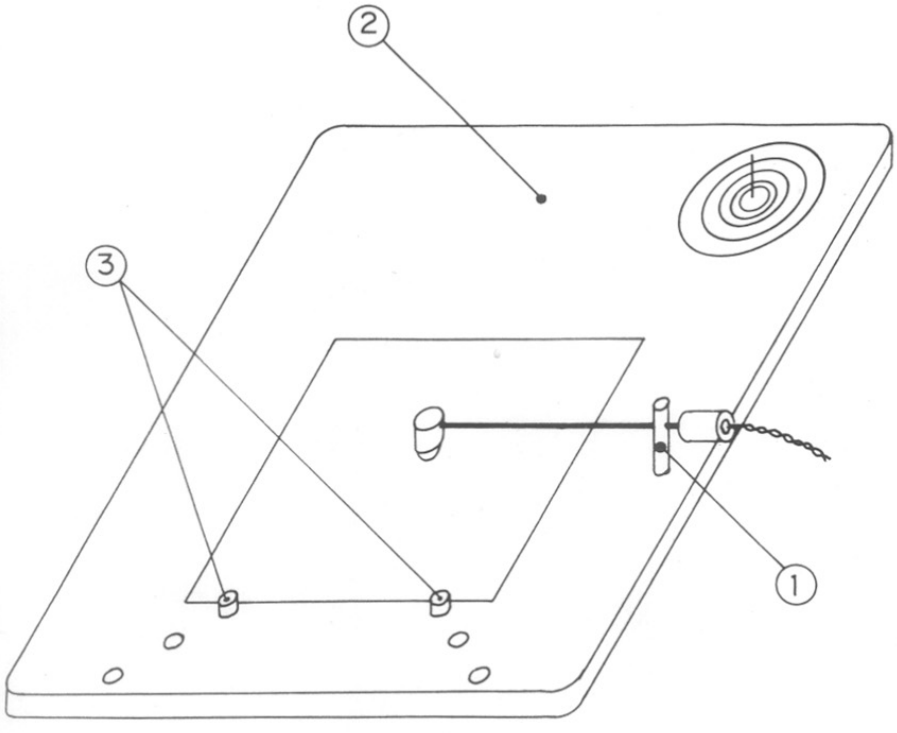

1) ALPHATOMETER DETECTER AND SUPPORT.

2) MOUNTING BORD WITH SUN ANGLE INDICATOR.

3) SAMPLE SUPPORT PEGS.

FIGURE 2·4. BLOCK DIAGRAM OF THE ALPHATO-METER MODEL A-1.

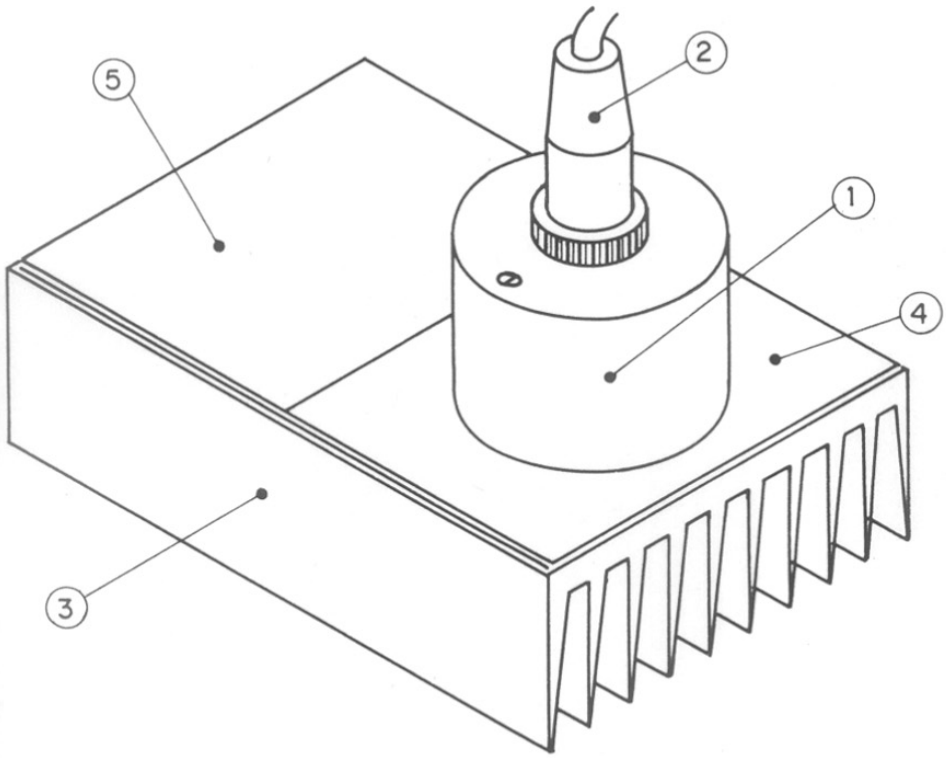

1) EMISSOMETER DETECTOR.

2) 4 PIN CONNECTOR & CABLE.

3) HEAT SINK.

4) FLAT BLACK PAINT — STANDARD.

5) LOW EMISSIVITY STANDARD - BARE ALUMINIUM.

FIGURE 2·5 BLOCK DIAGRAM OF THE EMISSOMETER MODEL — AE.

have to be heated. The detector responds only to radiation heat transfer and is designed to have a linear output with emissivity. The emissivity of an unknown surface is measured after the calibration of the detector with the standard surface of known emissivity, which is maintained at the same temperature as that of the sample. The radiation detector is a differential thermopile. The sensing surface of the detector is aluminum foil and black paint. This combination has nearly constant response to thermal wavelengths from 3μm to 30 μm.

The emittance (ϵ) of the sample was calculated using the relation,

$$\epsilon_{sample} = \frac{V_{sample}}{V_{standard}} \times 0.93$$

First a flat black standard surface and thesample were kept on the heat sink side by side. Sample must be flat and in good thermal contact with the heat-sink. To establish good thermal contact between the heat sink and the sample, either few drops of water were sprinkled over the heat sink or heat transfer grease was applied on the top of the heat-sink.

The emissometer was calibrated periodically with the standard Al foil whose emittance is 0.04. The detector is kept on the standard Al foil and voltage reading is adjusted in such a way that emittance is 0.04.

$$V_{Al} = \frac{V_{standard}}{0.93} \times 0.04$$

We measured emissivity (ϵ) on the sample, for which, deposition time was optimized.

RD1 digital voltmeter was used as voltage reading device.

2.6 Structural Properties

The structure of these selective black films was examined by electron diffraction and x-ray diffraction methods.

2.6.1 Electron diffraction

In order to identify the nature and their phases composition, these films were examined by using an electron diffraction camera. A Finch type (Finch & Wilman 1937) electron diffraction camera was used for the present study. A cold cathode was used as the source of electron beam. An accelerating voltage of 50-60 KV was generally used. The analysis of the electron diffraction pattern was carried out by using internal reference as the standard. The 'd' values were calculated by using the formula

$$d = \frac{L \lambda}{r}$$

where 'r' is the radius ofthe diffracting ring. The diffraction patterns of the film were analysed by comparing these 'd' values with the corresponding 'd' values from the ASTM data.

2.6.2 X-ray diffraction

X-ray diffraction studies were carried out using a Philips PW1730 diffractometer with CuK_α radiation (λ = 1.54 A^o). The diffraction intensity was recorded as a function of angle of diffraction (2θ). The 'd' values

were then calculated using the Bragg relation $2d \sin \theta = \lambda$, θ being the angle of diffraction maxima. The coating was then characterised by comparing the 'd' values and the intensity of diffraction used to identify the coatings by comparison with standard from the ASTM data file.

2.7 Surface Morphology Study Using Scanning Electron Microscope

A Cambridge Stereo Scan 150 Microscope was used in the present study to study the surface morphology. The samples were overcoated with a thin layer of aluminum to reduce the charging effect and to improve the contrast. The instrument was operated in the secondary emission mode at an angle of 45°. Scanning electron micrographs revealing the morphological features were recorded at suitable magnifications.

2.7.1 Electron probe micro analysis (EPMA) or EDAX energy dispersive analysis of x-rays

Elemental analysis of these films was carried out using energy dispersive analysis technique. The films were analysed non-destructively by this method and elemental analysis can be obtained with good accuracy.

2.8 Compositional Analysis

The analysis of the chemical composition of these coatings was carried out using X-ray Photoelectron Spectroscopy (XPS) and Auger Electron Spectroscopy (AES).

X-ray photoelectron spectra (XPS) on these samples were recorded with the help of ESCA-3, M-KII instrument using

MgK_α (1253.6 eV) or AlK_α (1486.6 eV) as radiation source. The instrument was calibrated using $Au4f_{7/2}$ (83.96 eV) and C1s peak as an standard (C1s 285eV). The calibration was regularly checked during the course of the work. Films were coated with a thin layer of gold or Al to avoid charging effects. The binding energy or peak position (BE), full width at half maximum (FWHM) have been compared with the available data to identify the chemical composition/or oxidation state etc.

AES was recorded on the above instrument using electron energy beam (10 KV) having diameter around 0.2 μm for excitation. The instrument was provided with sputter etching facility for cleaning the surface. AES depth profiling was carried out using a differentially pumped Ar ion gun with 0-10 KV energy which can be rastered over an area upto 10 mm x 10 mm. During AES depth profile studies a multichannel multiplex control was used for peak to peak height detection of Auger peaks as a function of sputtering time.

2.8.1 Chemical analysis

The standard chemical analysis techniques were used, wherever possible to determine the film composition.

CHAPTER – III

COPPER – BLACK

CHAPTER III

COPPER-BLACK

Introduction

Black copper oxide coating on copper or aluminum is the most commonly used selective surface for flat plate collectors. Several authors [3,44-45,47-48,119-123] investigated solar selective properties of the copper-black coatings prepared by various processes e.g. spraying, chemical conversion, chemical brightening and etching and thermal oxidation.

No studies have, however, been reported on selective copper-black films prepared by anodic oxidation method. We report the preparation of solar selective copper-black films by an electrolytic technique in this chapter and results on its characterization using different techniques are also presented.

3.1 Preparation of Films

The technique of anodic passivation by oxide film on copper metal in an alkaline medium is well known.[124] Copper plates of size 2 cm x 6 cm were cleaned as described in chapter II.(Section 2.2). Different runs were first taken, to optimize the preparation conditions namely bath composition, temperature, distance between two electrodes etc., using a bath containing sodium hydroxide (NaOH), and ammonium molybdate [$(NH_4)_2MoO_4$] solution in the setup

described in Chapter II. The chemicals used were all of the analytical reagent grade. A constant current was used as the power supply source. The plate was removed from NaOH solution after the current had been passed for a predetermined length of time and washed in distilled water several times and dried before measurements were taken. On the basis of these runs the following bath composition and deposition conditions were found to be the optimum and were kept fixed for subsequent studies.

(a) Bath composition -

(i)	Sodium hydroxide (NaOH)	10% by weight
(ii)	Ammonium molybdate $[(NH_4)_2MoO_4)]$	0.01% by weight

(b) Deposition conditions -

(i)	Temperature of the bath	$80^{o}C$
(ii)	Deposition time	60 sec
(iii)	Distance between two electrodes	7.5 cms
	Cathode - 2 cm x 6 cm	stainless steel plate
	Anode - 2 cm x 6 cm	cleaned copper plate
(iv)	Voltage across the two electrodes	1.25 volts

3.2 Results and Discussion

The films obtained by anodic oxidation process were found to be quite uniform and well adherent to the substrate as has been seen by the Scotch tape test. The anodizing time was optimized by changing the time of anodization from 10 seconds to 80 seconds to get high α and low ϵ.

The effect of anodizing time on the total reflectance of the copper-black films in the region 0.34 μm-0.76μm is presented in Figure 3.1. It is seen from Fig. 3.1, that as anodizing time is increased, the total reflectance of the film in this region decreases upto the time of 60 seconds and then onwards it remains more or less constant. This observation indicates that as anodizing time is increased upto 60 seconds, the absorptance in this region increases and it remains more or less constant on further increase in the time of anodization.

The effect of anodizing time on the normal spectral reflectance of the film in the IR region i.e. 1 μm - 15 μm is shown in Figure 3.2. It can be seen from Fig. 3.2, that as the anodizing time is increased, the normal spectral reflectance in this region goes down. This observation suggests that increase in the anodizing time decreased the reflectance, thereby increasing the emittance.

When the anodization time was kept equal to 60 sec we got the copper-black films with low total reflectance in the region 0.34 μm - 0.76 μm and with high reflectance in the

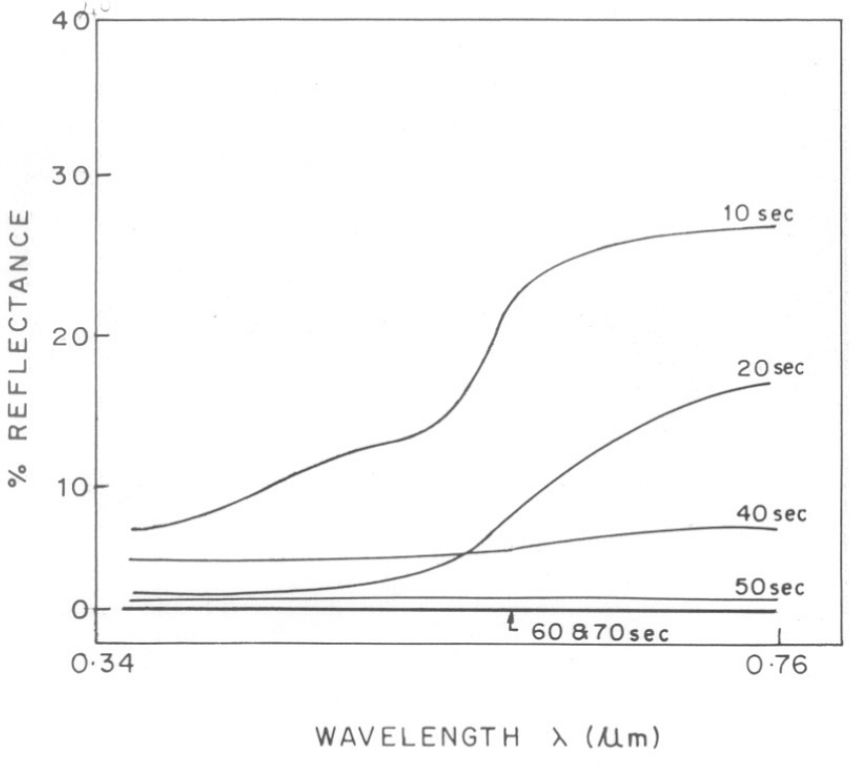

FIG. 3·1 EFFECT OF TIME OF DIPOSITION ON THE TOTAL REFLECTANCE OF THE COPPER BLACK FILM.

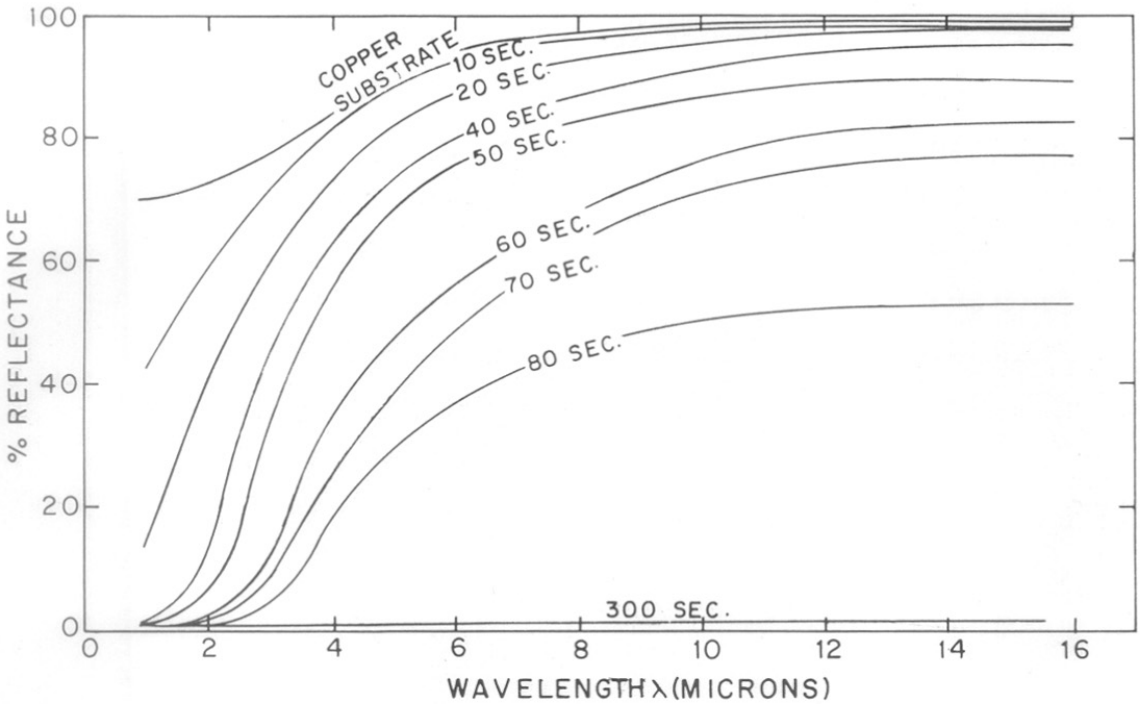

FIG. 3·2 EFFECT OF TIME OF DIPOSITION ON THE NORMAL REFLECTANCE OF COPPER–BLACK FILM.

region 1 μm - 15 μm. This observation indicates that at t = 60 seconds, the copper-black film has got just sufficient thickness, so that films are absorbing in the visible region but are transparent in the thermal IR region, since the reflectance of the substrate copper is not much affected. The Fig. 3.2 also shows the reflectance of the substrate copper for comparison. If the anodizing time is increased beyond 60 seconds, then it is observed that the transparency of the film in the IR region goes down, thereby increasing the emittance. This is expected because as the film thickness increases, the mass per unit area of the film also increases causing an increase in the emittance.

If the anodizing time is increased still further, say equal to 300 seconds, the transparency of the film in the IR region is affected to an extent that spectral selectivity is lost.

It is also seen from Figures 3.1 and 3.2 that if the anodizing time is made less than 60 seconds, the total reflectance in the region 0.34 μm - 0.76 μm is higher than that of the film prepared at t = 60 seconds, thereby lowering the absorptance and it is also found that the corresponding IR reflectance was higher than that in the film prepared at t = 60 seconds, thereby lowering the emittance.

It may also be seen from Figure 3.1 and 3.2 that $\lambda_{cut\text{-}off}$ shifts towards the higher wavelength side on increasing the anodizing time and vise-versa on decreasing it.

In the present study the selective copper-black film (A5) obtained when anodizing time was kept equal to 60 seconds and non-selective copper-black film (A6) obtained at t = 300 seconds of anodizing time were used for further experimental work.

Figure 3.3 shows the normal spectral reflectance of the film (A5) as a function of wavelength. The normal spectral reflectance of A5 film and substrate copper as measured by spectrometer is shown in Table 3.1 for comparison. The graph shows a near ideal spectral selectivity with $\lambda_{cut\text{-}off}$ at 3.5 μm. The total absorptance (α) over the solar spectrum (AM2 condition)[127] and total thermal emittance (ϵ) at 100°C were determined by graphical method [46] from the normal spectral reflectance measurement. The room temperature emittance (ϵ) as measured by emissometer was found to be equal to 0.2. The solar absorptance as measured by Alphatometer was 0.97. The values of α and ϵ thus obtained for A5 film are presented in Table 3.2. It may be noted from Table 3.2 that α/ϵ ratio is 4.8 at room temperature but the ratio changes to 2.798 at 100°C.

If we assume that the working temperature of the flat plate collector is 100°C and the incident radiation is AM2, then the desired cut-off should be around 2.5 μm. The film (A5) obtained under optimized conditions exhibits the required cut-off.

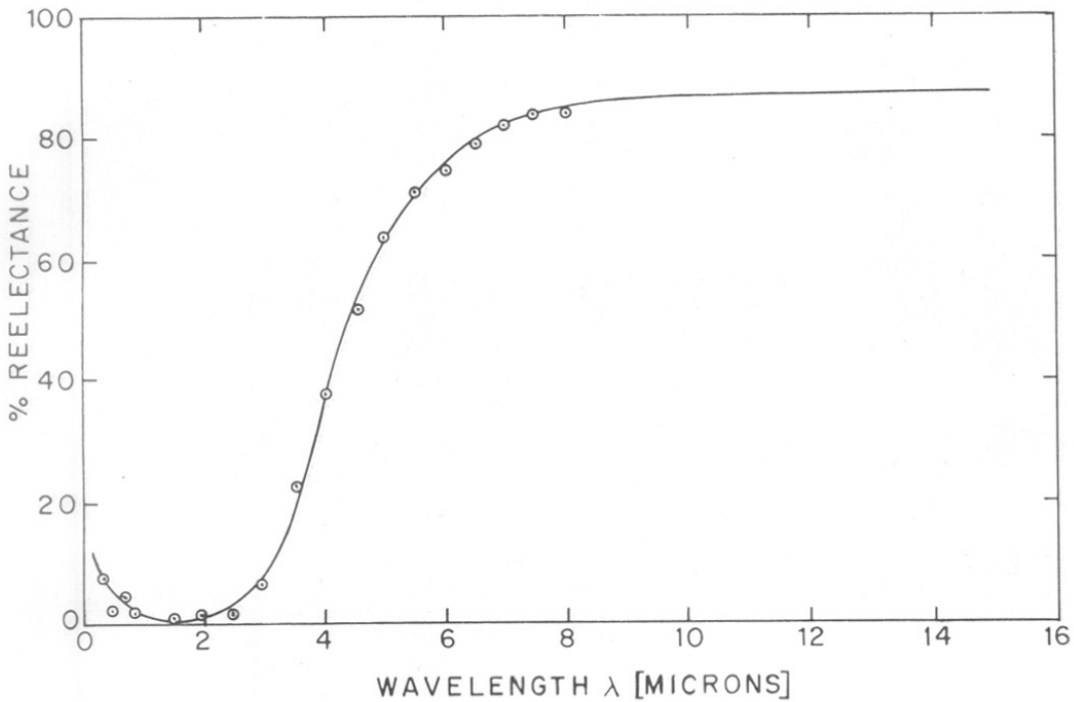

FIG. 3·3 REFLECTANCE OF SELECTIVE COPPER BLACK FILM (A_5).

TABLE 3.1

NORMAL SPECTRAL REFLECTANCE OF COPPER SUBSTRATE AND SELECTIVE COPPER BLACK FILM (A5)

$\lambda(\mu m)$	% Reflectance of film	% Reflectance of copper substrate
0.4	5.26	8.57
0.45	4.15	18.36
0.5	2.50	21.80
0.55	4.84	21.35
0.6	4.20	36.66
0.65	3.58	51.55
0.7	2.24	59.03

TABLE 3.2

VALUES OF α AND ϵ FOR THE SELECTIVE COPPER-BLACK FILM (A5)

Temperature ^{o}K	α	ϵ	α/ϵ
300	0.96	0.2	4.8
373	0.96	0.34	2.798

The values of α and ϵ of the selective copper-black film (A5) prepared by anodic oxidation method are comparable with the reported values prepared by other techniques such as spray pyrolysis,[47,48] chemical conversion,[44,122] thermal oxidation[48] etc. It is worthwhile to note the special feature of our films which are as follows. The graph shown in Figure 3.3, shows two distinctly different features as compared to the thermally oxidized samples one is the location of the reflectance step at longer wavelengths and other is the lack of interference fringes.

3.3 Structural Characterization (Electron Diffraction and X-ray Diffraction)

In order to know the nature of the film, phase composition and chemical composition, the electron diffraction and x-ray diffraction studies on these films were carried out.

The electron diffraction pattern of the selective copper-black film (A5) is shown in Figure 3.4. The 'd' values obtained for A5 film are presented in Table 3.3.

The first line is attributed to cuprous oxide (Cu_2O) as well as to cupric oxide (CuO), the second line to cupric oxide (CuO), while third one is attributable to cuprous oxide (Cu_2O) or copper. It is observed that the intensity of the third line is more than that of the first one, but if copper was absent, the relative intensity should have been other way (ASTM card No. 4-0836, 5-0667). From the comparison of the 'd' values from Table 3.3, the electron

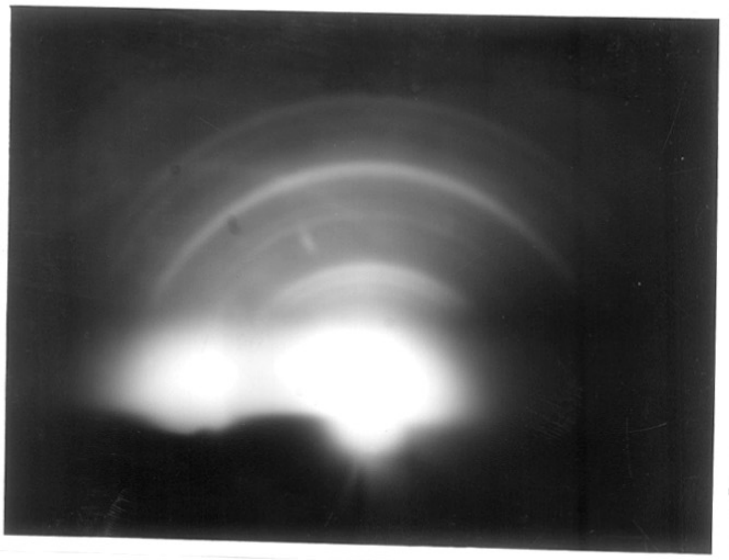

Figure 3.4: Electron diffraction pattern of selective copper-black film (A5)

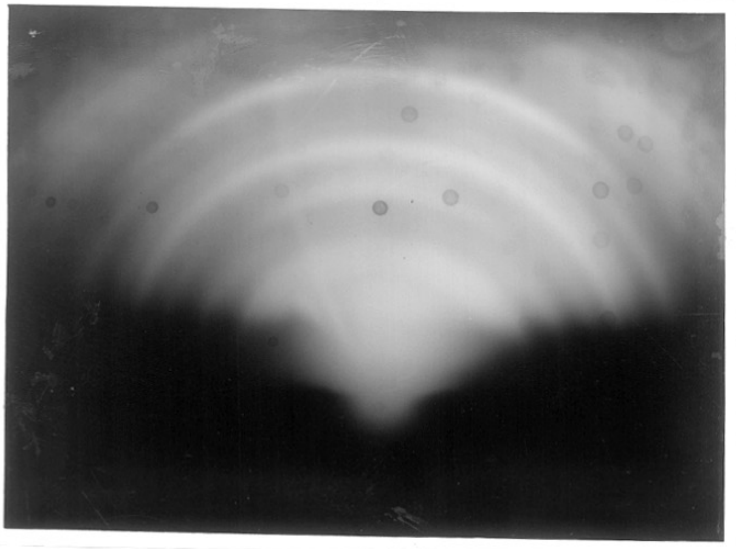

Figure 3.5 : Electron diffraction pattern of non-selective copper-black film (A6)

TABLE 3.3

ELECTRON DIFFRACTION DATA OF THE SELECTIVE COPPER-BLACK FILM (A5)

hkl			Intensity observed	'd' observed A^o	'd' standard A^o		
Cu	CuO	Cu_2O			Cu	CuO	Cu_2O
-	002, $\bar{1}11$	111	s	2.47	-	2.53 2.52	2.46
-	111	-	s	2.33	-	2.323	-
111	-	200	s	2.13	2.08	-	2.135
200	$\bar{2}02$	-	w	1.83	1.808	1.866	-
-	202	-	ms	1.60	-	1.581	-
-	$\bar{1}13$	-	w	1.51	-	1.505	-
-	220 113	-	s	1.37	-	1.375	-
311	-	-	w	1.10	1.09	-	-

s - strong
ms - medium
w - weak

diffraction pattern shows the presence of cuprous oxide (Cu_2O), cupric oxide (CuO) and copper in A5 film.

To solve the ambiguity in the intensity of third line (d = 2.13 A°), the electron diffraction pattern of thicker film (A6) was also examined. The pattern is shown in Figure 3.5 and 'd' values obtained are presented in Table 3.4. It is found that the intensity of the third line is reduced while intensities of first two lines are increased. This clearly indicates the presence of more cupric oxide(CuO) in the thicker film, but some intensity due to copper is also present. This copper line may be coming from the substrate because of low mass absorption character of the film or the porous nature of the film. This point is further clarified by SEM studies on the film.

It is also observed that as the thickness increases, the cupric oxide (CuO) tends to develop a preferred (11$\bar{1}$) orientation as can be seen by an arching on the lines. In other words, the 110 planes of cupric oxide, tend to align parallel to the substrate. The 'd' values from the Table 3.3 and 3.4 suggest, that the cuprous oxide (Cu_2O) in the film is cubic, while cupric oxide (CuO) is monoclinic. The presence of copper diffraction is attributed to the substrate copper.

To confirm the above analysis, x-ray diffraction study on the film A5 and A6 was carried out. Figure 3.6 and 3.7 show the diffractogrames of these two films respectively.

TABLE 3.4

ELECTRON DIFFRACTION DATA OF NON-SELECTIVE COPPER-BLACK FILM (A6)

'd' A^{o}	Intensity observed	Composition
2.47	s	CuO, Cu_2O
2.33	s	CuO
2.135	s	Cu, Cu_2O
1.83	w	CuO
1.60	s	CuO
1.50	w	CuO
1.32	s	CuO
1.20	w	CuO
1.09	w	Cu

s - strong
w - weak

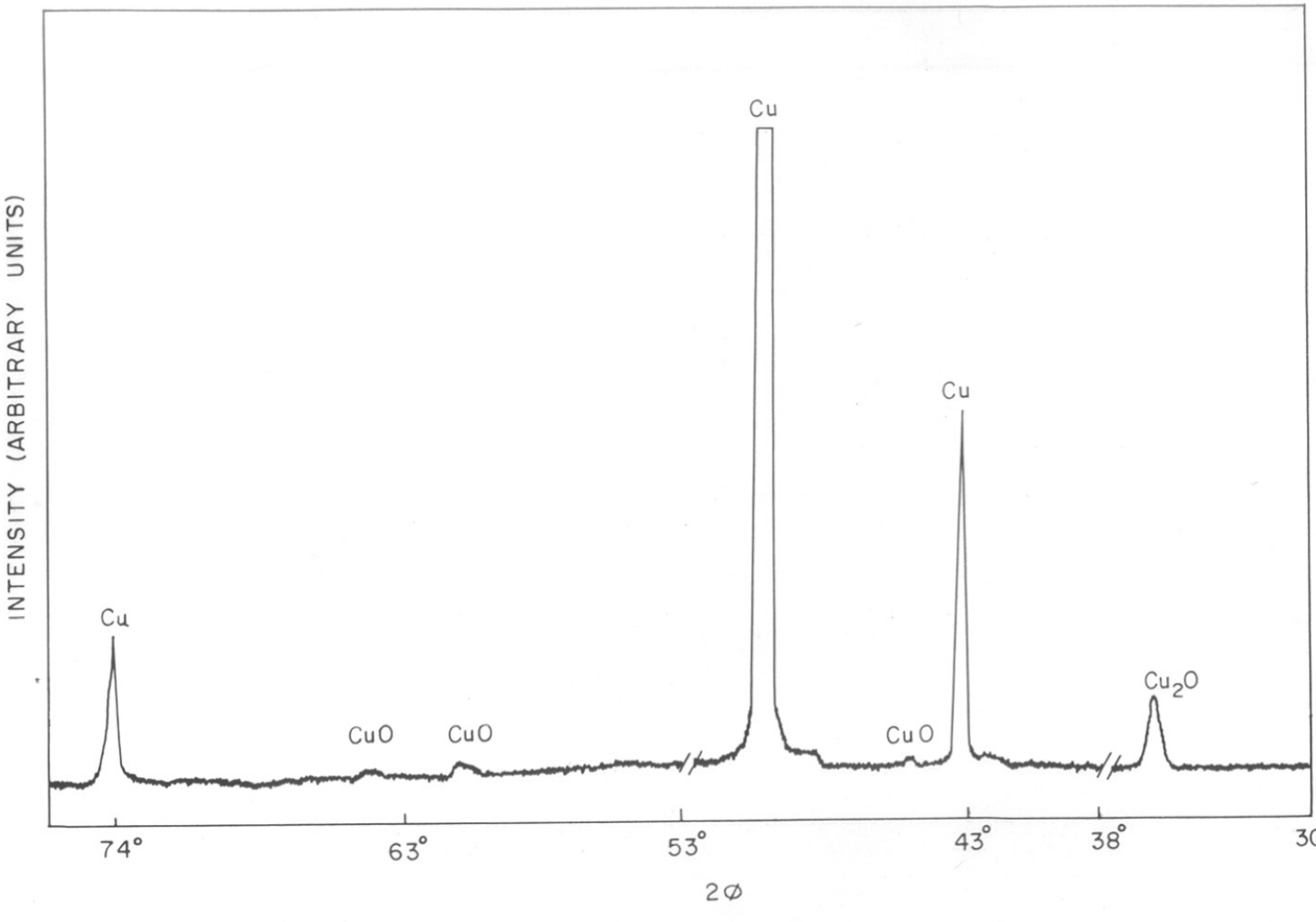

FIG. 3·6 X-RAY DIFFRACTOGRAM FOR SELECTIVE COPPER BLACK FILM (A_5).

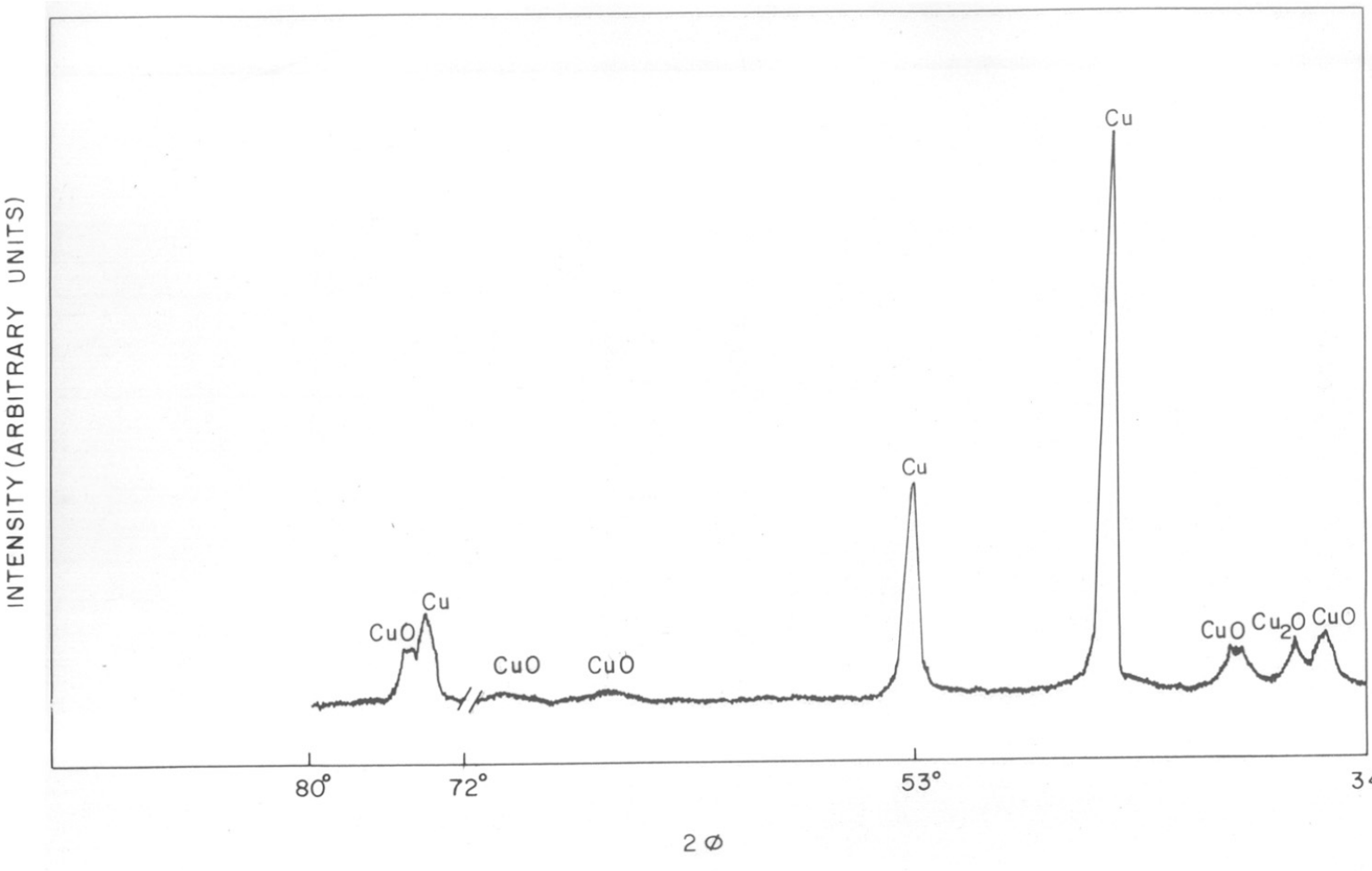

FIG. 3·7 X-RAY DIFFRACTOGRAM OF NONSELECTIVE COPPER BLACK FILM (A_5).

The 'd' values obtained are tabulated in Tables 3.5 and 3.6. From the comparison with standard 'd' values, it is possible to assign the peaks in Figures 3.6 and 3.7 to cuprous oxide (Cu_2O), cupric oxide (CuO) and copper. It is seen from the Figs. 3.6 and 3.7 that as anodic oxidation time increases, the percentage of cuprous oxide (Cu_2O) decreases and that of cupric oxide (CuO) increases. The 'd' values from Table 3.5 and 3.6 also suggest that cuprous oxide (Cu_2O) is in cubic form and cupric oxide (CuO) is monoclinic, which agree with electron diffraction results.

The peaks corresponding to cuprous oxide (Cu_2O) and cupric oxide (CuO) in A5 film are much broader as compared to sharp copper peaks. This observation indicates that the selective copper-black film (A5) consists mainly of cuprous oxide (Cu_2O) and cupric oxide (CuO) and large copper crystallites, the presence of which is shown from the substrate copper, considering the x-ray penetration depth.

Figures 3.6 and 3.7 also indicate that selective copper-black film (A5) contains more cuprous oxide (Cu_2O) than cupric oxide (CuO), while non-selective copper-black film (A6) contains more cupric oxide (CuO) than cuprous oxide (Cu_2O).

The crystallites sizes were calculated using the relation (125)

$$D = K\lambda / \beta \cos \theta$$

TABLE 3.5

X-RAY DIFFRACTION DATA OF SELECTIVE COPPER-BLACK FILM (A5)

d, A^{o}	hkl	Intensity
2.4727 (Cu_2O)	111	s
2.004 (CuO)	$\bar{1}12$	w
2.0924 (Cu)	111	s
1.8090 (Cu)	200	s
1.5043 (CuO)	$\bar{1}13$	w
1.4375 (CuO)	- 022 311, 310	w
1.2799 (Cu)	220	s

s - strong
w - weak

TABLE 3.6

X-RAY DIFFRACTION DATA OF NON-SELECTIVE COPPER-BLACK FILM(A6)

d A^o	hkl	Intensity
2.5197 (CuO)	$\bar{1}11$	s
2.4531 (Cu_2O)	111	s
2.3189 (CuO)	111	s
2.0780 (Cu)	111	s
1.8023 (Cu)	200	s
1.5043 (CuO)	$\bar{1}13$	w
1.4375 (CuO)	022, $\bar{3}11$, 310	w
1.2754 (Cu)	220	s
1.2654 (CuO)	004, $\bar{2}22$	s

s - strong
w - weak

Where 'D' is the mean crystallite dimension normal to diffracting plane, λ is the x-ray wavelength, β is the observed peak breadth at half maximum intensity corrected for K_α doublet separation and instrument line width broadening and θ is the Bragg angle. The crystallite size thus obtained for cuprous oxide (Cu_2O) and cupric oxide (CuO) is found to be between 100 A° to 200 A°.

To summarise, copper-black films are crystalline and consist of two phases namely cubic cuprous oxide (Cu_2O) and monoclinic cupric oxide (CuO) with crystallite sizes ranging from 100 A° to 200 A°. The selective film (A5) contains more cuprous oxide (Cu_2O), while non-selective film (A6) contains more cupric oxide.

3.4 Surface Morphology Study by SEM

It is now well established that optical properties of the selective-black films are dependent on the morphology of the surface[126]. A study on the surface morphology of the selective copper-black (A5) and the thicker copper-black (A6) was therefore carried out using scanning electron microscope. The electron micrographs obtained are shown in Figures 3.8 and 3.9 for films A5 and A6 respectively.

It is seen from the Figure 3.8, that selective copper-black film has got structure with uniform distribution of particles of sizes ranging from 0.5 μm to 1 μm. The voids of size of the order of 0.5 μm are seen.

Scanning

Figure 3.8 : Electron micrograph of selective copper-black film (A5)

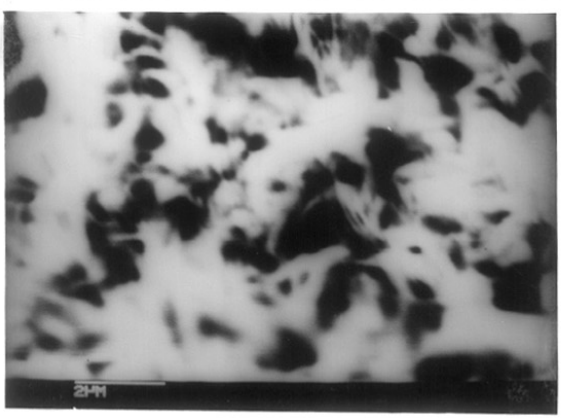

Figure 3.9 : Scanning electron micrograph of non-selective copper-black film (A6)

The surface morphology of the non-selective copper-black film (A6) is entirely different from that of A5 film. It shows structure with distribution of varied particles (Size > 3.5 μm) with more number of voids (size from 1 μm-10 μm). This observation suggests that the morphology of the film changes as the thickness of the film increases. If we compare the optical properties of the film A5 and A6, then it can be concluded that typical surface morphology of the film (A5) is responsible for the spectral selectivity to some extent, . . as in the case of thicker film (A6), due to morphology changes, the transmittance of the film in the thermal IR region is affected so much, that film (A6) loses its spectral selective behaviour as is seen from the reflectance measurement.

3.5 X-ray Photoelectron Spectroscopic Study

XPS study on selective copper-black (A5) and thicker copper-black (A6) was carried out to ascertain the chemical nature and/or oxidation state of the constituent surface atoms.

Figure 3.10 shows the XPS spectrum of the A5 film on 0-1000 eV binding energy (BE) scale. It indicates presence of mainly copper and oxygen and contamination from carbon. XPS spectra for copper and oxygen were taken on 100 eV full scale scan to know the exact BE. The XPS spectra is shown in Figure 3.11. It shows a broad assymetric peak at 934 eV, having a shoulder on the higher BE side. The asymmetric peak at 934 eV can be attributed to Cu-$2P_{3/2}$ level.

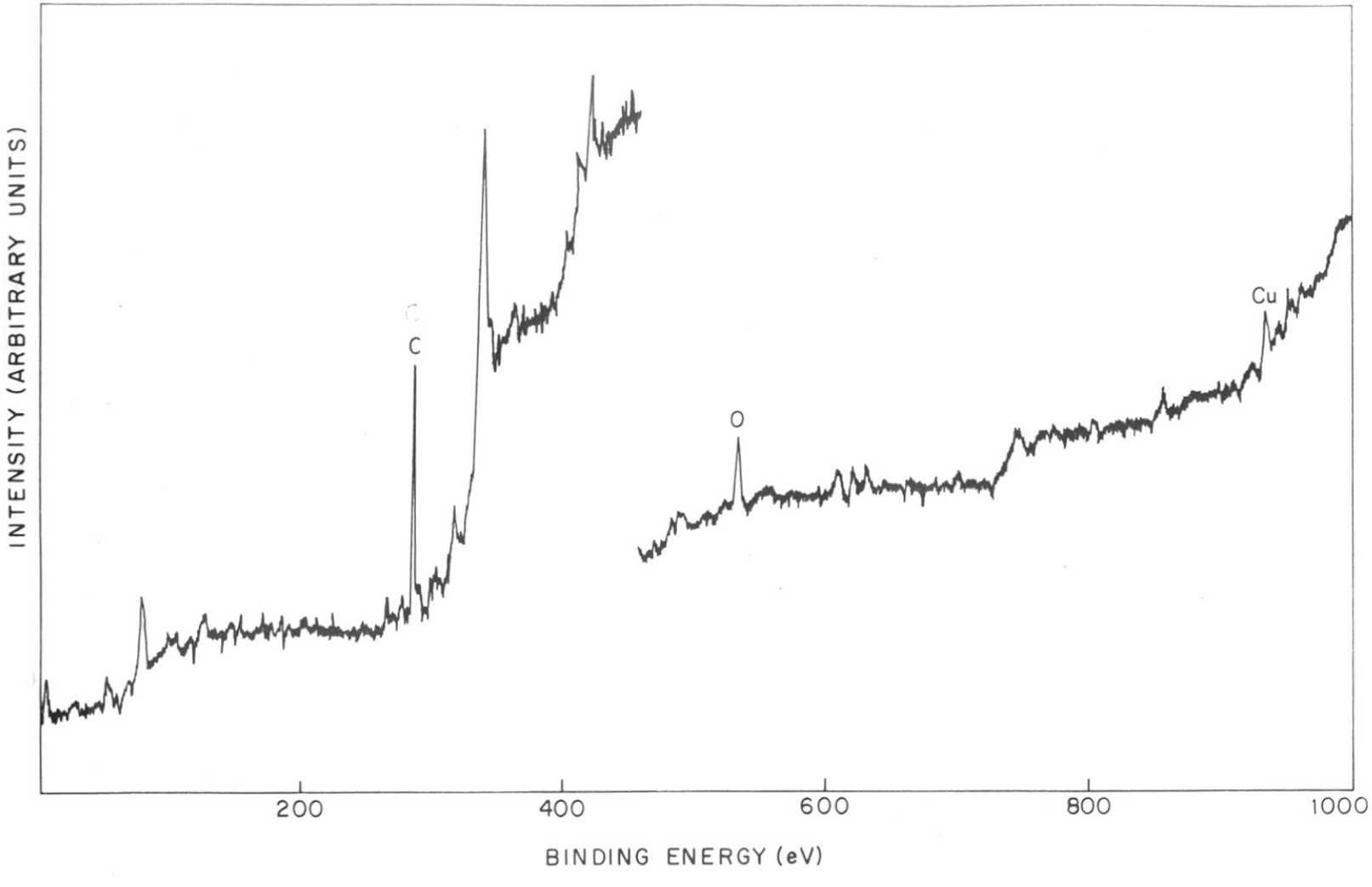

FIG. 3·10 FULL XPS OF SELECTIVE COPPER-BLACK FILM (A_5) ON 0-1000 eV BE SCALE

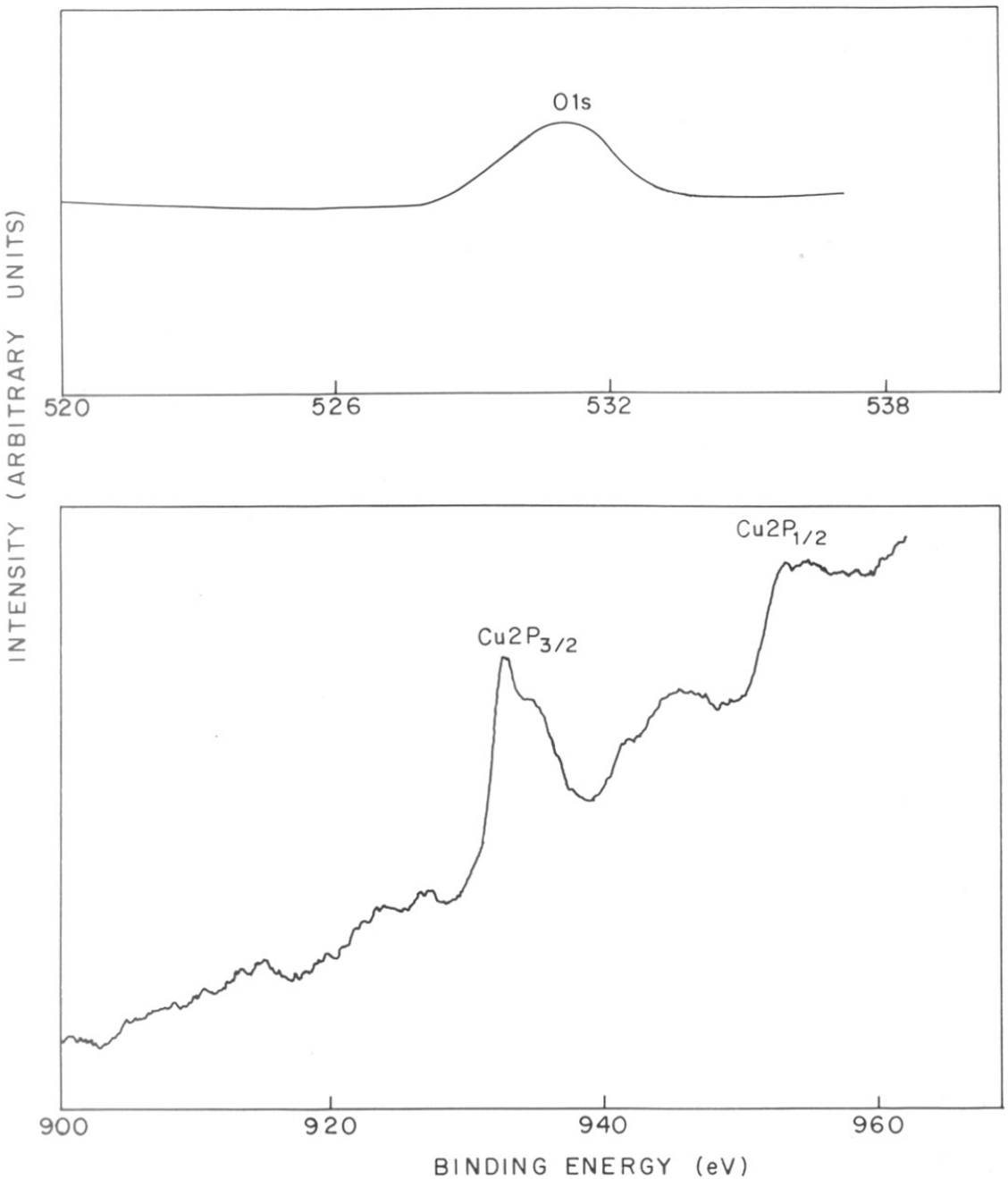

FIG. 3·11 XPS OF SELECTIVE COPPER-BLACK FILM (A_5).

This peak was resolved into two with maxima at 932.3 eV and 934.4 eV and is shown in Figure 3.12. In addition, there is a peak at 942.2 eV which is assigned to be a shake-up satellite.[80,131] The peak at 530.8 eV is due to oxygen (01s).

The BE of various levels obtained by us and corresponding reported values[128] are presented in Table 3.7. From the comparison of BE values, full width at half maximum (FWHM), g-energy separation between Cu $2P_{3/2}$ and 01s and presence of satellite structure characteristic of Cu^{+2} species, it can be concluded that selective copper-black film consists of cupric oxide (CuO), cuprous oxide (Cu_2O) and/or copper which is in agreement with Frost et al.[129] that cupric oxide exhibit multiplet line broadening with shake up satellite and cuprous compounds are nearly identical with copper spectrum in terms of line widths, BE and absence of satellite.

XPS study on thicker copper-black film (A6) was also carried out to know the composition. The spectra on 30 eV scale is presented in Figure 3.13. The peak at 934 eV is symmetric and a more intense satellite[130-131] structure is observed on the higher binding side of the main Cu $2p_{3/2}$ peak as compared with XPS spectra for selective film A5. The peak at 530.2 eV is due to 01s, which is found to be asymmetric. The asymmetric 01s peak indicates that lower BE side peak is due to the oxygen from the lattice whereas higher BE side peak can be attributed to adsorbed

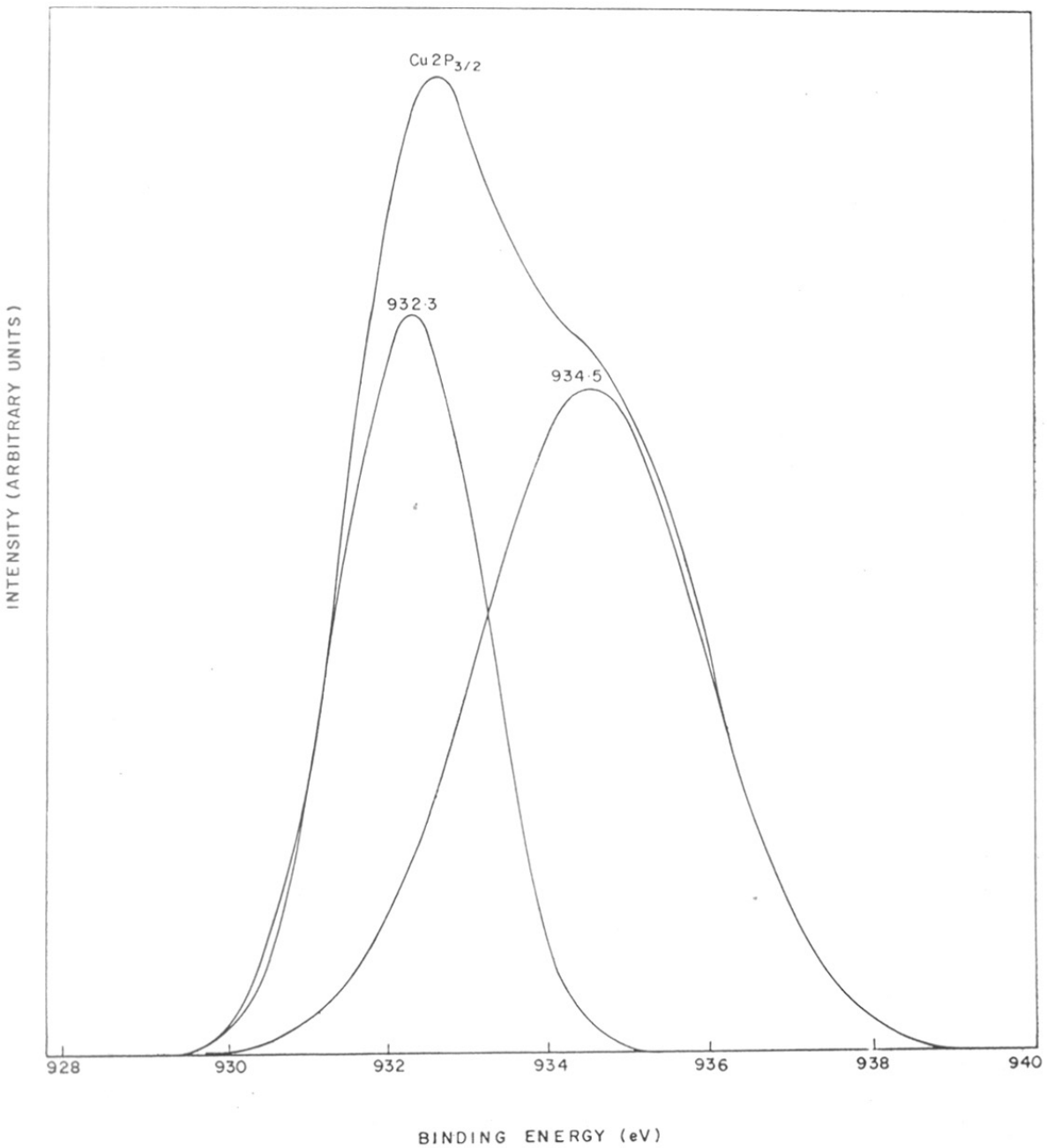

FIG. 3·12. XPS OF SELECTIVE COPPER BLACK FILM AFTER DECOVULSION.

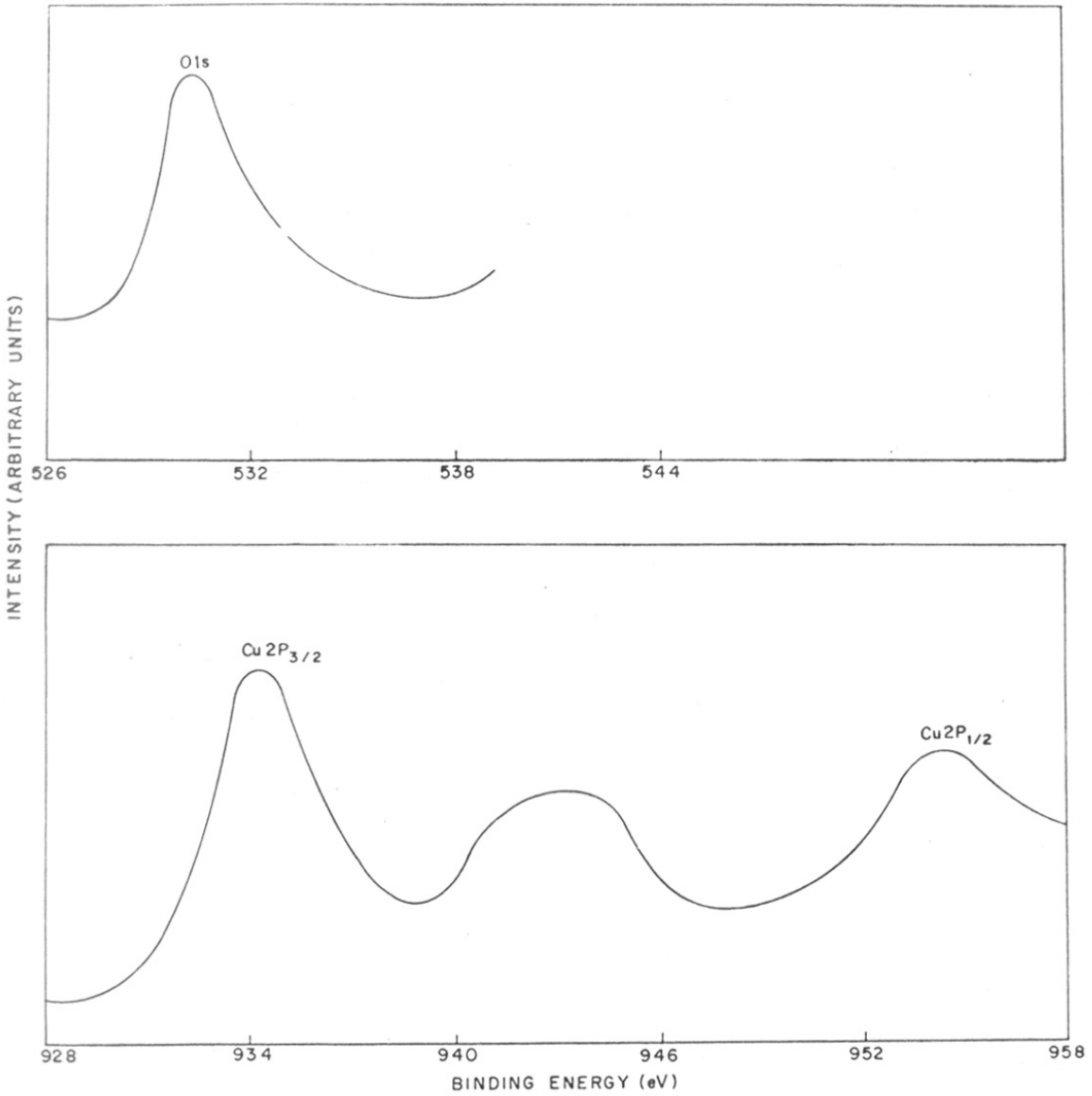

FIG. 3·13 XPS OF NONSELECTIVE THICKER COPPER-BLACK FILM (A_6).

TABLE 3.7

COMPARISON OF XPS DATA OF THE SELECTIVE COPPER-BLACK FILM (A5) AND NON-SELECTIVE COPPER-BLACK FILM(A6)

Sample	$Cu2p_{3/2}$	O1s	Δg	FWHM
Cu_2O (132,128)	932.7	530.6	402.1	1.8
Cu (132,128)	932.2	-	-	1.4
CuO(132)	933.6	529.7	403.9	3.7
Selective copper-black	934.5 932.3	530.8	403.7 401.5	3.4 2.0
Thicker copper-black	933.84	529.8	404.04	3.48

FWHM - full width at half maximum

Δg - splitting between $Cu2p_{3/2}$ and O1s

C 1s - 285 eV

Numbers in brackets denote the references

oxygen species. This observation is also found to be in agreement with the observation by Schon.[132] From the comparison of BE, FWHM, [illegible]g (Table 3.7), it can be concluded that thicker copper-black film (A6) consists of only CuO at the surface. Thus XPS study on selective (A5) and non-selective (A6) copper-black films shows that selective copper-black film consists of cuprous oxide (and/or copper) and cupric oxide, but non-selective (A6) film contains only cupric oxide (CuO) species within the penetration depth of XPS.

3.6 XPS Depth Profiling Study

The XPS depth profiling study on selective copper-black film (A5) was carried out to know the chemical composition or uniformity/gradation of the film along the depth. The sputtering was carried out using Argon ions at 8kV beam voltage and a current density equal to 50 μA. The sputtering rate and etching time (kept equal to 3 minutes) was kept constant during this study.

The XPS spectra i.e. Cu $2P_{3/2}$ and O 1s peak were scanned on 30 eV scale after each etching. They are shown in Figure 3.14.[a&b] The data obtained is presented in Table 3.8.

The sequential effect of Ar ion etching progressively can be summarised as follows:

(i) First etching

(A) Cu $2p_{3/2}$ asymmetric peak changes over to symmetric peak with rise in intensity.

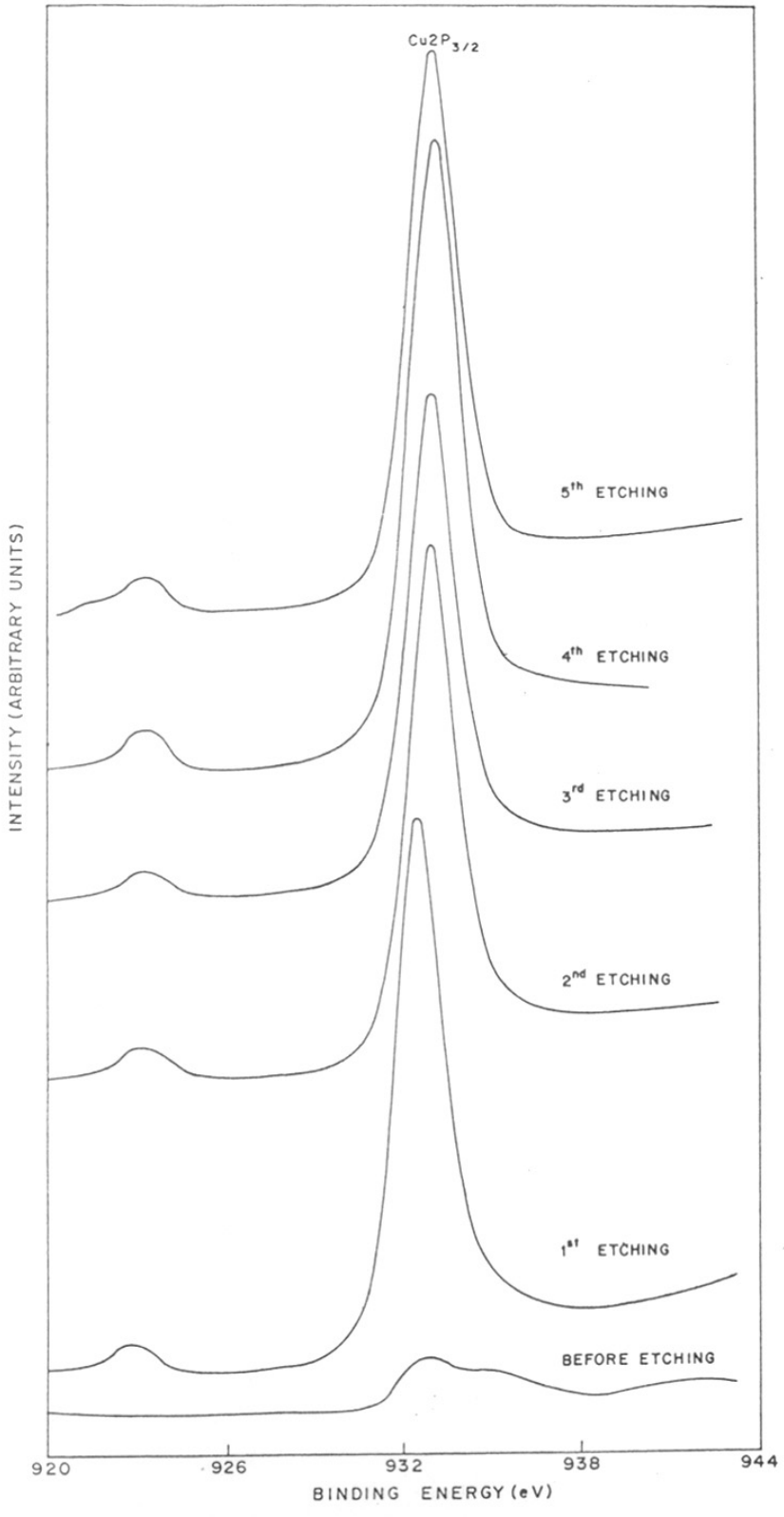

FIG. 3.14. XPS OF SELECTIVE COPPER-BLACK FILM (A_5) FOR COPPER.

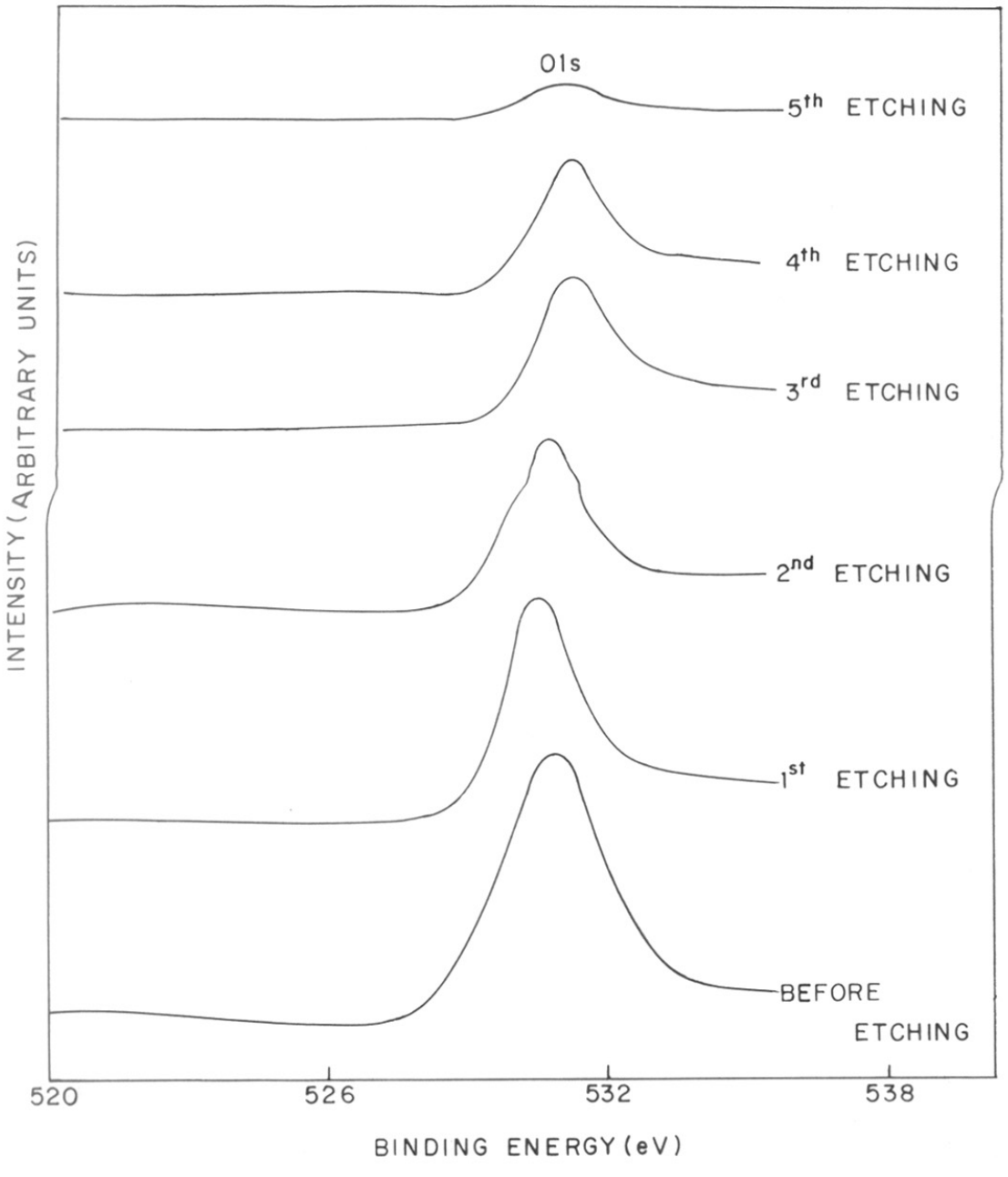

FIG. 3·14 b XPS OF SELECTIVE COPPER–BLACK FILM FOR OXYGEN.

TABLE 3.8

XPS-PROFILING DATA OF SELECTIVE COPPER-BLACK FILM (A5)

	$Cu2p_{3/2}$	01s	Δg	FWHM	Satellite
Unsputtered film	932.6 eV 934.5	530.8	401.8 403.7	2.0 3.4	Around 942 eV
1st etching	932.4	530.4	402.00	1.80	No satellite
2nd etching	932.36	530.4	401.96	1.68	"
3rd etching	932.36	530.92	401.44	1.80	"
4th etching	932.84	530.9	401.94	1.80	"
5th etching	932.96	530.8	402.16	1.68	"

FWHM - full width at half maximum

Δg - splitting between $Cu2p_{3/2}$ and 01s

(Reference C 1s - 285 eV)

(B) The intensity of O1s peak goes down.

(ii) Second etching

(A) Cu $2p_{3/2}$ peak remains unaltered

(B) The intensity of O1s peak goes down further.

(iii) Third and fourth etching

(A) Cu $2p_{3/2}$ peak remains unaltered

(B) The intensity of O1s peak goes down still further.

(iv) Fifth etching

(A) Cu $2p_{3/2}$ peak remains unaltered

(B) O1s peak almost vanishes

These observations can be explained if we visualize the processes as under.

It is reasonable to expect that during the etching process the adsorbed species would be lost. Also, the top surface would be removed and there is a likelyhood of the species present at the surface would be chemically reduced.[133] As concluded from our XPS results the film consists of CuO + Cu_2O and/or Cu with probably some oxygen adsorbed at the surface. After etching, as stated above, adsorbed oxygen was found be lost as O1s peak becomes symmetric. The asymmetric Cu $2p_{3/2}$ peak becomes symmetric possibly due to reduction of CuO by argon ions.[133] Since only one etching step was enough to remove or reduce CuO, it is reasonable to conclude that CuO was present only at the surface. The rise in the Cu $2p_{3/2}$ peak intensity is likely due to etching removal of contaminated carbon from the fresh sample.

Subsequent etchings do not change copper peak intensity. The only change in the observation was a decrease in the intensity of O 1s peak. This can be explained by the possible formation of copper due to reduction by argon ions at the surface which will make less and less oxygen available for XPS. Since we have kept etching rate and time constant during the study, alternatively, if the layers from the top to bottom have continuously varying composition from CuO to distorted Cu_2O, then obviously oxygen intensity would be continuously reduced from top to substrate (compare Tables 3.8 and 3.7).

From the XPS depth profiling study it can be concluded that:

(i) CuO layer is present only as a top layer of the selective (A5) film.

(ii) The layers below CuO possibly may have Cu_2O composition with reducing oxygen upto the substrate.

3.7 Auger-electron Depth Profiling Study

The XPS spectrum readily identifies Cu(II) species but fails to distinguish between Cu(0) and Cu(I). However, Auger chemical shifts are even larger for cuprous than cupric compounds[132b] and therefore readily identify the Cu(I) and Cu(0) species. Auger depth profiling study on A5 film was therefore carried out to know the variation of Cu^{+2} and Cu^{+1} species along the thickness. The sputtering

was carried out using the Argon gun at 8kV beam voltage and 50 μm current density. Sputtering rate and time (3 min) were kept constant during the study. $CuL_3M_{45}M_{45}$ on KE scale & O1s peak on Binding Energy Scale were recorded on 30 eV full scale scan after each etching.

Auger electron spectroscopy is usually carried out with an electron beam as exciting source where penetration depth is of the order of 5-10 A°. But Auger electrons are also created under x-ray radiation where contribution to the AES signal would be from the depth of 30-40 A° which is the penetration depth for XPS. A $L_3M_{45}M_{45}$ Auger electron is created when a vacancy in the $2p_{3/2}$ level is filled by a 3d electron with simultaneous ejection of another 3d electron.

The $L_3M_{45}M_{45}$ Auger spectrum from the A5 sample is shown in Figure 3.15. The figure shows that $L_3M_{45}M_{45}$ Auger peak is broad and asymmetric. It is resolved into two peaks with maxima at 916.2 eV and 918.2 eV. The peak at 916.2 eV is assigned to Cu_2O and peak at 918.2 eV is attributed to CuO on the basis of the literature data. The peak at 530.8eV is attributed to O1s from the oxide lattice. Thus Auger study from XPS indicates that the as prepared layer consists of cuprous oxide and cupric oxide.

After each etching with argon ions the $CuL_3M_{45}M_{45}$ peak was recorded on 10 eV full scale kinetic energy and O1s peak on BE scale was recorded on 30 eV full BE scale. The results are shown in Figure 3.16. We note three

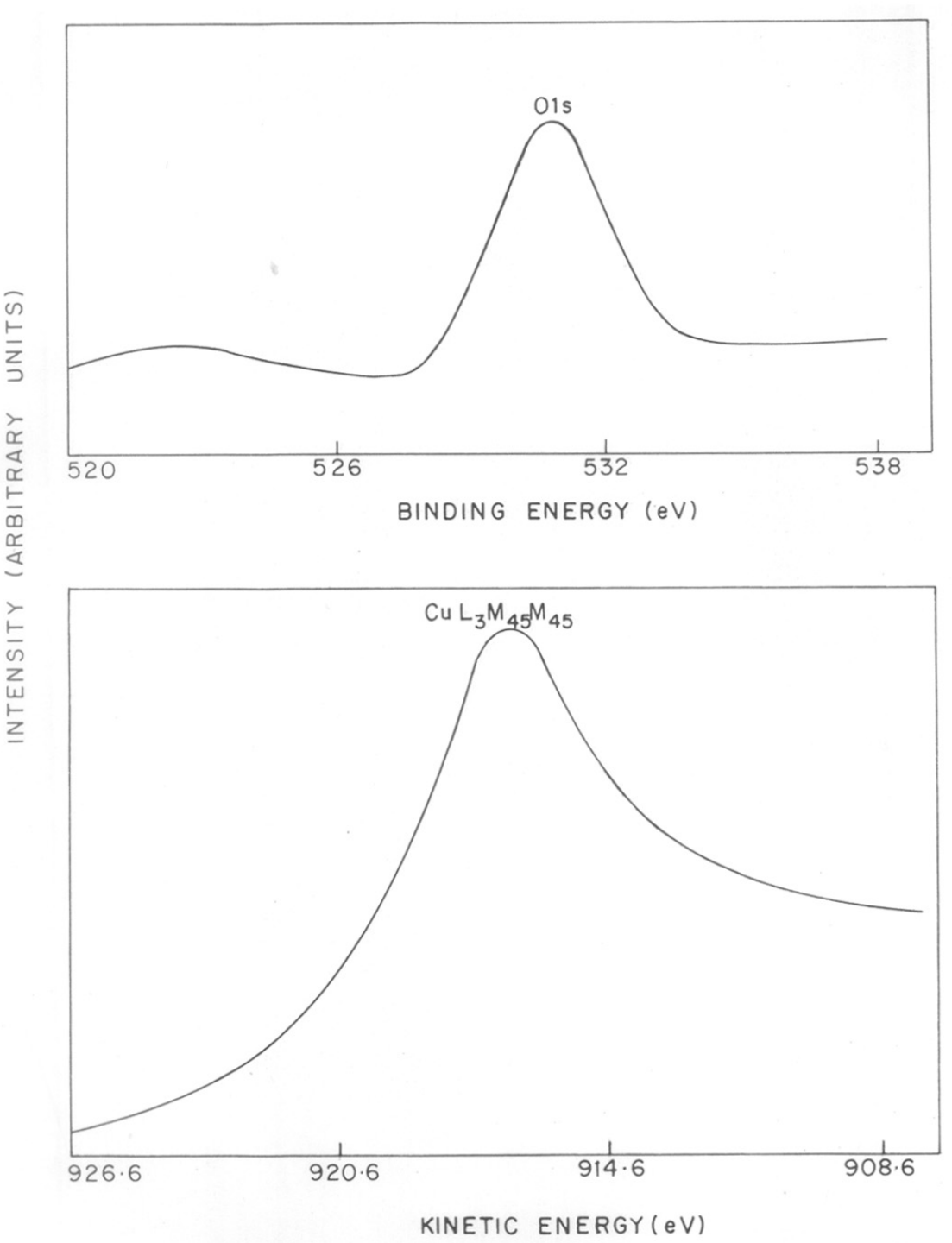

FIG 3·15 AUGER SPECTRUM OF SELECTIVE COPPER BLACK FILM (A_5).

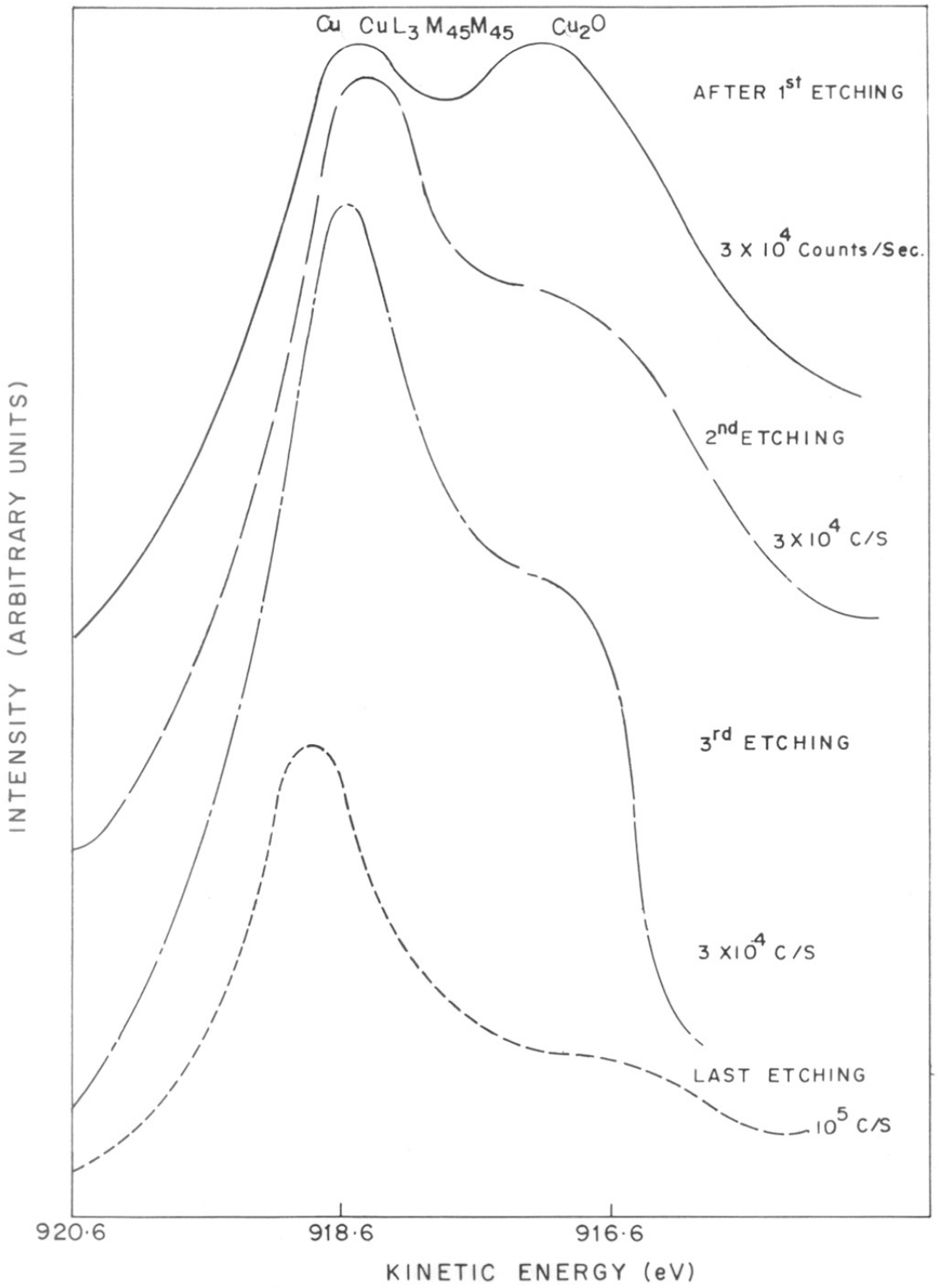

FIG. 3·16 AUGER SPECTRUM FOR COPPER-BLACK FILM (A_5)

observations:

(i) 'Cu' intensity increases with number of etching [$L_3M_{45}M_{45}$ for Cu(0) = 919 eV]

(ii) Intensity of Cu_2O peak decreases from top to bottom

(iii) Intensity of O 1s peak decreases with successive etchings. [See Fig. 3.14b]

The Auger electron is excited by x-rays having a penetration depth of 30-40 A^o but the XAES spectrum would not indicate the quantitative presence of the species as shown by their respective intensities in the spectrum, since the sensitivities for the species vary along the depth. Therefore, single spectrum does not give additional information to what has been obtained by XPS profiling. However, as mentioned above the observations after successive etchings give the idea about the gradation of concentration of various species along the depth. Here we would like to indicate that the presence of Cu in AES after etching might be due to reduction of oxide by Argon ions[133], since the as prepared XAES does not show 'Cu' presence.

The observations given in Figure 3.16 can be explained as follows. During the 'Ar' ion etching,[133] Cu_2O or CuO is reduced to Cu and some oxygen is lost. If this is true, then successive etchings show the presence of more 'Cu' (indicated by higher intensity) as we see from top to bottom indicating that more and more species reducible to Cu are available along the depth for successive etchings. This is possible if Cu_2O is non-stoichiometric

(oxygen deficient) along the depth, so that more Cu is formed. Since 'Cu' formation is at the cost of Cu_2O, obviously Cu_2O intensity would be lower for successive etchings and also since oxygen concentration in the form of Cu_2O also reduces along the depth, oxygen intensity would go down.

The explanation above is supported by the observations reported in the literature regarding the mechanism of film deposition by this method, that initially lower oxidation species of Cu are formed on the substrate and as the film thickness increases higher and higher oxidation states of Cu are observed. The species from the substrate to the top in thick film formed are reported to be in the order of $Cu\text{-}Cu_2O\text{-}CuO\text{-}Cu_2O_3$.[134-138]

This explanation is consistent with an observation of AES depth profiling which is explained later.

3.8 AES Depth Profiling Study

Auger electron spectroscopic study on selective copper-black film (A5) was carried out using electron beam as the source, where penetration depth is of the order of 5-10A°. Figure 3.17 shows the AES spectrum for A5 film on 1100-200 eV kinetic energy scale. It indicates the presence of copper and oxygen at the surface along with some contamination of carbon. The intense peak of copper $L_3M_{45}M_{45}$ and oxygen $OKL_{23}L_{23}$ was chosen for the depth profile study and peak to peak height was recorded as a function of etching time.

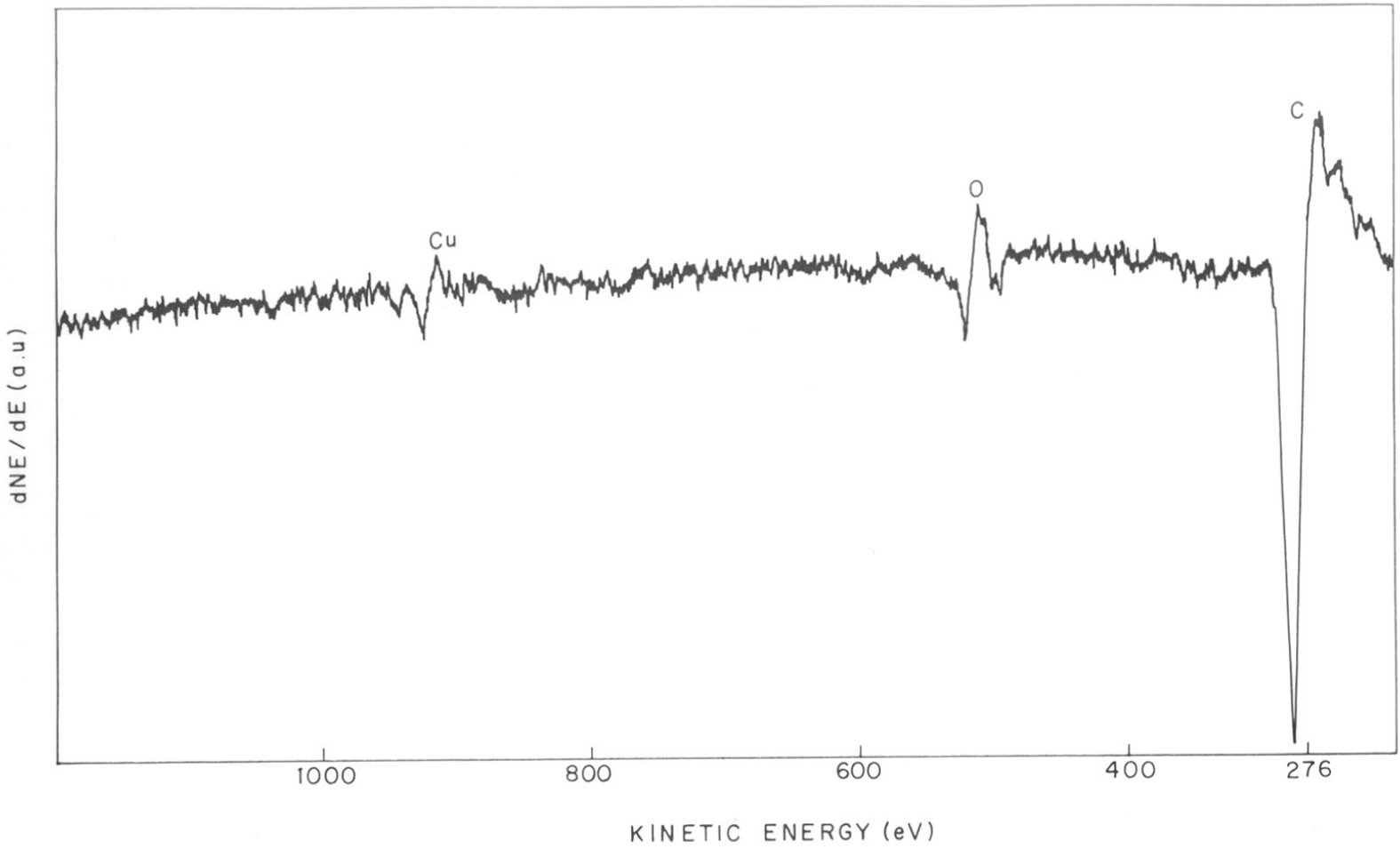

FIG. 3·17 AES OF THE SELECTIVE COPPER–BLACK FILM (A_5)

The depth profile i.e. peak to peak height of copper and oxygen as a function of etching time was carried out using differentially pumped Argon at pressure of 10^{-5} mm at 9kV beam voltage and 30 μA current density. The depth profile obtained is shown in Figure 3.18. The profile study revealed more oxygen per copper atom at the surface. The copper to oxygen ratio varies from 1.35 to 0.40. It can also be noted that near the interface copper and oxygen signals do not increase sharply. This observation suggests that at the interfacial region between oxide layer and copper substrate, the film contains more copper. This observation along with those from XPS, XAES studies suggest that copper-black film (A5) is composed of upper cupric oxide (CuO) layer and layers of non-stoichiometric cuprous oxide (Cu_2O) below down to substrate.

3.9 Discussion

From the different characterization studies on selective copper-black film, the following model is proposed for the film, which explains the observed optical and structural properties. The model consists of a polished copper substrate, which provides the necessary high IR reflectance (Figure 3.19).

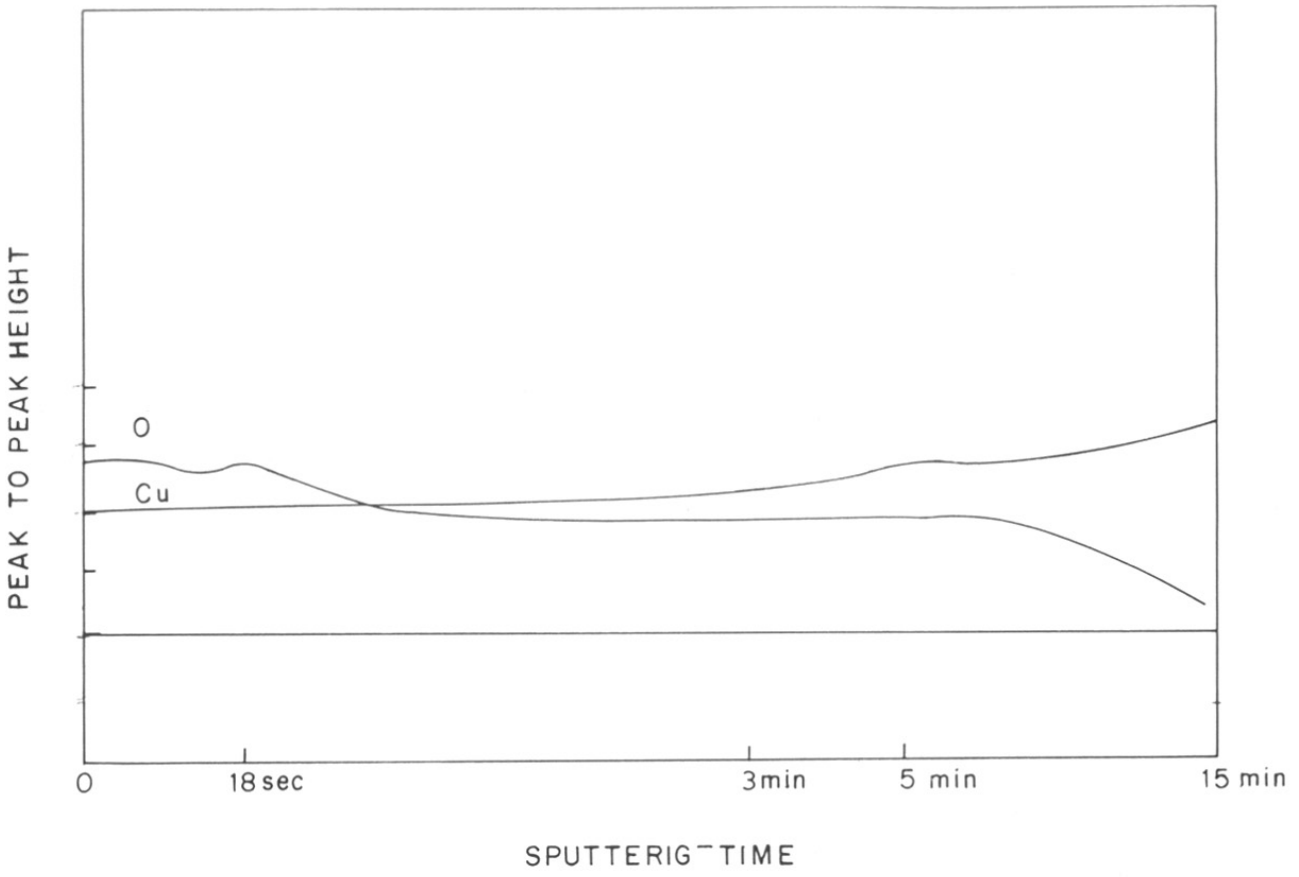

FIG. 3·18 AES DEPTH-PROFILE OF SELECTIVE COPPER-BLACK FILM (A_5).

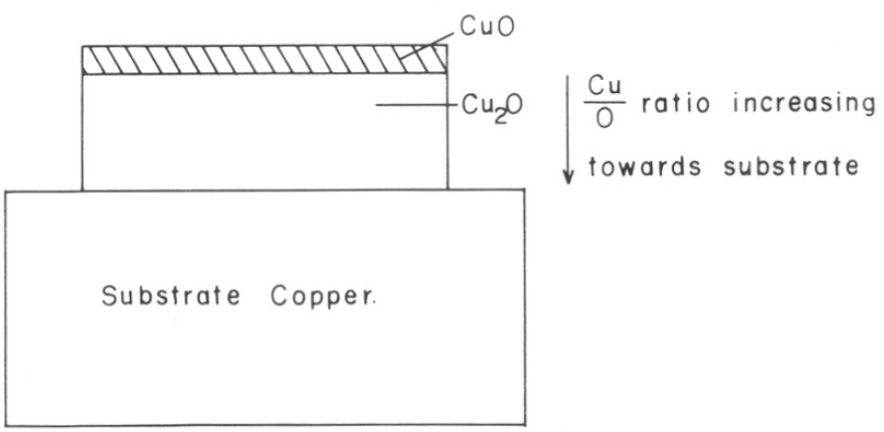

FIG. 3·19 PROPOSED MODEL FOR SELECTIVE COPPER-BLACK FILM (A_5)

The film composed of cupric oxide (CuO) and cuprous oxide (Cu_2O) with sufficient thickness lie on this substrate. The film has always cupric oxide (CuO) layer at the top and subsequent layers of cuprous oxide (Cu_2O) with $\frac{Cu}{O}$ ratio increasing towards the substrate. This layered structure with sufficient thickness would absorb all incident photons of energy greater than 1.5 eV or 2.17 eV. [Band gaps (E_g) of CuO = 1.5 eV and Cu_2O = 2.17 eV].[121] The mechanism of absorption will be, that the photons of energy greater than the band gap would be absorbed in exciting electron from valence band to conduction band whereas for photons with energy less than Eg, the above film would be transparent. High reflectivity in the IR region would be maintained by the substrate copper.

It is reported in the literature[121] that homogeneous layers of either cuprous oxide (Cu_2O) or cupric oxide (CuO) of sufficient thickness do not produce absorptance greater than 0.9, because of the position of $\lambda_{cut\text{-}off}$ and refractive indices[121] [n for Cu_2O = 2.7 and n for CuO = 2.9].

However, the copper-black films prepared by anodic oxidation method show solar absorptance of the order of 0.96 so we propose that high α in our films has resulted due to intrinsic absorption of both Cu_2O and CuO species along with the morphological[139] contribution resulting from geometric effects and the graded structure of the film.

Since the above structure is transparent in the IR

region, the low emittance ($\epsilon \simeq 0.2$) obtained is due to the substrate copper.

Conclusions

1. Solar selective copper-black films are prepared successfully using anodic oxidation technique with $\alpha \simeq 0.98$ and $\epsilon = 0.2$. The $\lambda_{cut\text{-}off}$ lies at 3.5 μm. The films obtained are found to be well adherent to the substrate. The optical and thermal properties of the films are found to be producible. This method can therefore be useful for the large area fabrication of solar selective copper-black films useful for the flat plate collector applications.

2. The absorption in this film is primarily due to semiconducting cupric oxide (Eg $\simeq$ 1.5 eV) and cuprous oxide Cu_2O [Eg $\simeq$ 2.17 eV] along with influences from surface morphology and graded structure. The low thermal emittance (ϵ) = 0.1 is due to the copper substrate.

3. The study reveals that films are crystalline and non-homogeneous and mainly consist of upper layer of cupric oxide (CuO) and lower layer of cuprous oxide (Cu_2O) below the top layer with $\frac{Cu}{O}$ ratio increasing towards the substrate.

4. As the thickness of the film increases, the morphology of the film also changes.

5.* Preliminary study on thermal cycling shows that the films are stable upto 100°C and therefore can be used in flat plate collector applications.

(* This study is not included as a part of the thesis but will be published elsewhere)

CHAPTER – IV

MOLYBDENUM–BLACK

CHAPTER IV

MOLYBDENUM-BLACK

Introduction

For efficient solar energy conversion at operating temperatures greater than 150°C for concentrating type solar collectors, the selective surfaces should not only absorb the incident solar radiation, but also suppress reradiation losses in the thermal-IR region and should also possess thermal stability. The copper-black films reported in the earlier chapter are not stable at temperature greater than 350°C and hence is not suitable material for higher temperature applications.[81b] Thin films of cermet black-chrome[76] composed of Cr and Cr_2O_3 have been tried as selective absorber for high temperature application. However, it is reported that black-chrome also degrades at temperature greater than 300°C.[81a] It is reported that specific forms of black molybdenum (consisting mainly MoO_2) satisfy the obvious need for the high absorptance along with low thermal emittance and stability at temperatures of operation for extended periods of time.[154,156]

Molybdenum films with partial selectivity were prepared earlier by the decomposition of $Mo(CO)_6$ or by hydrogen reduction of $MoCl_5$[140-152] Molybdenum-black films (consisting mainly MoO_2) with good selectivity had been prepared by CVD under oxidising conditions followed by post

deposition annealing and passivation by Si_3N_4.[153,154,156] This passivation layer is used as an antireflection coating. The solar absorptance $\alpha \simeq 0.91$ and thermal emittance $\epsilon \simeq 0.11$ were obtained.

No studies have, however been reported on the selective molybdenum-black films prepared by cathodic electro-deposition technique. We report the preparation of solar selective molybdenum-black films by an electrolytic technique in this chapter and results on their characterization using different techniques are also presented.

4.1 Preparation

Nickel plated copper strips size 2 cmx 6 cm were cleaned as described in Chapter II. The cleaned nickel plated copper strips were coated with the molybdenum-black film from a bath[157] containing ammonium molybdate $[(NH_4)_2MoO_4]$, nickel sulphate ($NiSO_4$), boric acid (H_3Bo_3) and copper sulphate ($CuSO_4$) solution using the experimental setup described in Chapter II. The molybdenum-black films were then washed with distilled water several times and dried using IR lamp and then these films were used for the measurements. The bath composition and the deposition conditions used are given below.

(a) Bath composition -

Nickel sulphate ($NiSO_4$)	144 gms/l
Ammonium molybdate $[(NH_4)_2MoO_4]$	30 gms/l
Boric acid (H_3BO_3)	22.5 gms/l
Copper sulphate ($CuSO_4$)	2 gms/l

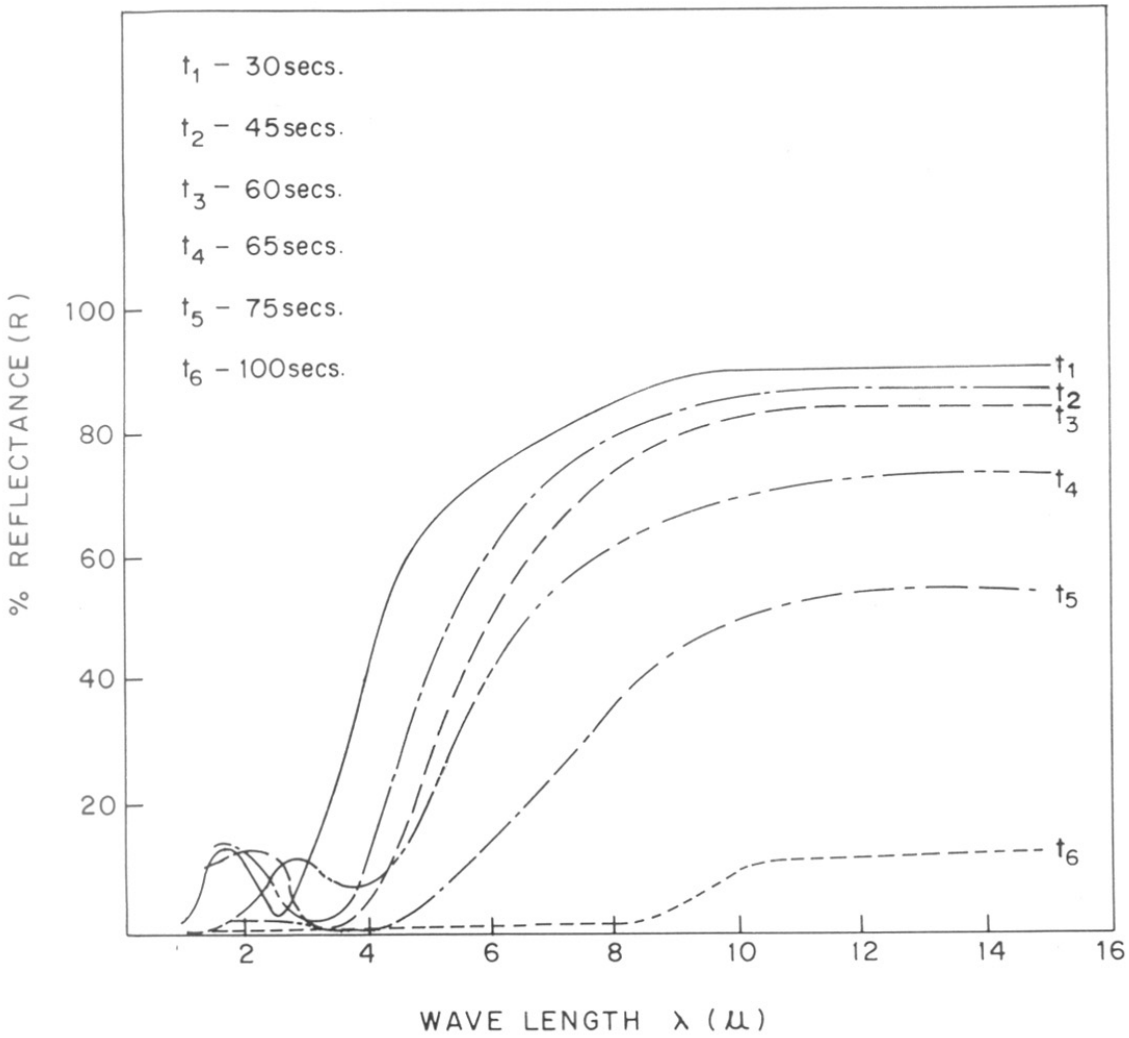

FIG. 4·2 EFFECT OF THE DEPOSITION TIME ON IR REFLECTIVITY OF THE MOLYBDENUM–BLACK FILM.

(b) Deposition conditions -

(i)	Temperature of the bath	35-45°C
(ii)	Current density	4 mA/cm^2
(iii)	Deposition time	50 sec
(iv)	Distance between two electrodes	4.5 cm
	Cathode - 2 cm x 6 cm nickel plated copper strip	
	Anode - 2 cm x 6 cm copper strip with thicker nickel plating	
(v)	Voltage across the two electrodes	2.5-3 Volts

The deposition time was optimized by varying it from 30 sec to 75 sec to get high α over solar spectrum region and low emittance in the thermal IR region.

4.2 Results

The molybdenum-black films obtained by electrolytic technique were found to have good adherence to the substrate as is seen by schotch tape test.

In Figure 4.1, the effect of the deposition time on the total reflectance of the molybdenum-black film in the region 0.38-0.76 μm is presented. It is seen from Figure 4.1, that the total reflectance goes down as the time of deposition is increased, indicating increase in the absorptance in 0.38-0.76 μm.

The effect of deposition time on the normal spectral reflectance of the film in the region 1 μm to 15 μm is shown in Figure 4.2. It is seen from the Figure 4.2 that, as the

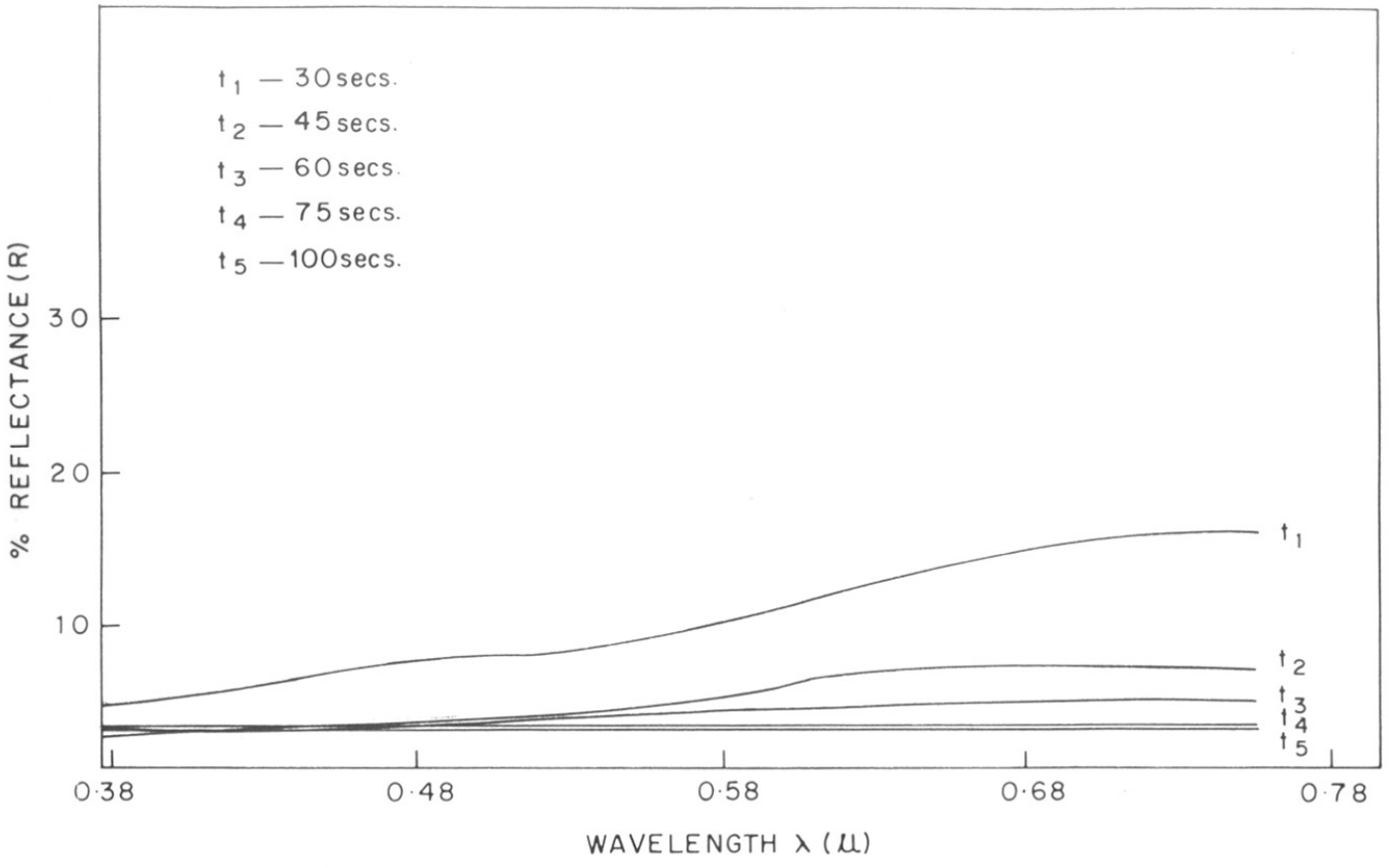

FIG. 4·1 EFFECT OF DEPOSITION TIME ON THE TOTAL REFLECTANCE OF THE MOLYBDENUM–BLACK FILM.

deposition time is increased, the normal spectral reflectance of the film decreases, indicating increase in the emittance.

It is found that the time of deposition to get high absorptance (α) in the visible and low thermal emittance (ϵ) in IR is critical. It is observed that if the time of deposition is kept less than the critical time (t = 60 sec), then although IR reflectance increase, the solar absorptance is considerably less. If the deposition time is more than the critical time, the solar absorptance increases slightly but IR reflectance decreases considerably, thus increasing the emittance. For example, the film deposited at t = 75 sec has $\alpha \simeq 0.91$ but the emittance (ϵ) also increases to 0.55. This is expected, because as the time of deposition increases, thickness as well as mass per unit area of the film increases affecting the transparency of the film in the IR region. It is observed, that as deposition time increases, the $\lambda_{cut\ off}$ was found to shift towards the higher wavelength side.

Figure 4.3 gives the normal spectral reflectance as a function of wavelength for the molybdenum-black film deposited at 40°C and at optimized deposition time t=60 sec. The graph shows near-ideal selective property as described in Chapter I with λ_{cutoff} at 3.5 μm. The total absorptance (α) over solar spectrum region for AM2 condition[127] and total thermal emittance (ϵ) at 100°C were calculated by graphical method[46] as described earlier. The room temperature emittance of the film as measured by emissometer was

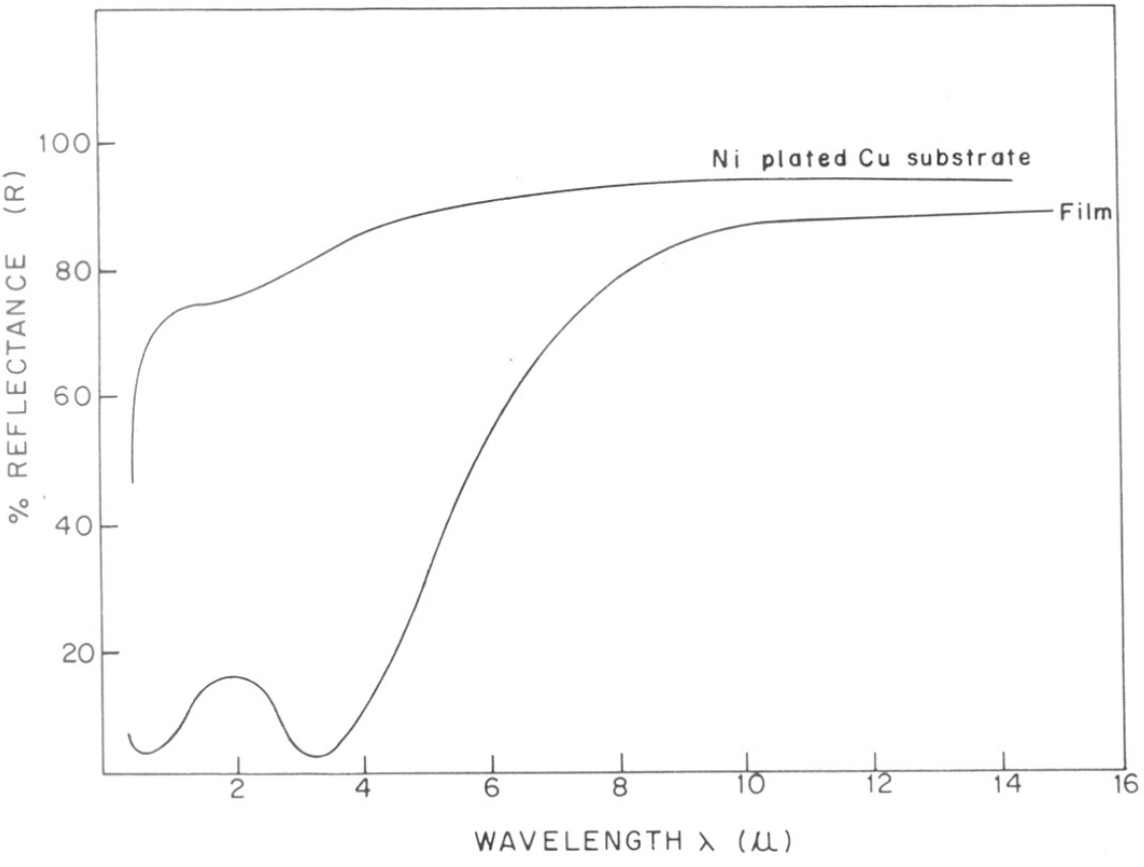

FIG. 4·3 REFLECTANCE (R) AS A FUNCTION OF WAVE LENGTH OF THE SELECTIVE MOLYBDENUM-BLACK FILM & Ni PLATED Cu SUBSTRATE.

0.11. The total absorptance over solar spectrum region as obtained by Alphatometer was 0.86. The values of α and ϵ thus obtained are presented in Table 4.2. The values of reflectance in the wavelength region 0.4-0.7 μ as measured by spectrophotometer[118] fabricated in our laboratory on the molybdenum-black film and nickel plated copper substrates are tabulated in Table 4.1 for comparison.

The values of α and ϵ of the film obtained by the electrodeposition technique are comparable with reported values for the films prepared by CVD and chemical conversion technique.[70,112,113] It may be noted that α/ϵ ratio is 7.7 for the molybdenum black film at room temperature but α/ϵ ratio changes to 2.6 at 100°C.

4.3 Electron diffraction and x-ray diffraction studies

To characterize the structure of the film, the chemical composition and phases present, the electron diffraction and x-ray diffraction studies on the selective molybdenum-black film were carried out. These studies revealed that the films were non-crystalline in nature. Therefore, it was not possible to know the phases present as well as the chemical composition of the film.

Figures 4.4a, and b give the diffractogram of the selective molybdenum-black film on nickel plated copper and stainless steel substrate. It shows peaks corresponding to substrate . Figure 4.5 gives the diffractogram of the selective molybdenum-black film on stainless steel heated in

TABLE 4.1

% REFLECTANCE OF THE MOLYBDENUM-BLACK FILM AND NICKEL-PLATED Cu SUBSTRATE

λ μm	% reflectance for Mo-Black film	% reflectance for Ni plated Cu
0.40	6.89	46.42
0.45	4.02	49.31
0.50	4.10	57.74
0.55	3.47	59.85
0.60	8.57	60.00
0.65	18.69	68.23
0.70	15.21	66.44
0.75	9.25	73.68

TABLE 4.2

α & ϵ VALUES OF THE MOLYBDENUM-BLACK FILM ON NICKEL PLATED COPPER SUBSTRATE

Temperature ^{o}K	α	ϵ	α/ϵ
300	0.85	0.11	7.7
373	0.85	0.32	2.6

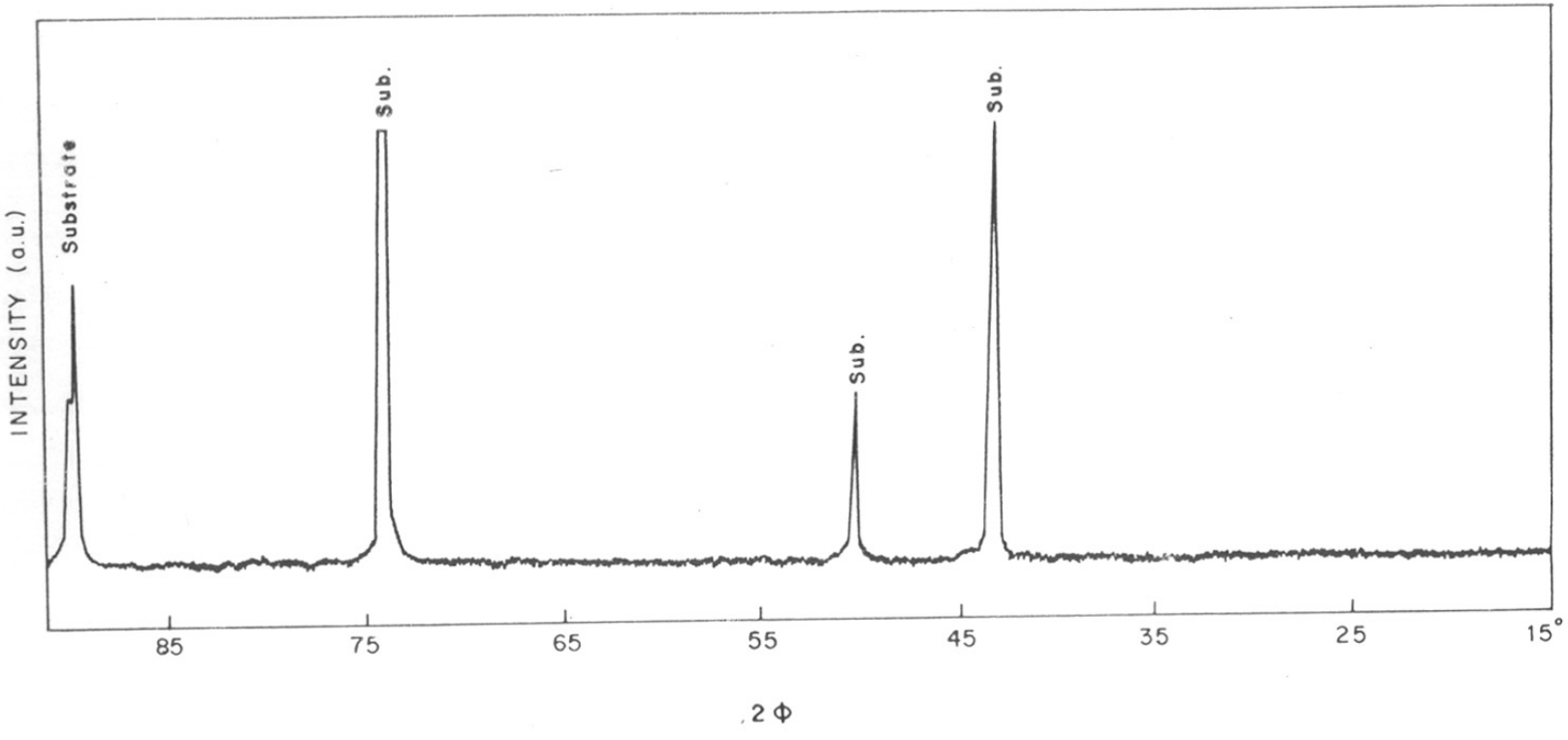

FIG. 4·4 a X-RAY DIFFRACTOGRAM OF SELECTIVE MOLYBDENUM-BLACK FILM ON NICKEL PLATED COPPER SUBSTRATE.

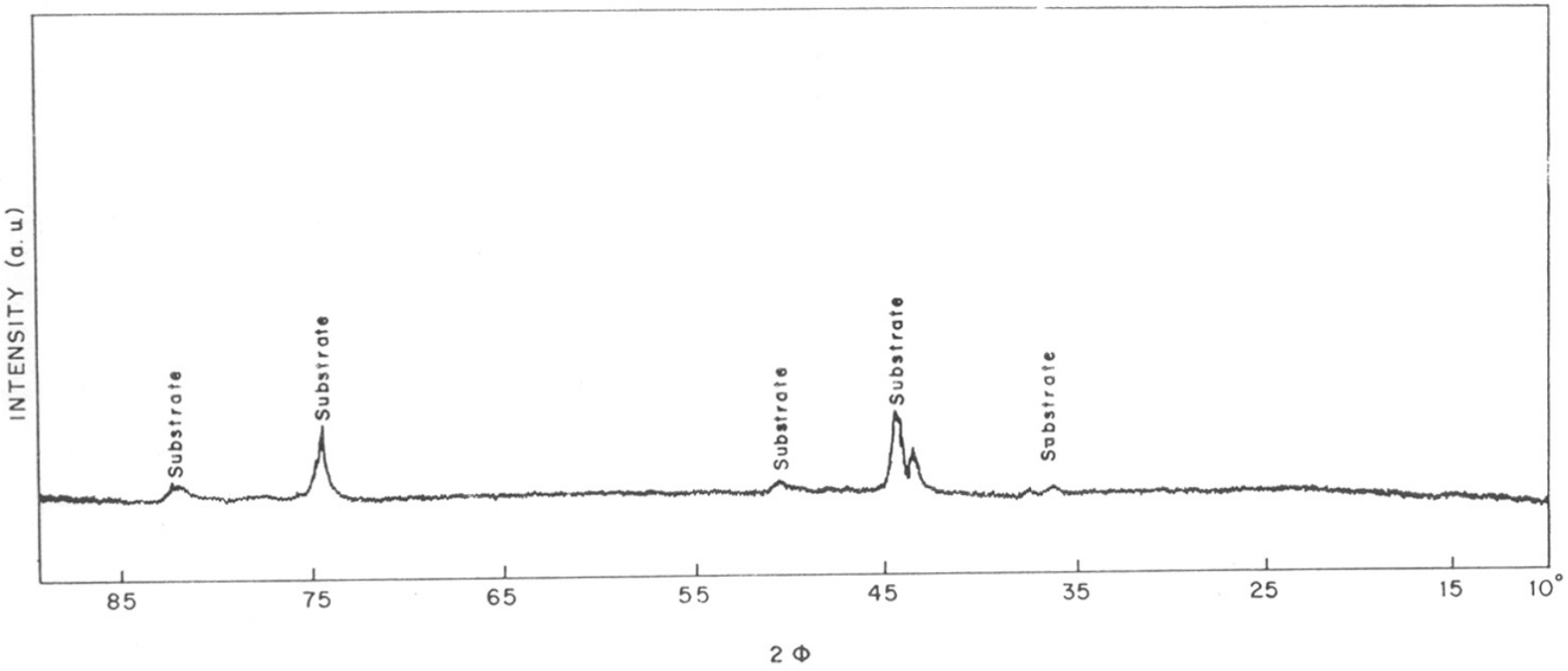

FIG. 4·4b X-RAY DIFFRACTOGRAM OF SELECTIVE MOLYBDENUM BLACK FILM ON STAIN-LESS STEEL SUBSTRATE.

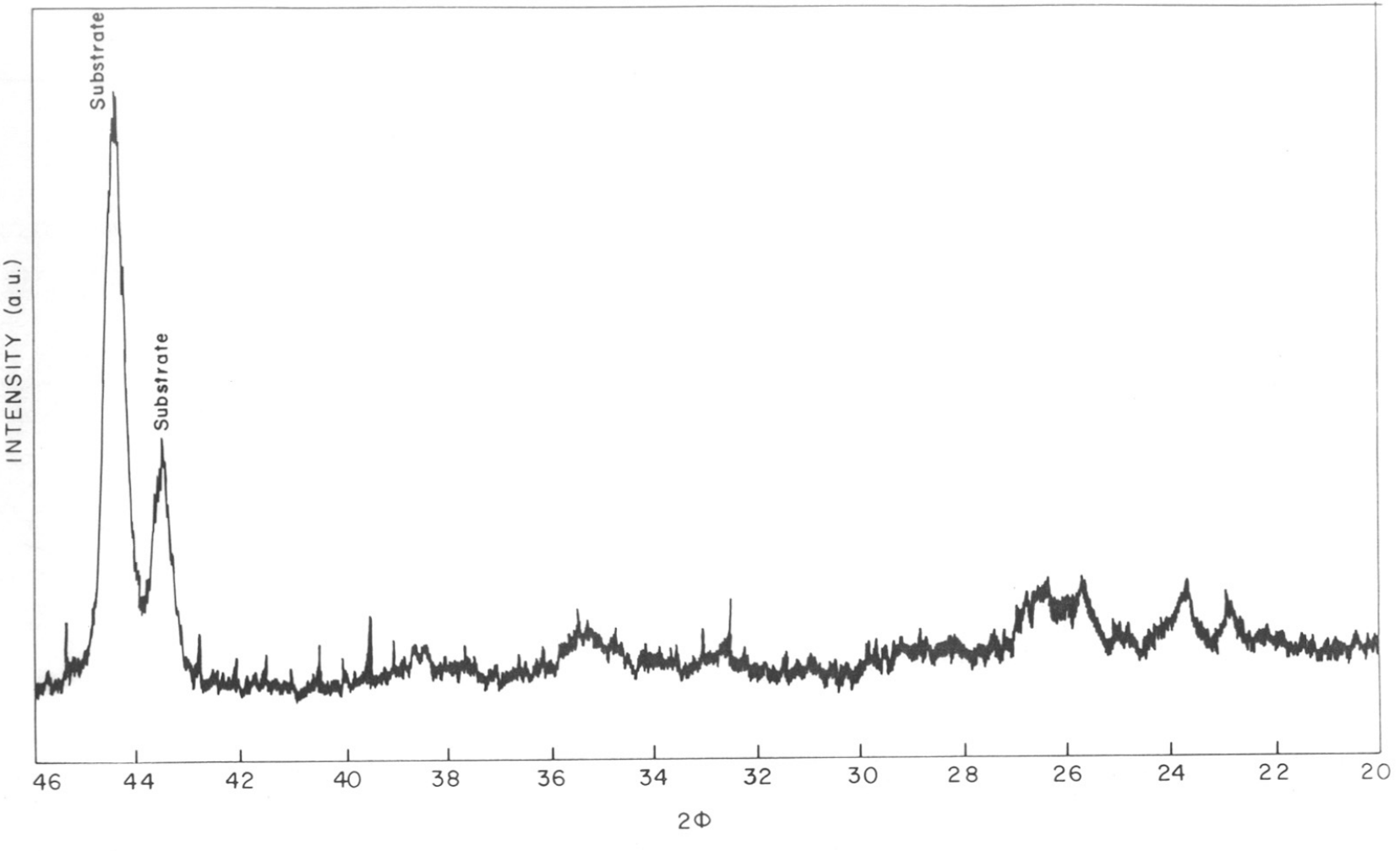

FIG. 4·5 X-RAY DIFFRACTOGRAM OF SELECTIVE MOLYBDENUM-BLACK FILM HEATED AT 350°C FOR 7 HRS.

air at 350°C for 7 hrs. It shows broad peaks along with sharp peaks characteristic of the stainless steel substrate. The 'd' values obtained are tabulated in Table 4.3. From the comparison with standard 'd' values from ASTM cards for Mo oxides, the calculated 'd' values match with Mo_4O_{11} oxide.

4.4 Elemental Analysis by EDAX Technique

Elemental analysis of the selective molybdenum-black film was carried out by using EDAX technique. The thickness of the film was such that there was a considerable contribution from the substrate. It was therefore necessary to deposit these films on various substrates under identical conditions to delineate the substrate counts from those of the film.

Since these films on different substrates were deposited under exactly identical conditions, it is reasonable to expect that these films would have the same chemical composition. Furthermore, their optical properties are found to be more or less similar, which gives an additional support to our conclusion that these films have the same chemical composition on different substrates.

Figures 4.3, 4.6a and b show the reflectance as a function of wavelength for the molybdenum-black film deposited on nickel plated copper, stainless steel and copper substrates under identical conditions. The spectra were found to be similar.

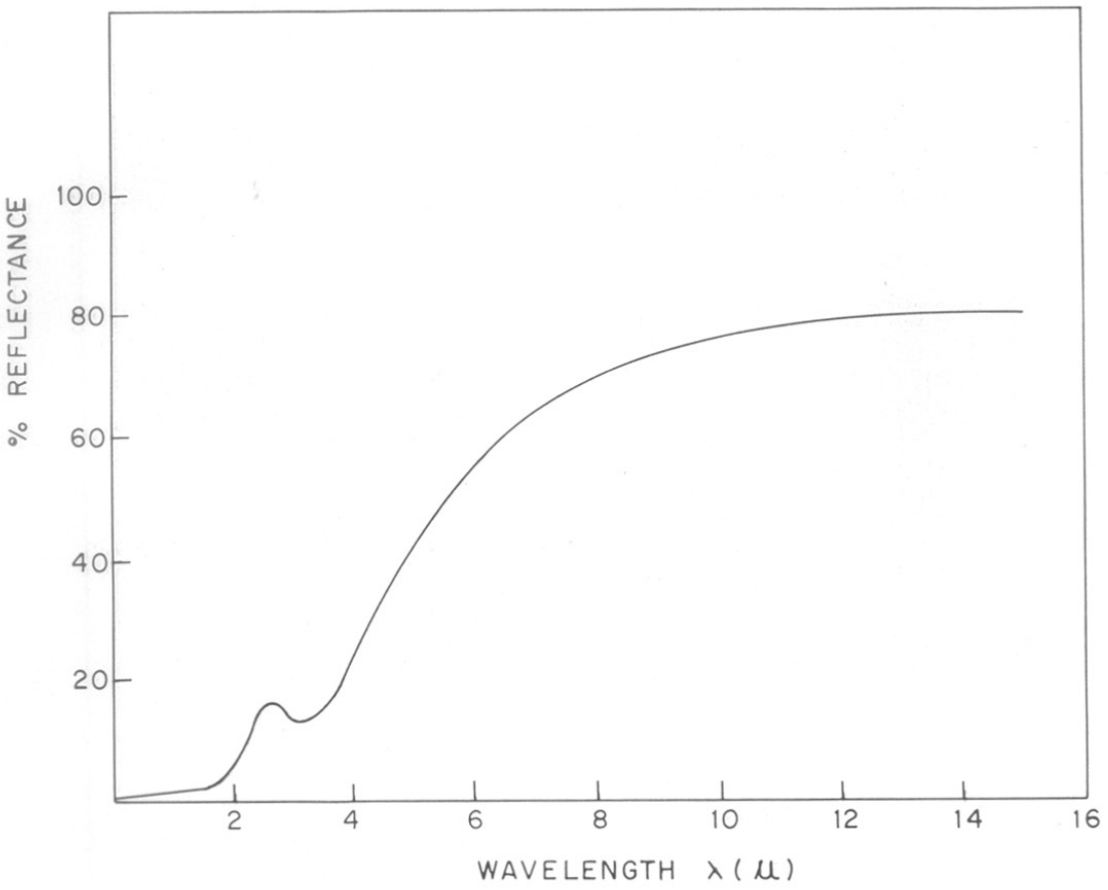

FIG. 4·6a REFLECTANCE OF MOLYBDENUM-BLACK FILM ON STAINLESS STEEL SUBSTRATE

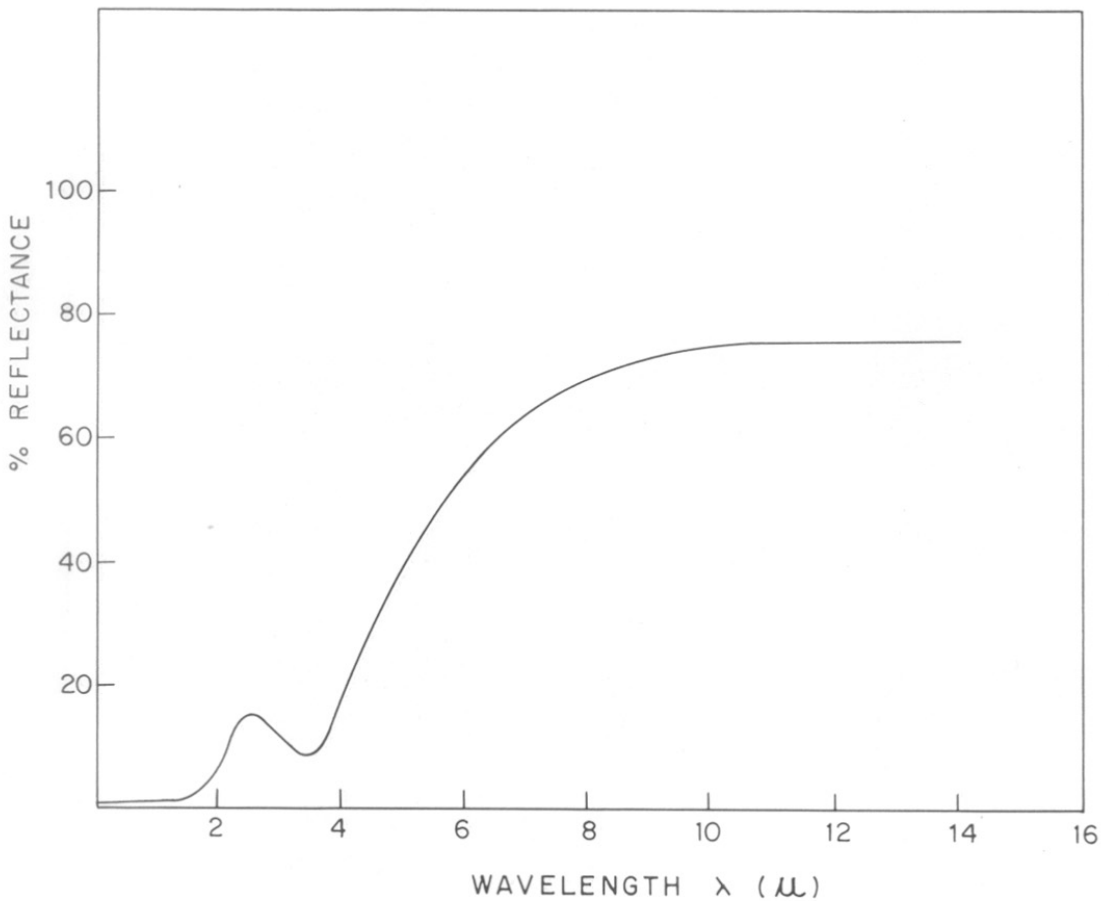

FIG. 4·6 b REFLECTANCE OF MOLYBDENUM-BLACK FILM ON COPPER SUBSTRATE

TABLE 4.3

'd' VALUES OF THE SELECTIVE Mo-BLACK FILM HEATED AT 350°C

'd' calculated A°	Intensity observed
3.95	MS
3.75	s
3.48	s
2.79	w
2.72	w
2.67	w

MS = medium
s = strong
w = weak

The EDAX counts from the deposit on nickel plated copper are as follows. (Mo - 25531, Ni - 25481, Cu - 21304). In this large part of the nickel and copper counts are due to the substrate.

However, the selective molybdenum-black film deposited on the copper substrate also give the nickel signal in addition to that of molybdenum and copper. This observation indicates the presence of small amount of nickel in the film along with large amount of molybdenum. The counts obtained were as under. (Mo - 24675, Ni - 610, Cu - 75065).

The EDAX counts on the film deposited on stainless steel substrates were also measured. Here copper signal was seen in addition to that of molybdenum and nickel, indicating the presence of copper in the film. The counts obtained on the film deposited on stainless steel substrate are as follows. (Cr - 14834, Fe - 43200, Ni - 3536, Mo - 28629, Cu - 2221).

The EDAX count analysis on the films of molybdenum-black on different substrates indicated the presence of molybdenum, nickel and copper in the film. Relative comparison of counts in EDAX analysis shows that the film contains large amount of molybdenum as compared to the copper or nickel in the film.

4.5 Surface Morphology Study by SEM

As discussed earlier, the optical and thermal properties are dependent on the morphology[126] of the film. Changes

taking place in the morphology of the surface of the selective molybdenum-black film deposited at t = 60 sec and thicker molybdenum-black film deposited at f = 100 were therefore studied by SEM.

The typical surface morphology of the selective molybdenum-black film is shown in Figure 4.7, which indicates a uniform distribution of particles ranging from 0.1-0.5 μm in size with only a few clusters and voids. The morphology of this film was found to be similar with the reported morphology for the selective chromium-black film.[7] The morphology of the thicker film was also observed for comparison and is shown in Figure 4.8, which indicates a distribution of the bigger particles (size > 1μm) as compared to the particles in the selective film, with more clustering.

It can be seen from SEM studies that as the thickness of the film increases, the morphology of the film also gets affected, modifying mainly the transparancy of the film in the IR region as is seen by reflectance measurements, causing an increase in the emittance.

4.6 Chemical Composition by XPS and AES

XPS study on these films was carried out to get information about the oxidation state of molybdenum, copper and nickel, the presence of which was seen by the EDAX technique. XPS spectrum of pure MoO_3 powder was also recorded for comparison.

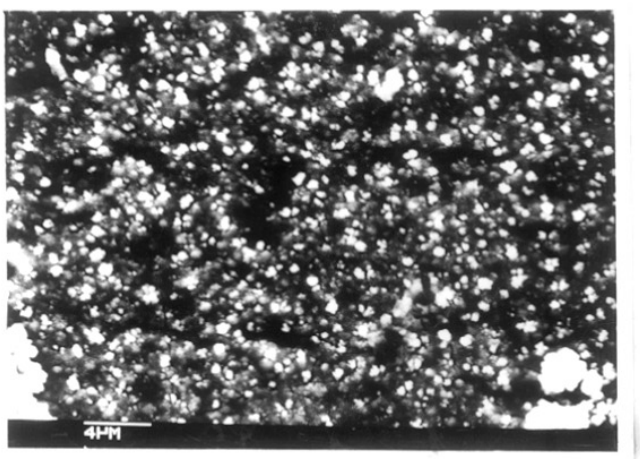

Figure 4. 7 : Scanning electron micrograph of selective molybdenum-black film

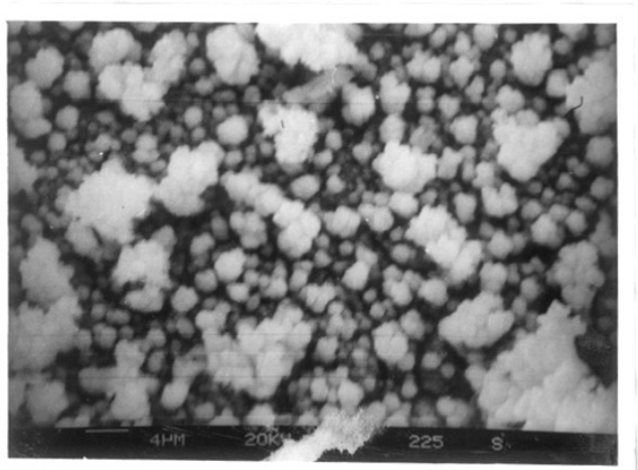

Figure 4.8 : Scanning electron micrograph of thicker molybdenum-black film

The XPS spectrum for selective molybdenum-black film is shown in Figure 4.9 which shows a scan on 0 - 1000 eV scale. It indicated the presence of molybdenum, copper, nickel, oxygen and contaminated carbon. This observation is in agreement with EDAX count analysis result. The XPS spectrum for each constituent of the film was recorded on 30 eV full scale scan to know the exact binding energy (BE), while other spectrameter parameters were kept constant during this work.

Figure 4.10a gives the XPS spectrum of the selective molybdenum-black film on the nickel plated copper substrate for Mo region. The first peak at 232.2 eV corresponds to $Mo_3d_{5/2}$ and second peak at 235.2 eV is attributed to $Mo3d_{3/2}$. There is a shift of 6.1 eV in BE as compared to the BE of pure Mo ($3d_{5/2}$ - 226.1 eV)[158]. The 3 eV separation between the $3d_{5/2}$ and $3d_{3/2}$ level which is characteristic of Mo compounds is also observed.[158,159] Figure 4.10b also gives the XPS spectrum for the pure MoO_3 powder.

Figures 4.10c,d,e give the XPS spectrum of the selective molybdenum-black film for copper, nickel and oxygen respectively. Figure 4.10c shows peak at 932.8 eV, which is due to $Cu2p_{3/2}$ and peak at 952.6 eV is due to $Cu2p_{1/2}$.

Figure 4.10d shows the XPS spectrum for the nickel region. The peak at 953.24 eV is attributed to $Ni2p_{3/2}$. The peak at 531.6 eV is attributed to O 1s and is shown in Figure 4.10e.

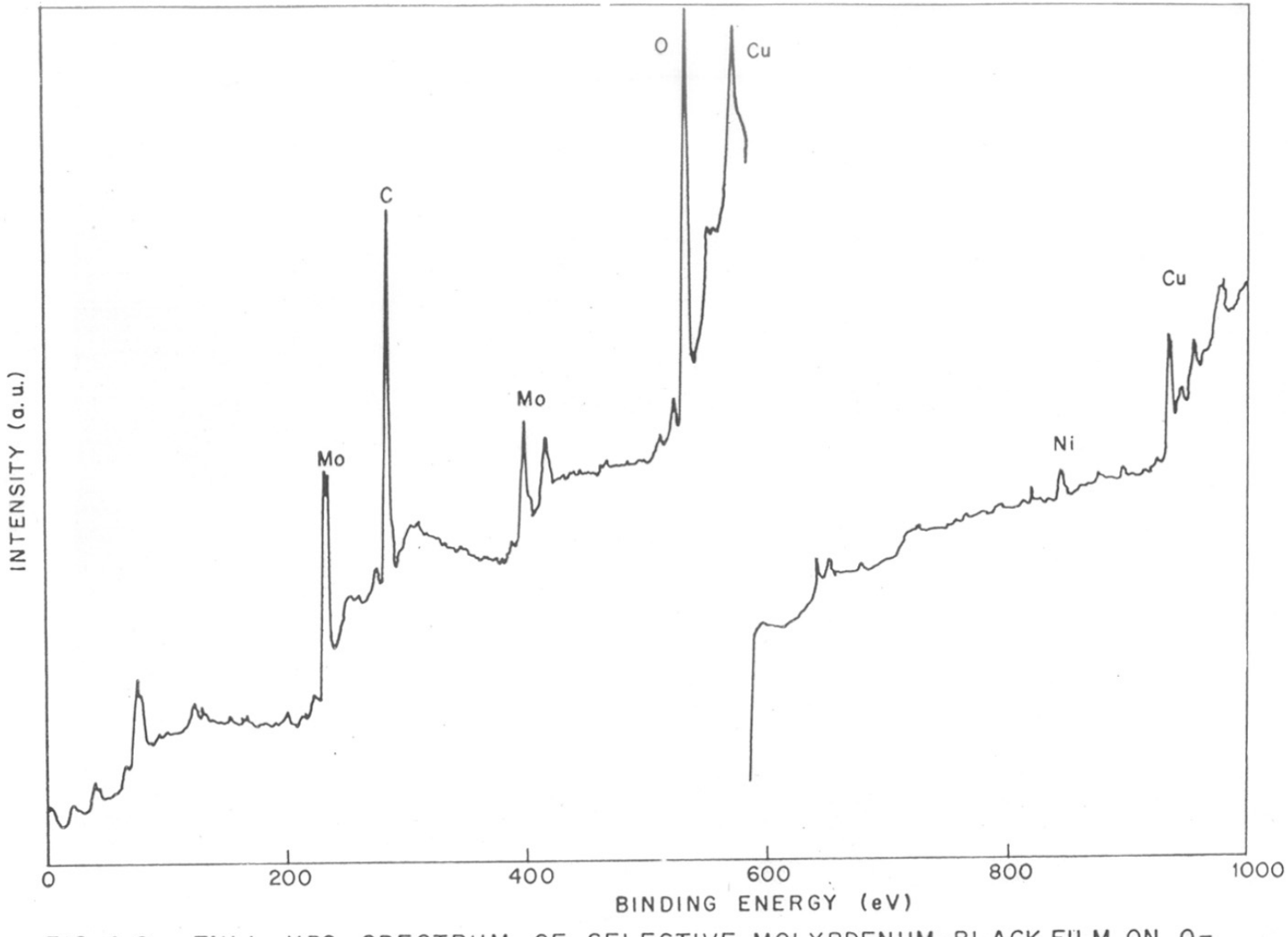

FIG. 4·9. FULL XPS SPECTRUM OF SELECTIVE MOLYBDENUM-BLACK FILM ON 0-1000eV SCALE.

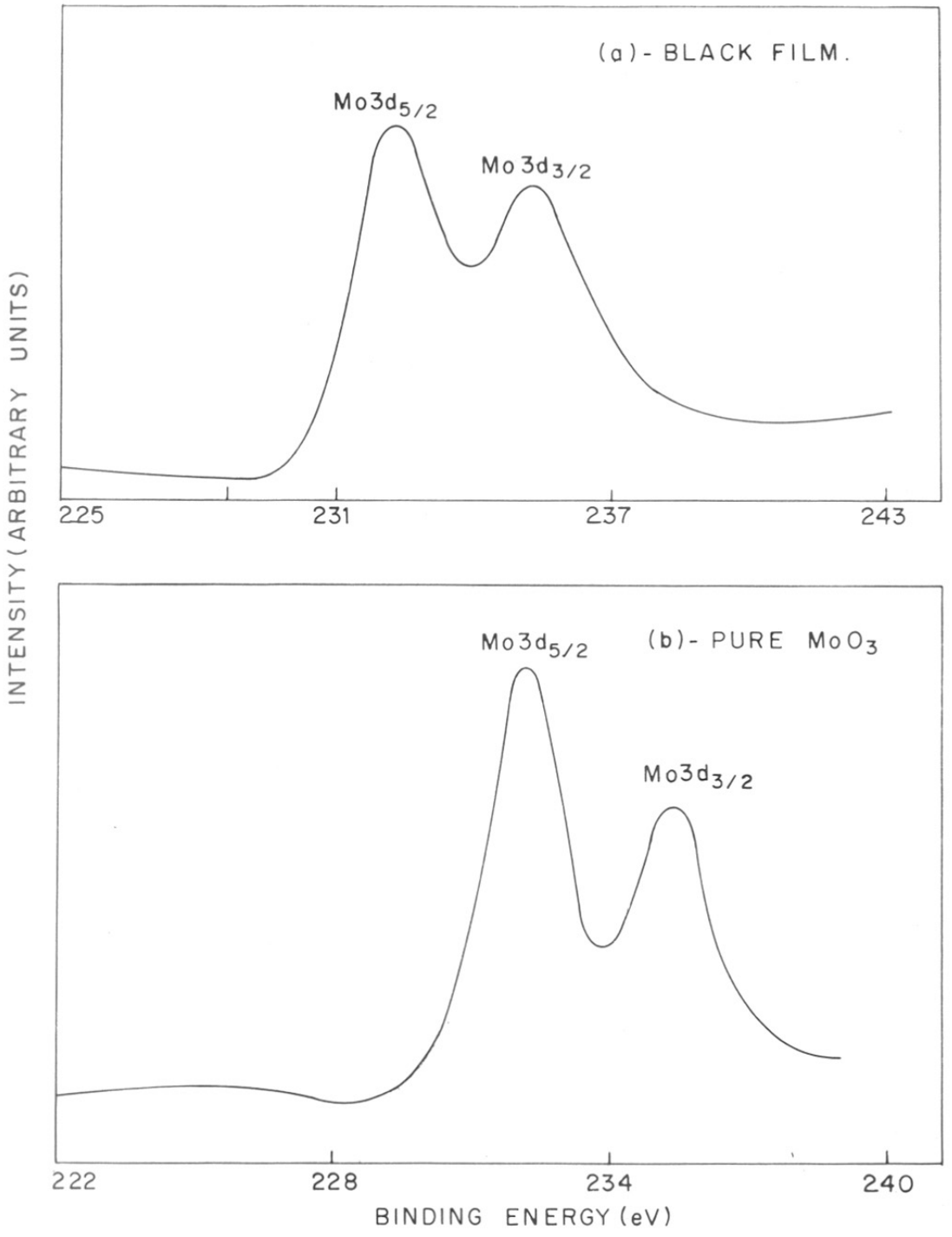

FIG. 4·10 XPS SPECTRUM OF MOLYBDENUM–BLACK FILM & MoO_3

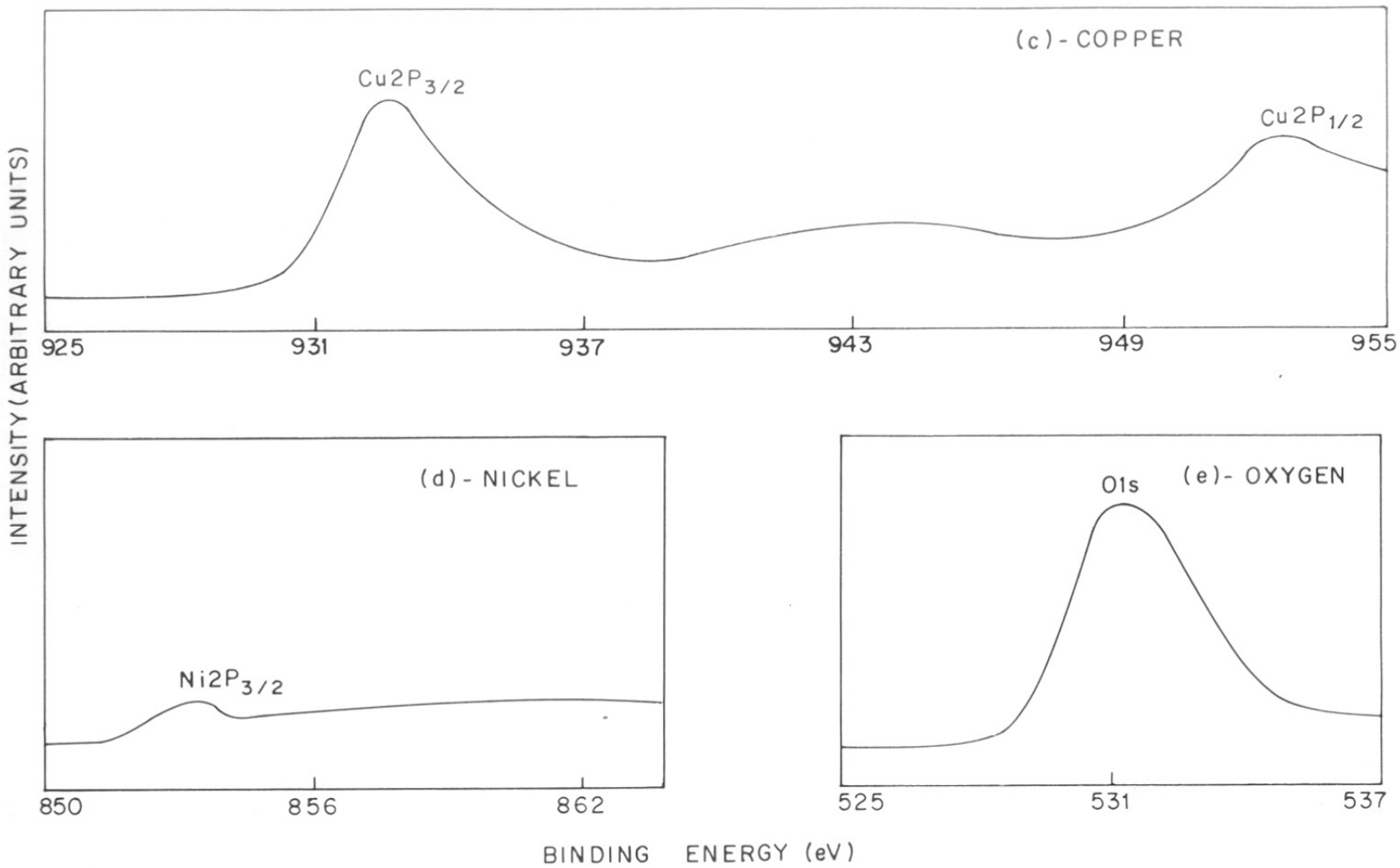

FIG. 4·10 XPS SPECTRUM OF MOLYBDENUM-BLACK FILM.

The values for the BE, ΔE - shift in binding energy, FWHM - full width at half maximum are presented for the molybdenum-black film and pure MoO_3 powder in Table 4.4a. In Table 4.4b reported data of BE values on MoO_3, MoO_2, Cu & Ni comps is presented for comparison.

It is obvious from Table 4.4a and b that molybdenum-black film contains Mo in the form of oxide mainly MoO_3 at the surface. From the comparison of BE value for Ni and Cu with reported Ni and Cu compounds (Table 4.4b), it can be concluded that nickel is present in Ni(0) state and copper may be present in either Cu(0) or Cu(I) state, because XPS does not distinguish between Cu(0) and Cu(I) species. Therefore, to confirm the presence of Cu(0) or Cu(I), AES spectrum was taken using x-ray as the source as Cu(I) species[132b] have got more chemical shift. The Auger L_3M_{45} M_{45} peak is shown in Figure 4.11. The Auger L_3M_{45} M_{45} peak position matches with reported Cu(0)[132] peak position (919 eV on kinetic energy scale). This observation confirms that Cu is present in Cu(0) state.

The XPS study on the selective molybdenum-black film has shown that the film contains Mo in the form of MoO_3 while Cu and Ni are present in metallic form within the penetration depth of XPS.

4.6.1 AES studies

AES studies on the selective molybdenum-black film was carried to know the composition at the surface as the penetration depth is smaller for AES than XPS, using electron

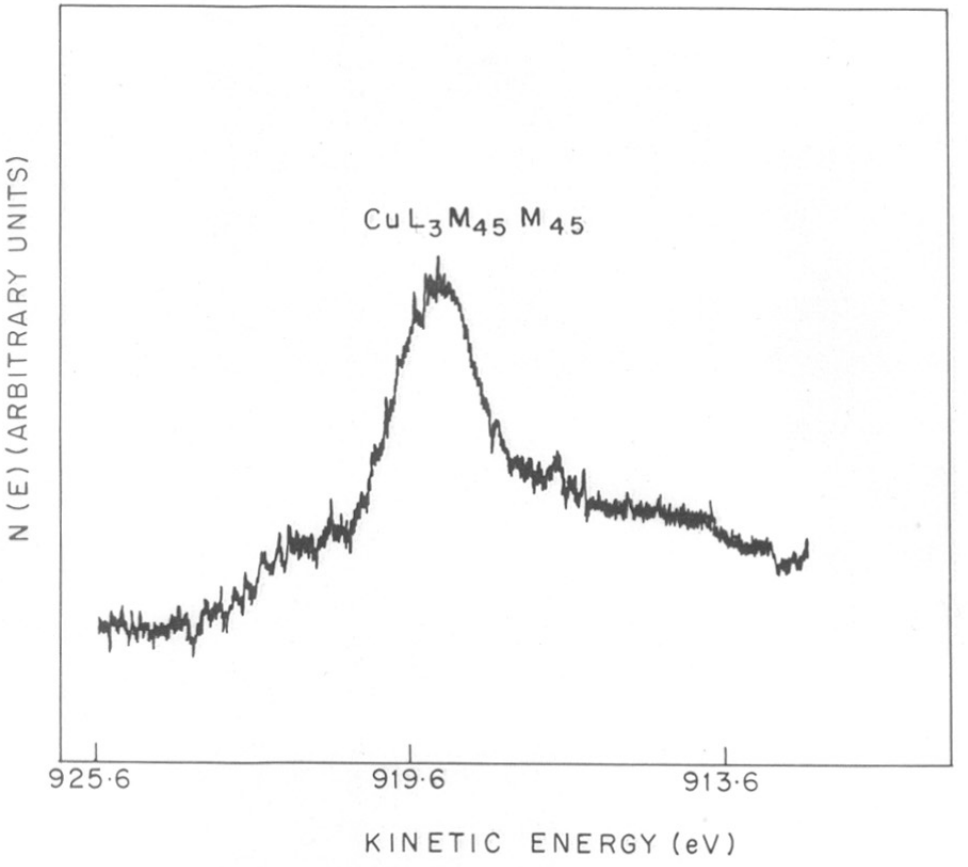

FIG. 4·11 XAES OF SELECTIVE MOLYBDENUM–BLACK FILM FOR COPPER.

TABLE 4.4a

BE, SHIFT IN BE, AND FWHM DATA FOR PURE MoO_3 AND Mo-BLACK FILM

Sample	BE eV $3d_{5/2}$	Shift in BE Δ E eV	Spin-orbital aplitting	FWHM eV
Pure MoO_3	232.1	6.0	3.2	1.92
Mo-black film	232.2	6.1	3.0	2.40
Mo-black film after treating with HCl	232.6	6.1	3.0	2.14
Pure Mo foil (158)	226.1	-	-	-

BE - Binding energy
E - Shift in BE
FWHM - Full width at half maximum
Ref - C 1s = 284.8 eV

Numbers in bracket denote reference

TABLE 4.4b

REPORTED BE DATA ON Mo, MoO_3, MoO_2, Cu & Ni COMPOUNDS

Material		Level	BE (eV)
Mo	(158)	$3d_{5/2}$	226.1
MoO_3		$3d_{5/2}$	232.5
MoO_2	(171)	$3d_{5/2}$	229.4
Cu	(132)	$2p_{3/2}$	932.7
Cu_2O		$2p_{3/2}$	932.6
CuO		$2p_{3/2}$	933.6
Ni	(132)	$2p_{3/2}$	852.9
NiO		$2p_{3/2}$	854.2
Ni_2O_3		$2p_{3/2}$	855.6

Numbers in bracket denote the reference

beam as the source. AES scan on 1100 - 100 eV kinetic energy scale indicated presence of molybdenum and oxygen (Figure 4.12). But no signal for copper and nickel was seen. For the purpose of chemical shift measurement in AES, we have chosen $M_{45}N_{23}V$ transition peak. AES was scanned on 440 - 140 eV region as shown in Figure 4.13. It shows doublet structure with peak position at 186 eV and 182.6 eV respectively. The intense peak at 182.6 eV is attributed to + 6 oxidation state of Mo and less intense peak at 186 eV is due to + 4 oxidation state of Mo. These values were found to be in agreement with the reported values.[160,161]

AES on the same sample was taken after etching with Argon ions for three minutes. The spectrum is shown in Figure 4.14a,b. The spectrum indicates singlet structure at 186 eV characteristic for + 4 oxidation state of Mo. After etching with Argon ions AES does not show signal for copper or nickel (Figure 4.14c,d), but XPS of etched sample shows the presence of copper and nickel (Figure 4.15).

These observations suggest that there is no copper or nickel present at the surface of the film and film has only MoO_3 composition at the surface. The less intense peak may be due to MoO_2, which has been shown in the AES of the as prepared sample, is, due to the partial reduction of MoO_3 to MoO_2 by electron beam exposure.[161] After etching with Argon ions MoO_3 in the film gets further reduced to

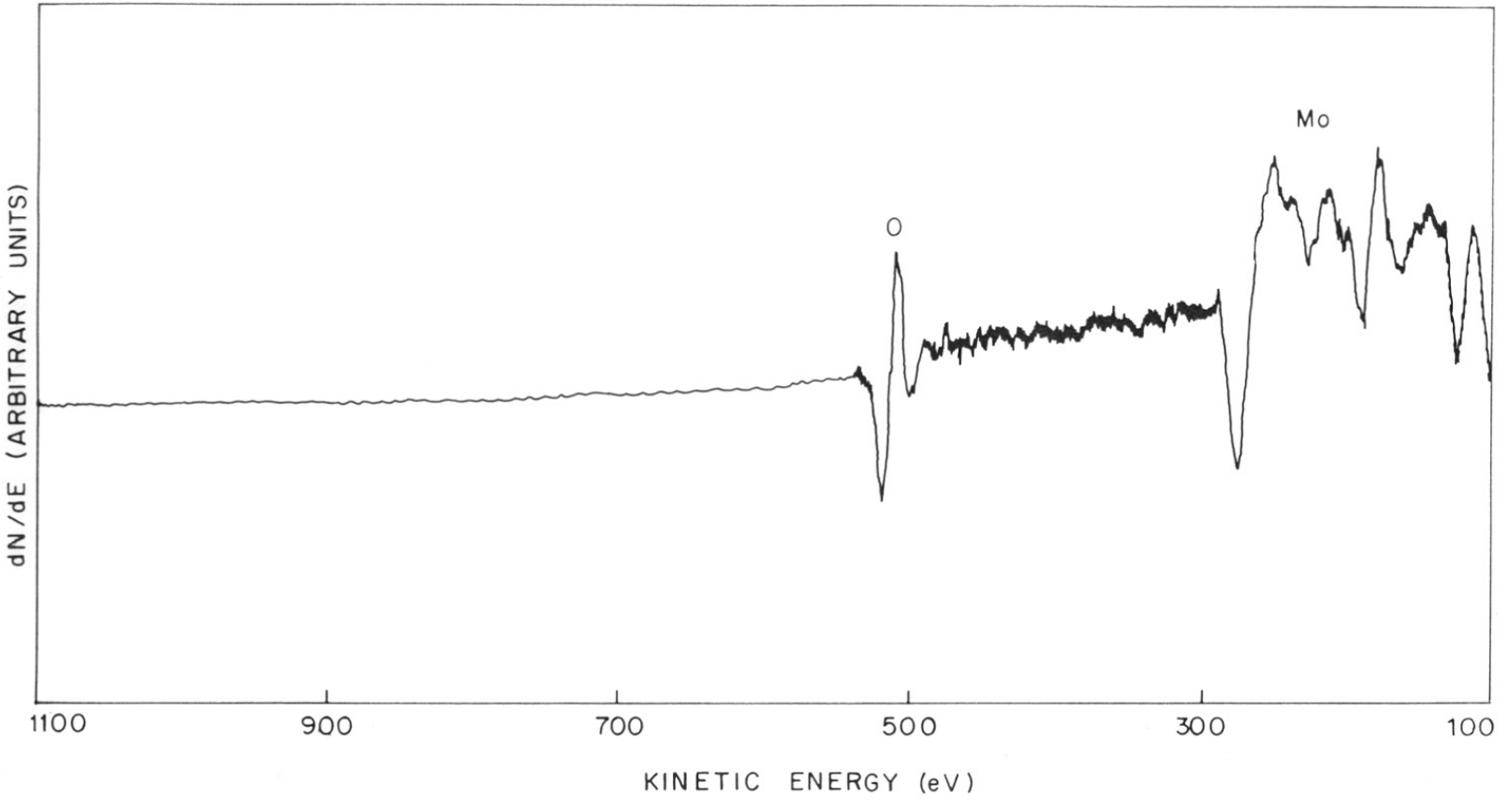

FIG. 4·12 FULL AES OF MOLYBDENUM-BLACK FILM ON 1100-100 eV SCALE.

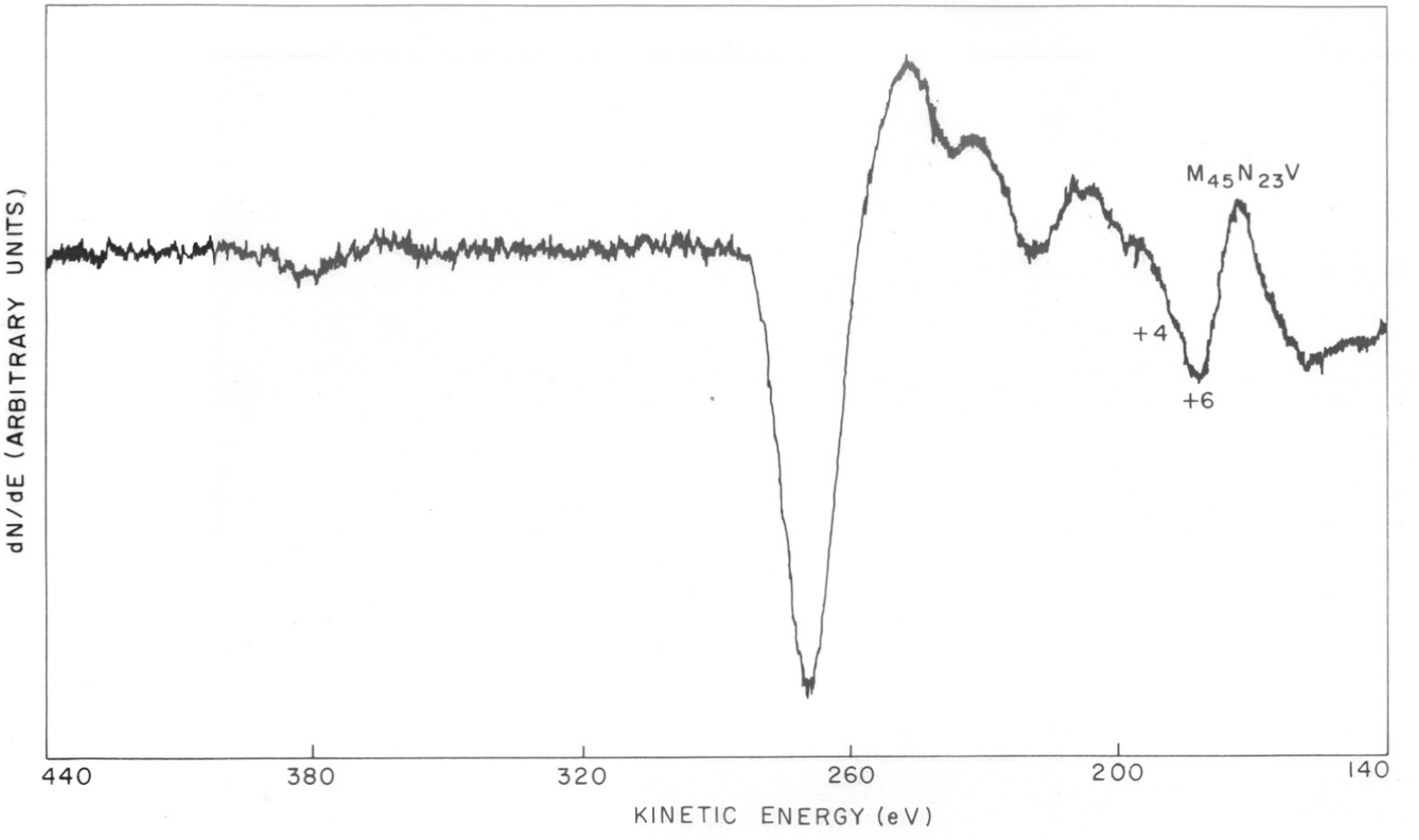

FIG. 4·13 AES OF A SELECTIVE MOLYBDENUM-BLACK FILM ON 440–140 SCALE.

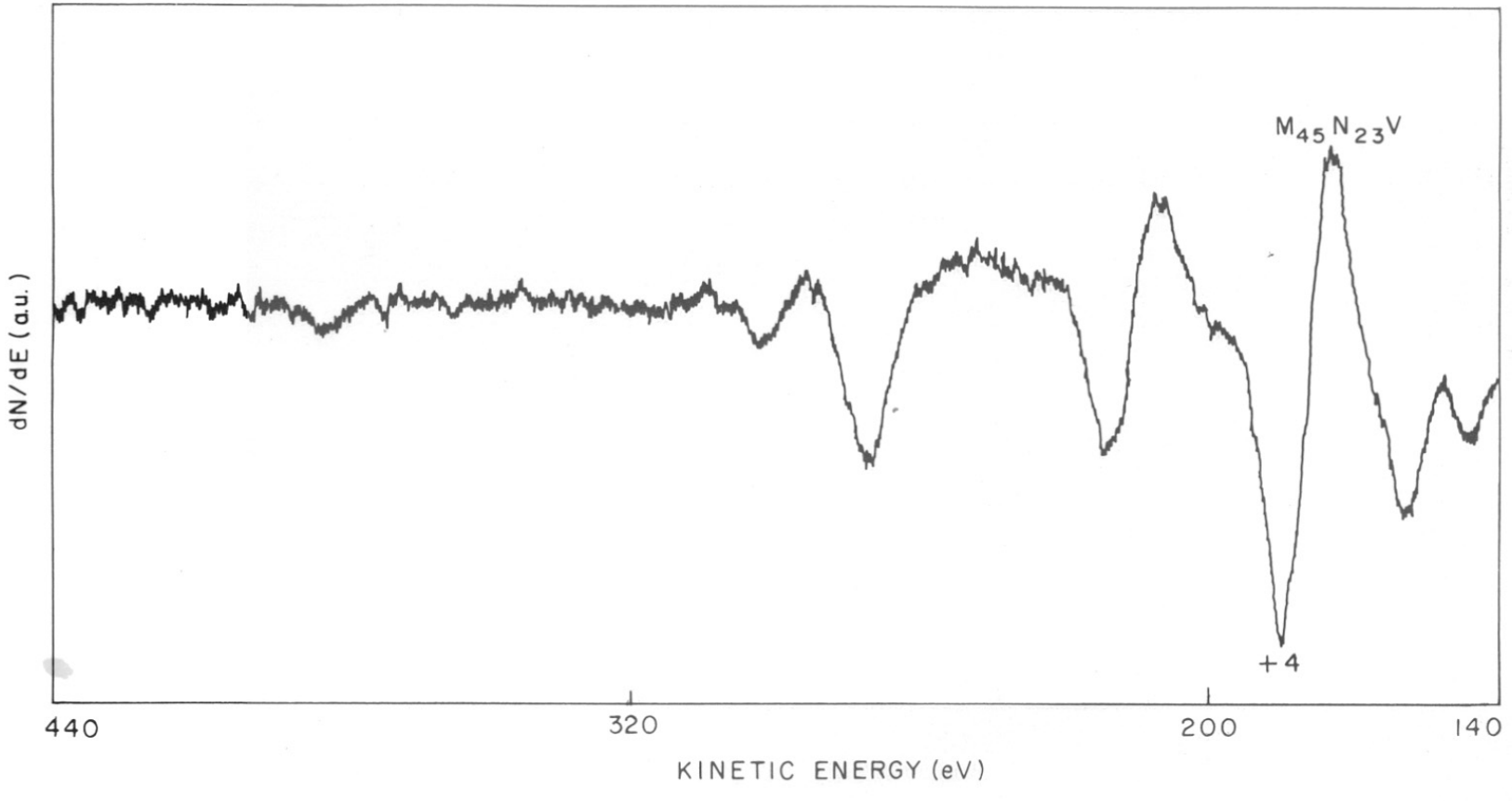

FIG. 4·14(a) AES OF SELECTIVE MOLYBDENUM-BLACK FILM AFTER FIRST ETCHING WITH Ar IONS FOR THREE MINUTES.

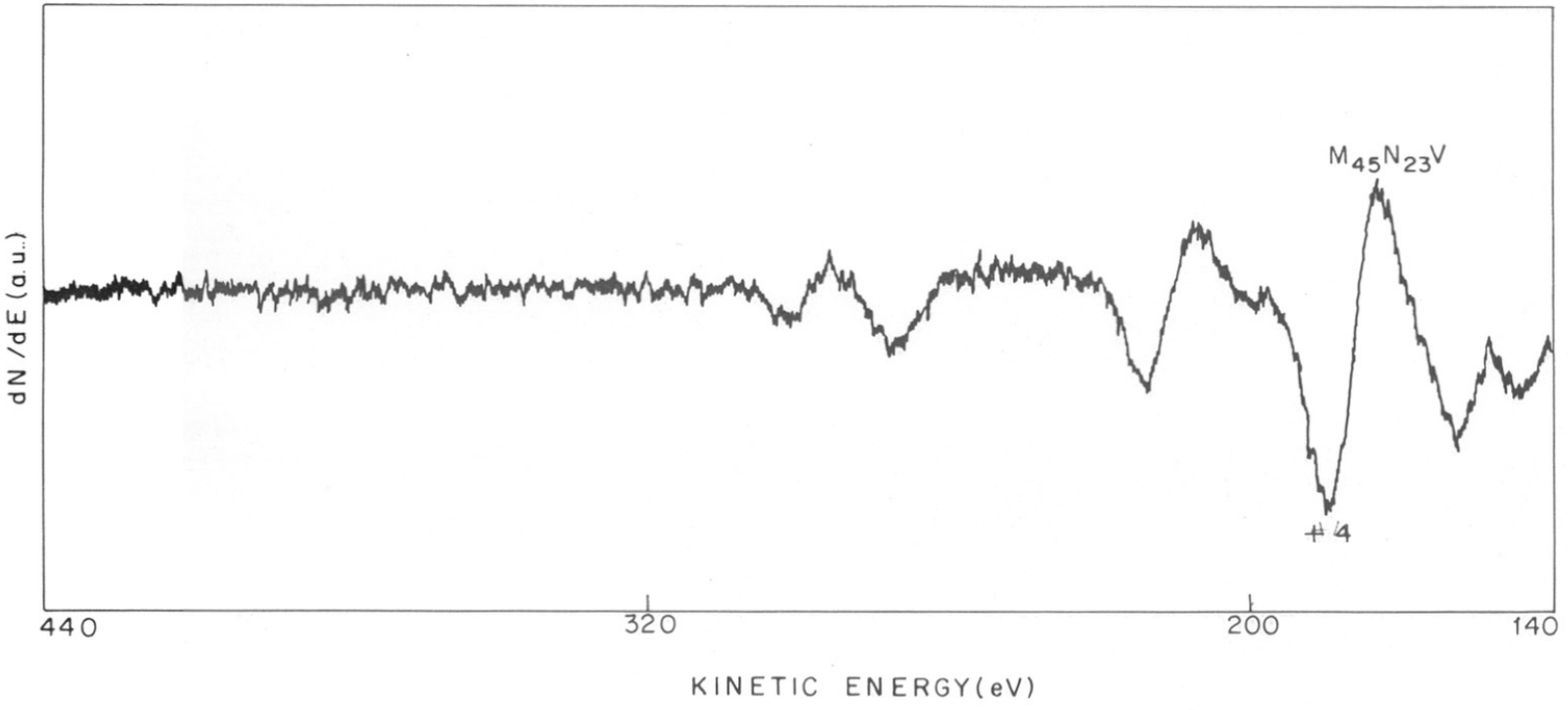

FIG. 4.14 (b) AES OF SELECTIVE MOLYBDENUM-BLACK FILM AFTER 2nd ETCHING FOR THREE MINUTES.

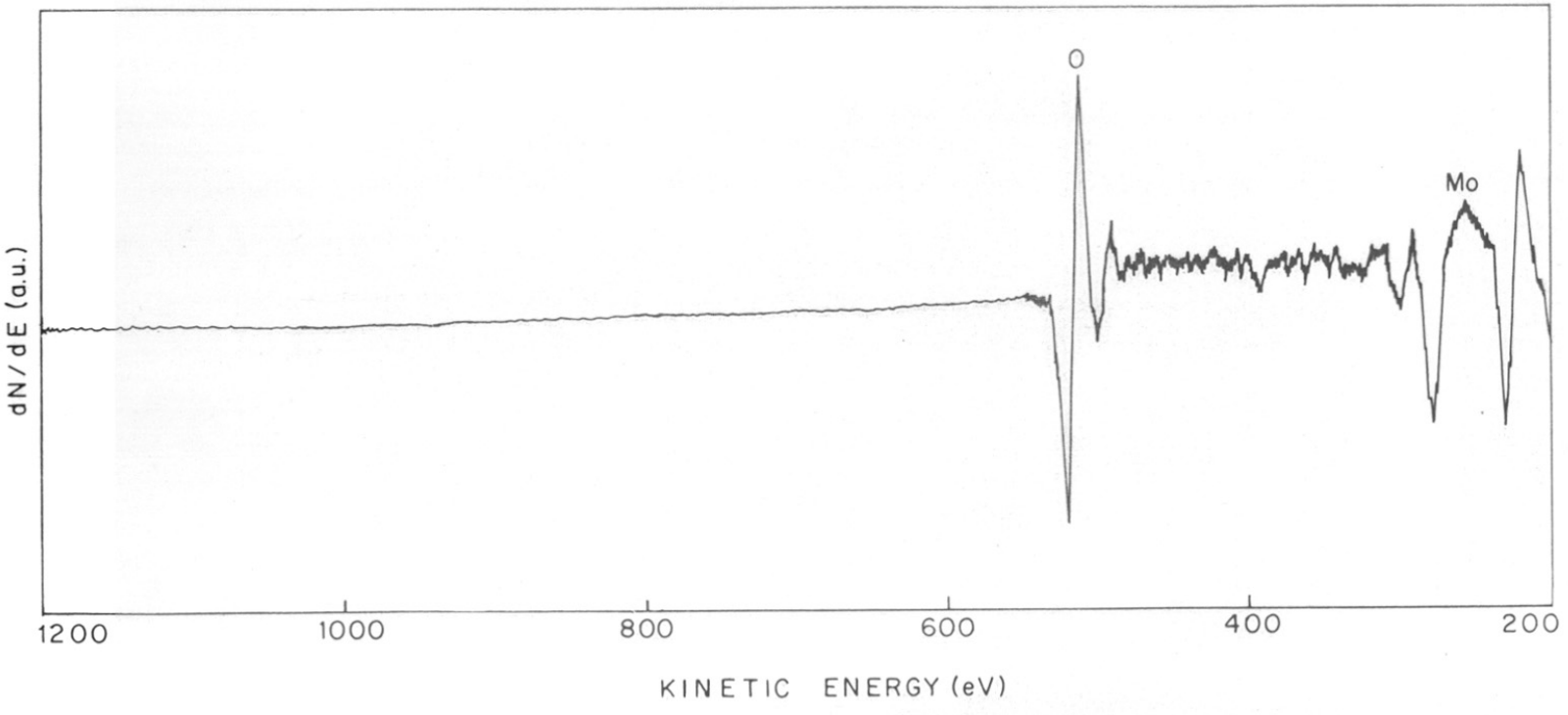

FIG. 4·14(c) AES OF MOLYBDENUM–BLACK FILM WITH Ar IONS FIRST ETCHING FOR THREE MINUTES.

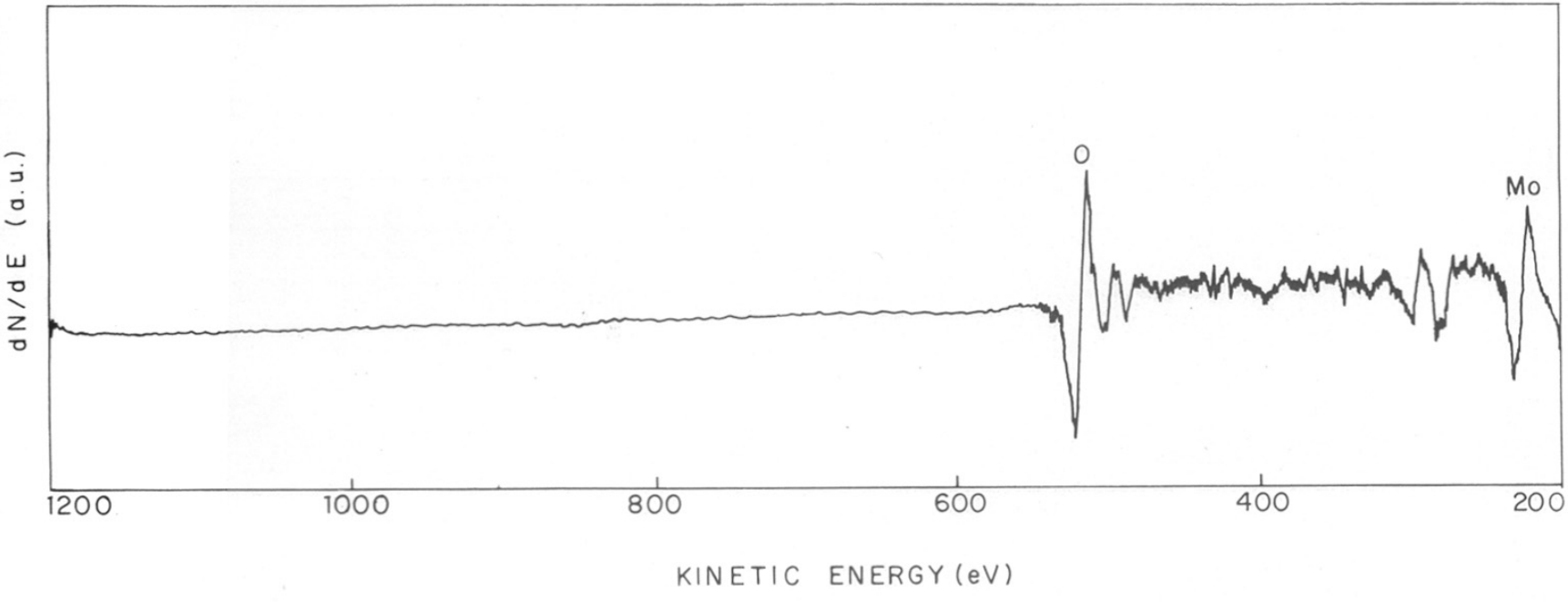

FIG. 4·14(d) AES OF SELECTIVE MOLYBDENUM–BLACK FILM AFTER 2nd ETCHING FOR THREE MINUTES

MoO_2 due to Argon ion reduction,[133,162] therefore singlet structure at 186 eV is shown in Figure 4.14a,b. AES taken after etching with Ar ions does not show signals for copper or nickel, but the presence of which is shown by XPS (Figure 4.15), leads to the conclusion that copper and nickel particles are embedded in MoO_3 matrix and cannot be seen by AES as penetration depth (5-10 A^o) is small as compared to XPS, where the penetration depth is 30-40 A^o. This observation was found even after second etching, which confirms the conclusion.

4.6.2 XPS and AES profiling study

To know the composition of the film along the thickness as well as uniformity of the composition, XPS and AES depth profiling study on the selective molybdenum-black film was carried out.

XPS profiling study - XPS profiling was carried out using Argon ion gun (8 KV, 100 μA). The $Mo3d_{5/2}$, $Mo3d_{3/2}$, $Ni2p_{3/2}$ and $Cu2p_{3/2}$ and O 1s peaks were recorded after successive etching. BE for each constituent was determined and is tabulated in Table 4.5.

Figure 4.16a gives the XPS spectrum for the as prepared molybdenum-black film for Mo, Cu, Ni and O region.

Figures 4.16b, 4.16c, 4.16d, 4.16e and 4.16f show the XPS spectra of the film after Argon ion etching for two, five, eight, ten and seven minutes respectively. The cronological effect of Ar ions is given below.

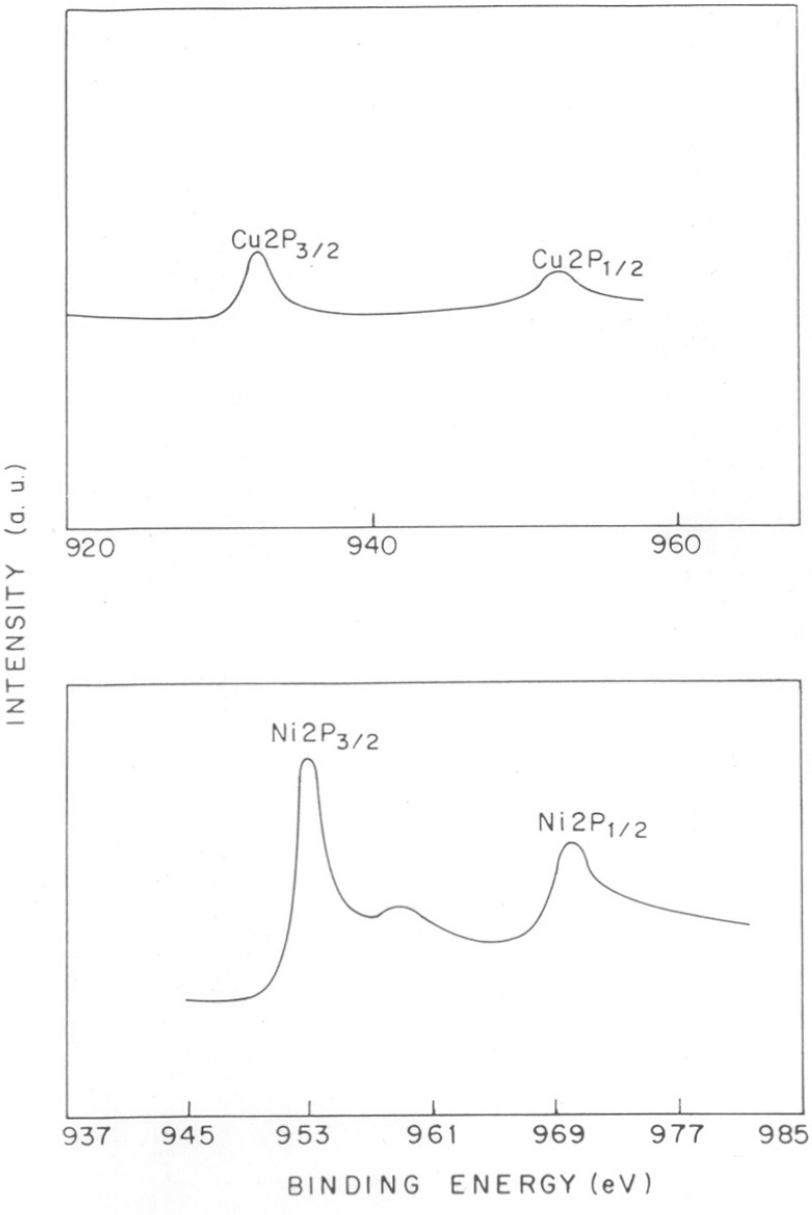

FIG. 4·15 XPS OF ETCHED MOLYBDENUM BLACK FILM FOR THREE MINUTES

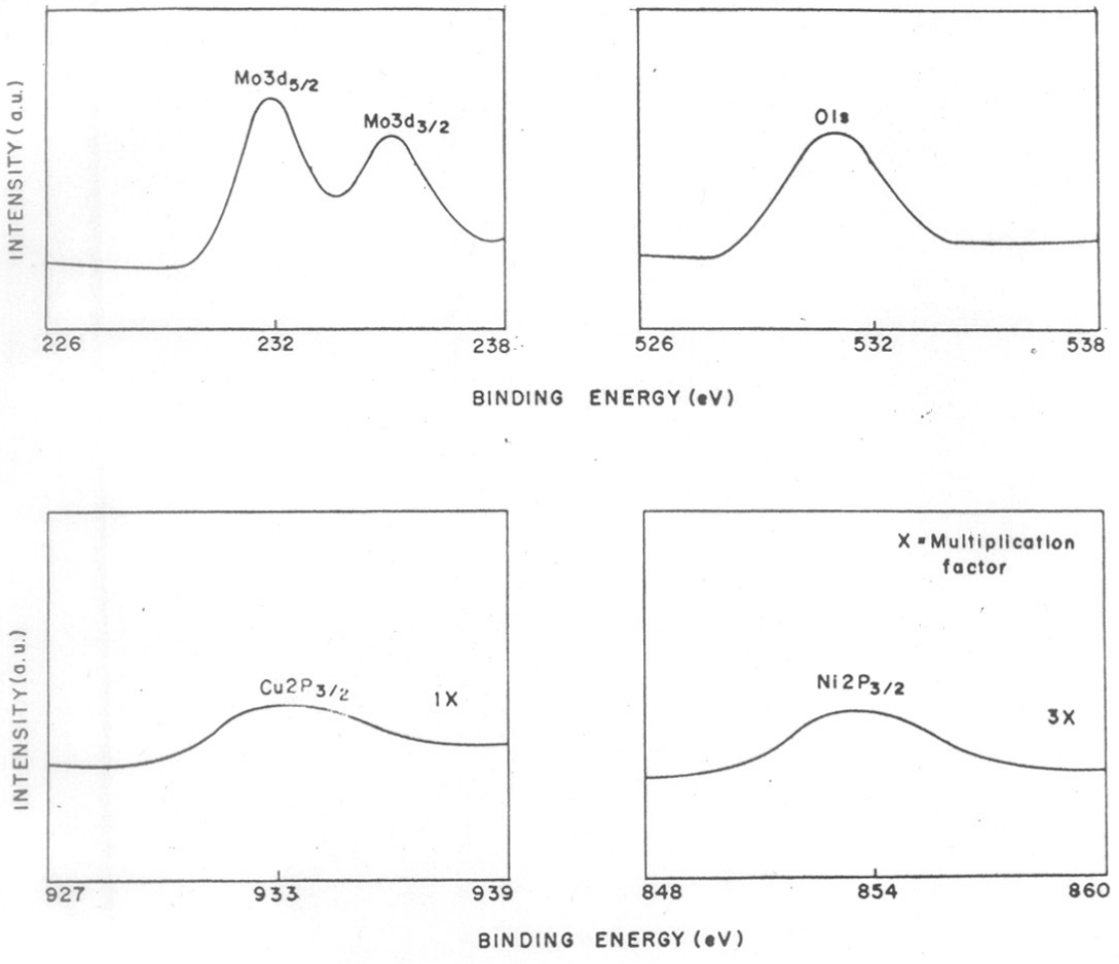

FIG. 4·16 (a) XPS OF SELECTIVE MOLYBDENUM-BLACK FILM.

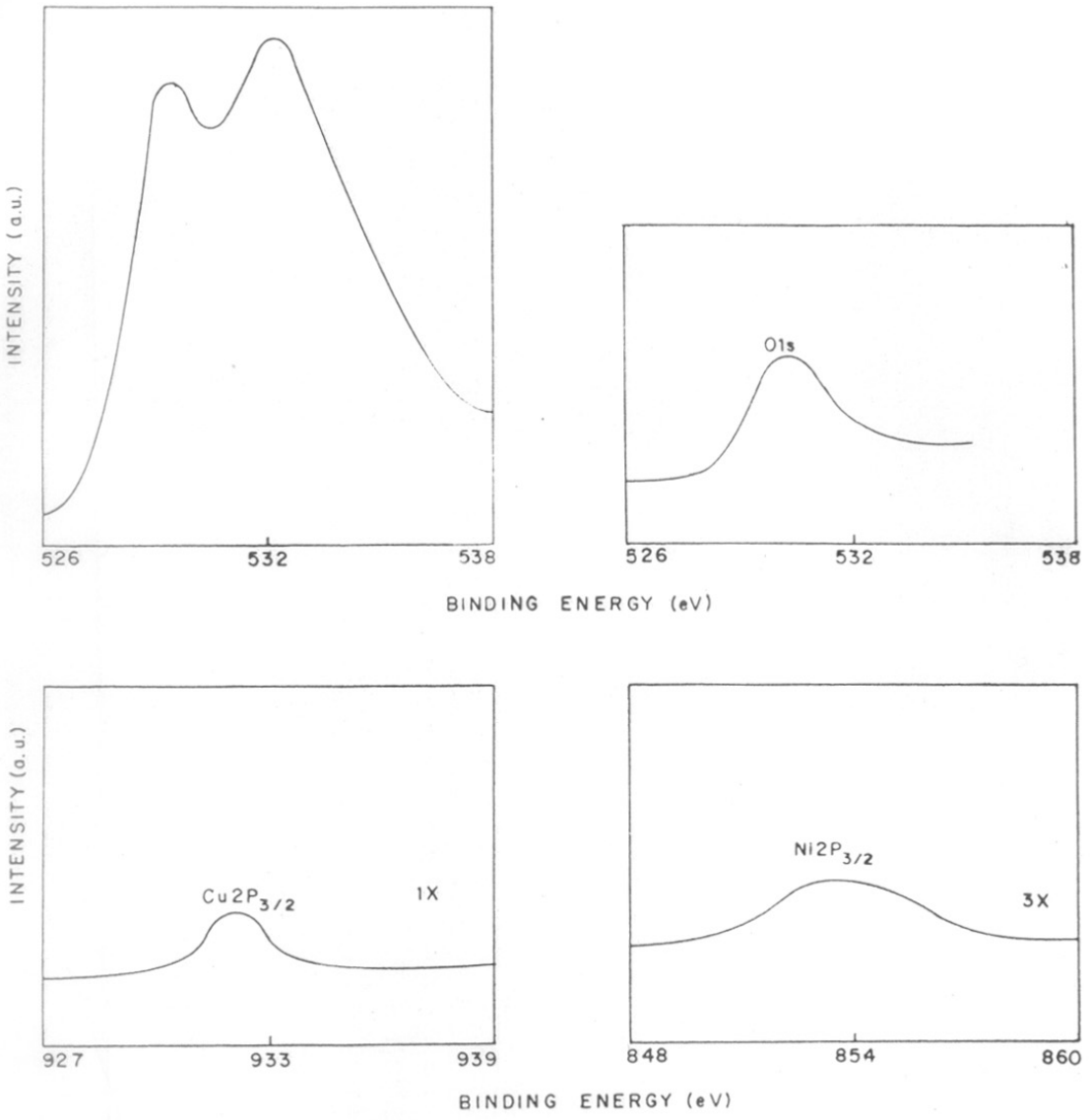

FIG. 4·16(b) XPS OF SELECTIVE MOLYBDENUM–BLACK FILM AFTER FIRST ETCHING.

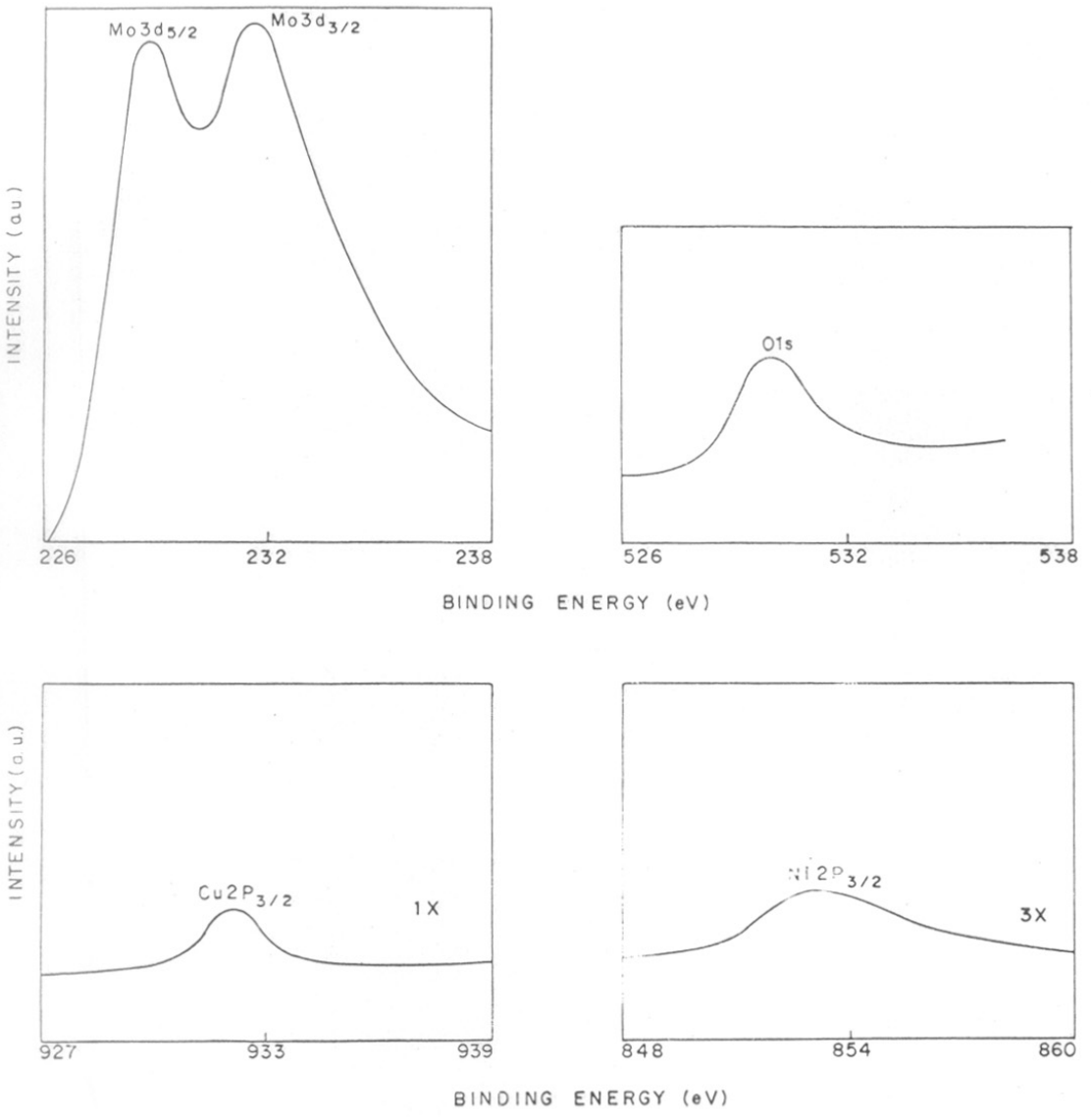

FIG. 4·16(c) XPS OF SELECTIVE MOLYBDENUM–BLACK FILM AFTER SECOND ETCHING.

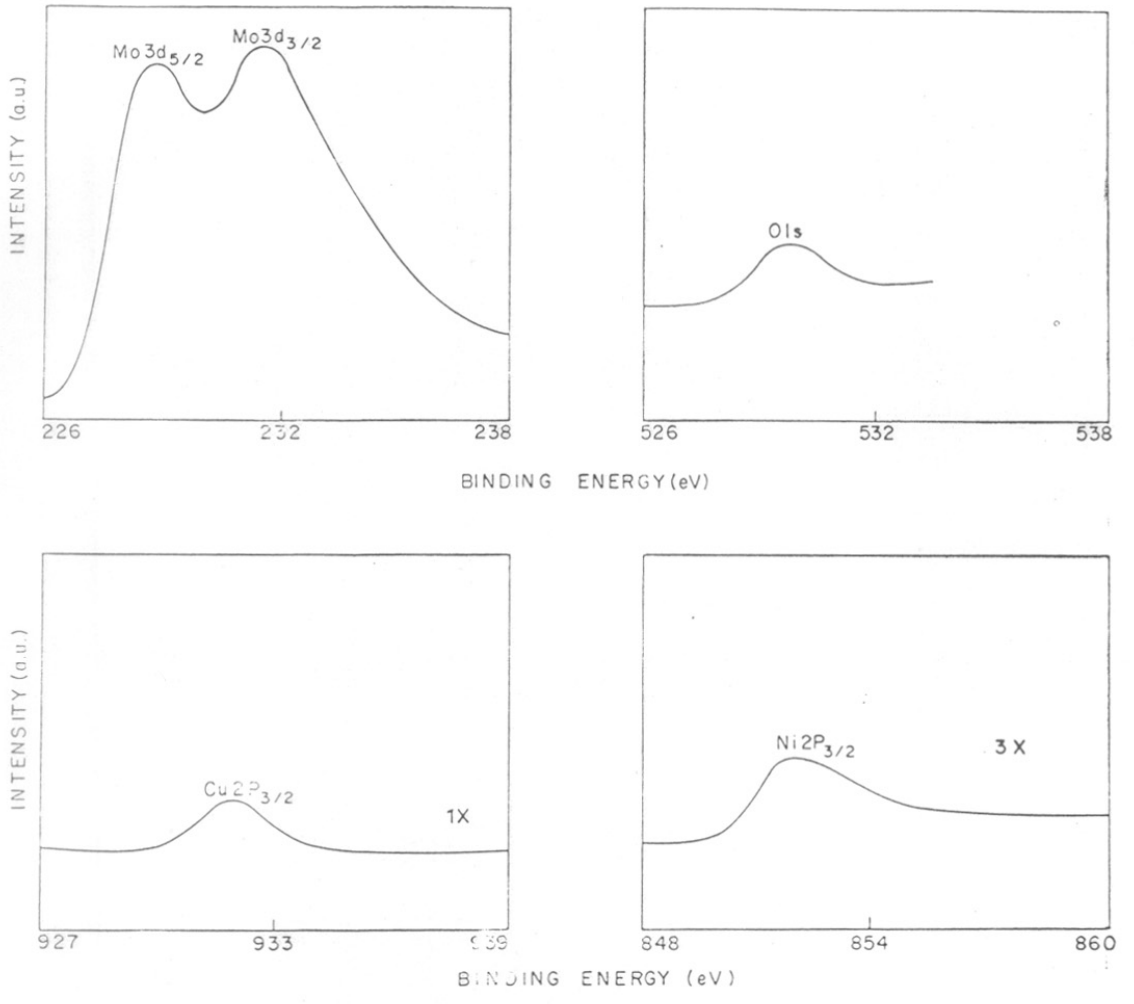

FIG. 4·16(d) XPS OF SELECTIVE MOLYBDENUM BLACK FILM AFTER THIRD ETCHING.

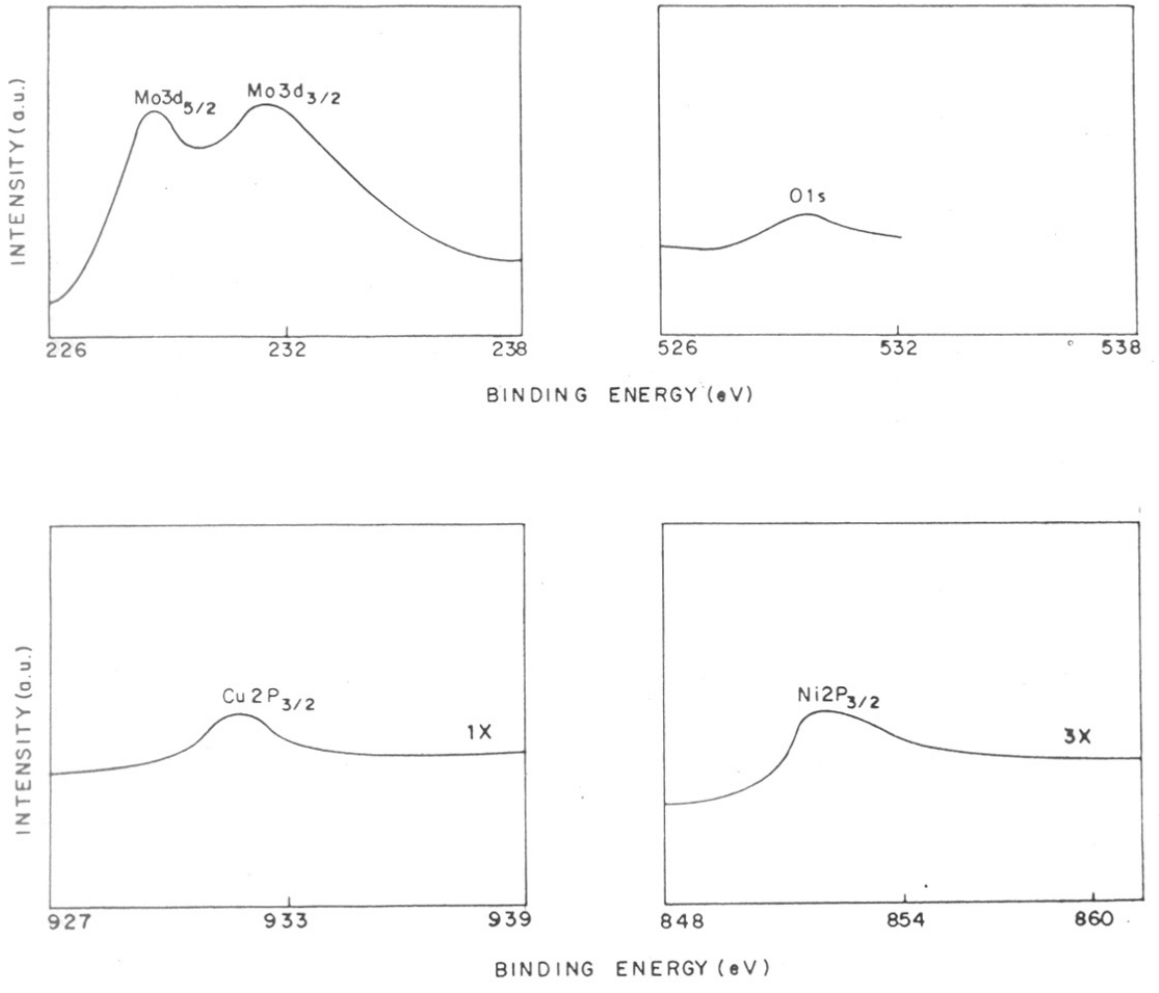

FIG. 4·16 (e) XPS OF SELECTIVE MOLYBDENUM-BLACK FILM AFTER FOURTH ETCHING.

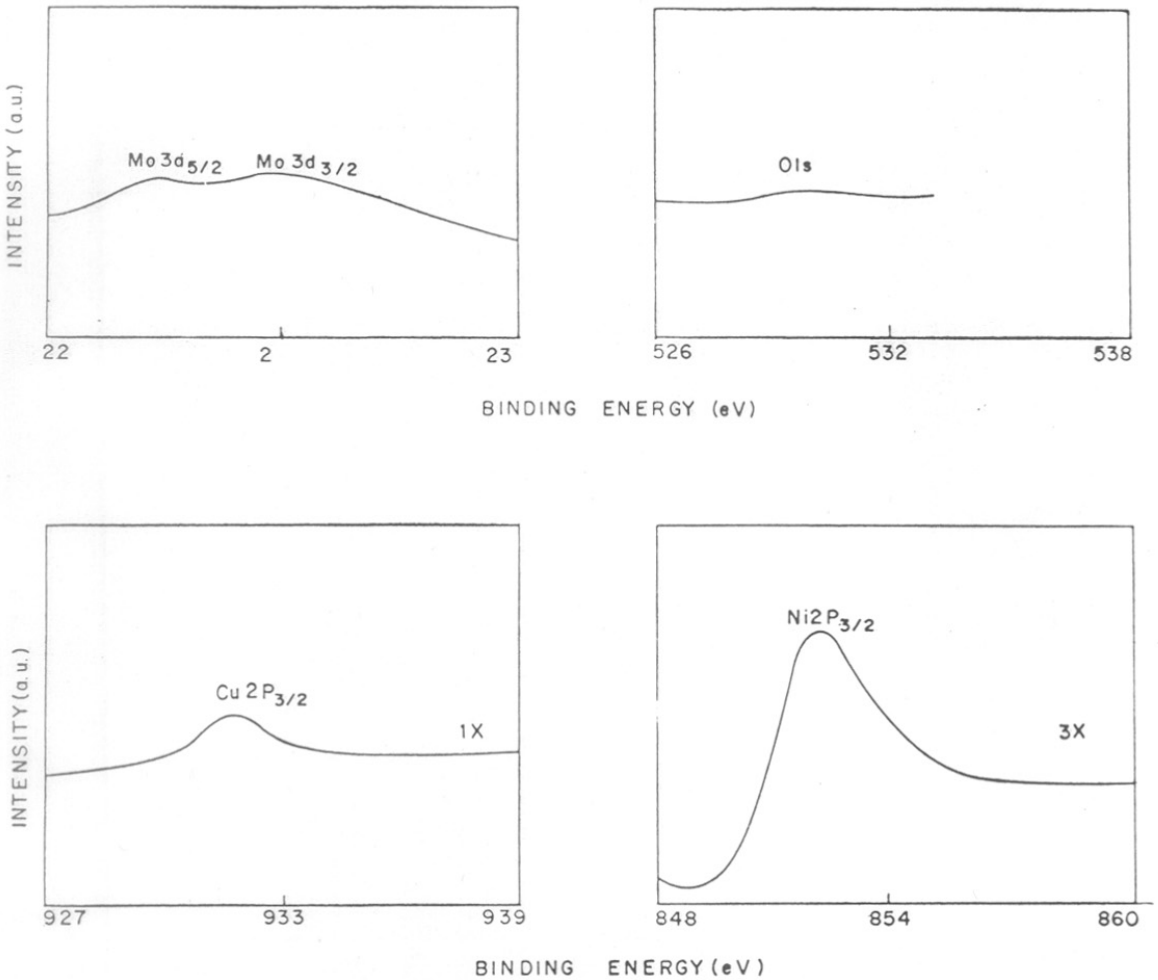

FIG. 4·16 (f) XPS OF SELECTIVE MOLYBDENUM–BLACK FILM AFTER 5th ETCHING.

TABLE 4.5

XPS PROFILING DATA OF SELECTIVE MOLYBDENUM-BLACK FILM AND PURE MoO_3 POWDER

	Atomic level				
	$Mo3d_{5/2}$	$Mo3d_{3/2}$	O1s	$Cu2p_{3/2}$	$Ni2p_{3/2}$
Unsputtered film	232.24	235.48	531.72	932.8	853.6
1st etching	229.36	232.24	530.6	932.36	853.4
2nd etching	229.96	232.84	530.9	932.7	853.6
3rd etching	229.68	232.44	530.8	932.8	853.6
4th etching	229.32	232.44	531.6	932.5	853.1
5th etching	229.2	232.40	-	932.5	853.1
Unsputtered MoO_3	232.1	235.2	-	-	-
1st etching	229.24	232.24	-	-	-
2nd etching	229.36	232.36	-	-	-

Ref. C1s = 284.8 eV

(a) $Mo3d_{5/2}$ and $Mo3d_{3/2}$ peaks are shifted towards lower binding energy side.

(b) The intensity of $Mo3d_{3/2}$ peak is found to be more or equal than that of 3d5/2 peak.

(c) The $Mo3d_{5/2}$ and $3d_{3/2}$ is broader as compared to the unetched sample.

(d) $Cu2p_{3/2}$ and $Ni2p_{3/2}$ peak position and intensity remains the same throughout the etching process, but $Ni2p_{3/2}$ peak intensity increases when substrate is reached.

(e) $Mo3d_{5/2}$ and O 1s intensity was found to decrease simultaneously after 3rd and further etchings.

These observations can be explained as follows. The as prepared film contains MoO_3 in which copper and nickel particles are embedded. After etching, the MoO_3 gets reduced to MoO_2 due to Argon ion reduction.[133,162] So BE position matches with MoO_2 as is seen from Table 4.4a,b. But XPS sees both MoO_2 formed at the surface along with MoO_3 layers below. Therefore, the Mo3d peak was found to be much broader as compared to Mo peak in unetched sample. The intensity of $3d_{3/2}$ peak is found to be more than that of $3d_{5/2}$ can be explained as follows. The peak $Mo3d_{3/2}$ of MoO_2 formed due to reduction overlaps with $Mo3d_{5/2}$ peak from MoO_3 below the reduced layer.

Since as prepared film of Mo-black does not show peaks for MoO_2 and peak intensity of $Mo3d_{3/2}$ is higher than that of $Mo3d_{5/2}$ after successive etching indicates that

film may have MoO_3 composition throughout the bulk. But the presence of MoO_2 along with MoO_3 below the top layer cannot be ruled out.

To confirm whether the film has MoO_3 composition throughout the film or contain MoO_2 along with MoO_3, the use of a chemical property of MoO_3 namely its reaction with HCl or NaOH is used. MoO_2 does not react with either HCl or NaOH solution.

When the film was treated with NaOH/HCl solution, all the film material goes into solution without any residue, showing the absence of MoO_2 in the bulk of the film. Similarly, the molybdenum-black film was treated with dil. HCl or dil. NaOH solution for few seconds and then the remaining film was washed with distilled water several times to remove excess HCl or NaOH. The film was then dried and XPS was taken. The Figure 4.17 shows the XPS spectrum of molybdenum-black film treated with HCl or NaOH. BE position, FWHM of $Mo3d_{5/2}$ and $Mo3d_{3/2}$ levels match with Mo(+6) state indicating thereby absence of MoO_2 (Table 4.4a).in the film.

The observations D and E in XPS depth profiling results suggest that Ni and Cu concentration (relative) increases systematically towards the substrate.

Thus the XPS profiling study on the molybdenum-black film confirmed that film has MoO_3 composition throughout the bulk. Some Ni and Cu are also present in free state incorporated in the matrix of MoO_3. Their concentration is

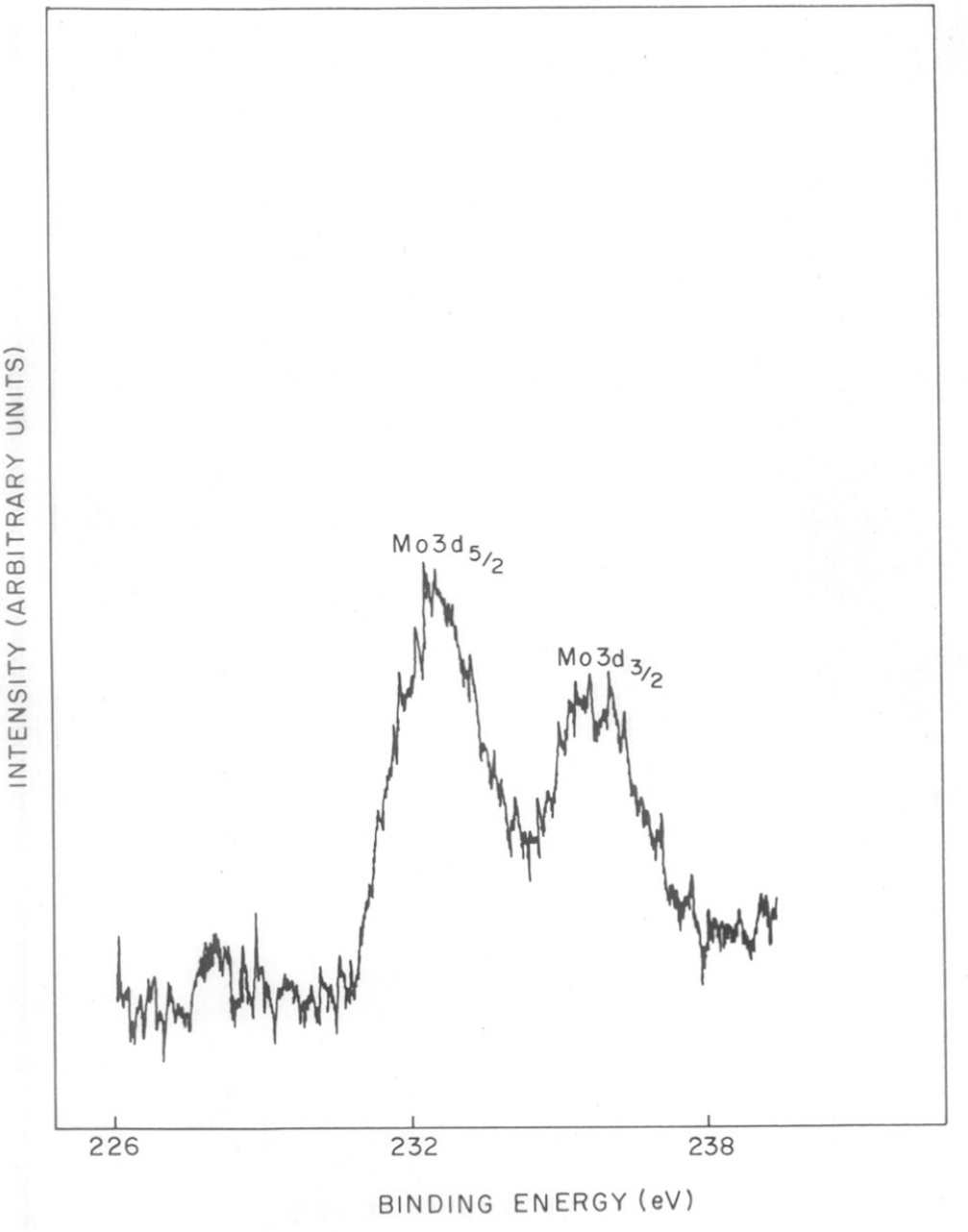

FIG. 4·17 XPS OF SELECTIVE MOLYBDENUM-BLACK FILM AFTER TREATING WITH HCl

increasing towards the substrate. To support the above conclusion XPS depth profiling study on pure MoO_3 powder was also carried out. The XPS profiling results obtained are shown in Figure 4.18. The cronological effects are given below.

(a) $Mo3d_{5/2}$ and $Mo3d_{3/2}$ peaks are shifted towards lower binding energy side.

(b) The intensity of $Mo3d_{3/2}$ peak is found to be equal to that of $Mo3d_{5/2}$ peak.

(c) The $Mo3d_{5/2}$ and $Mo3d_{3/2}$ peak is broader as compared to the peak in unetched pure MoO_3.

These results are identical with results obtained for the molybdenum-black film (Compare Figures 4.16 and 4.18 and Table 4.5). This observation supports the conclusion that film has MoO_3 composition throughout the bulk.

4.6.3 AES depth profiling study

AES depth profiling study was carried out using differentially pumped Argon at 10^{-5} mm of Hg pressure using 9.8 KV and 20 μA current. The peak to peak height for Mo and O was recorded as a function of etching time. The profile obtained is shown in Figure 4.19. It indicated that peak to peak ratio for $\frac{O}{Mo}$ is 2.8 at the surface, but it changes to 2.0 after etching and then remains more or less constant upto the substrate.

It is known that electron beam exposure[162] and argon ion bombardment reduce Mo (+6) to (+4) as is seen in

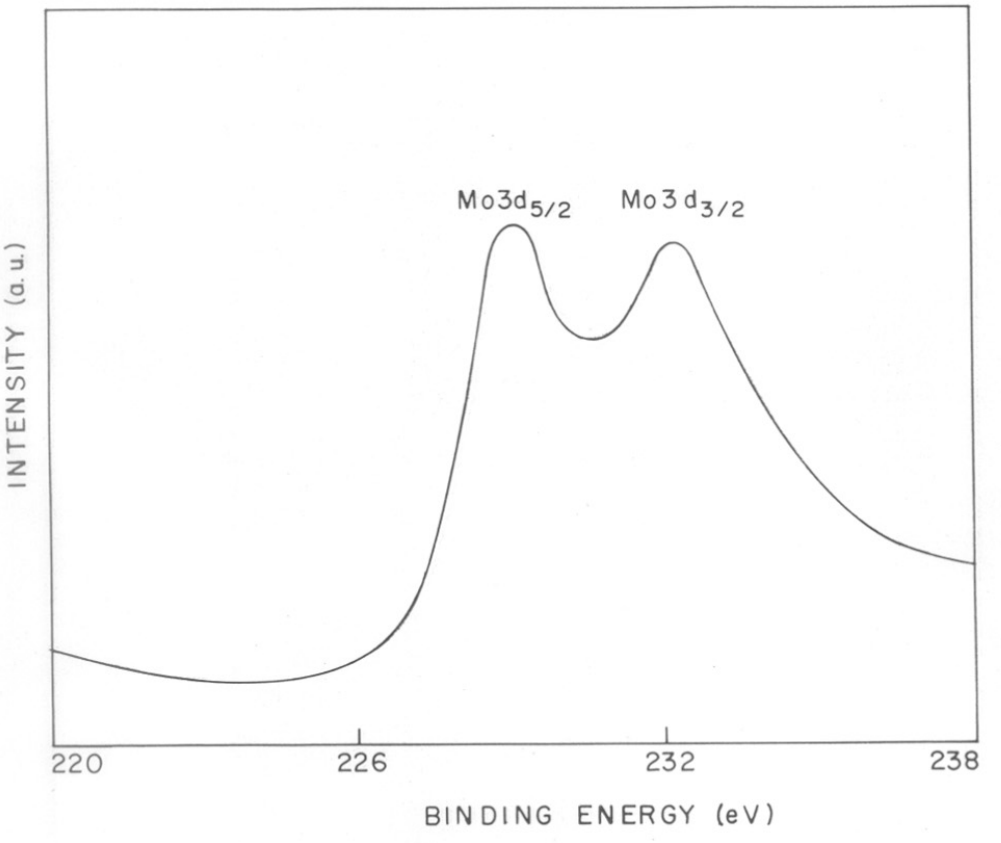

FIG. 4·18(a) XPS OF PURE MoO_3 POWDER AFTER FIRST ETCHING FOR TWO MINUTES

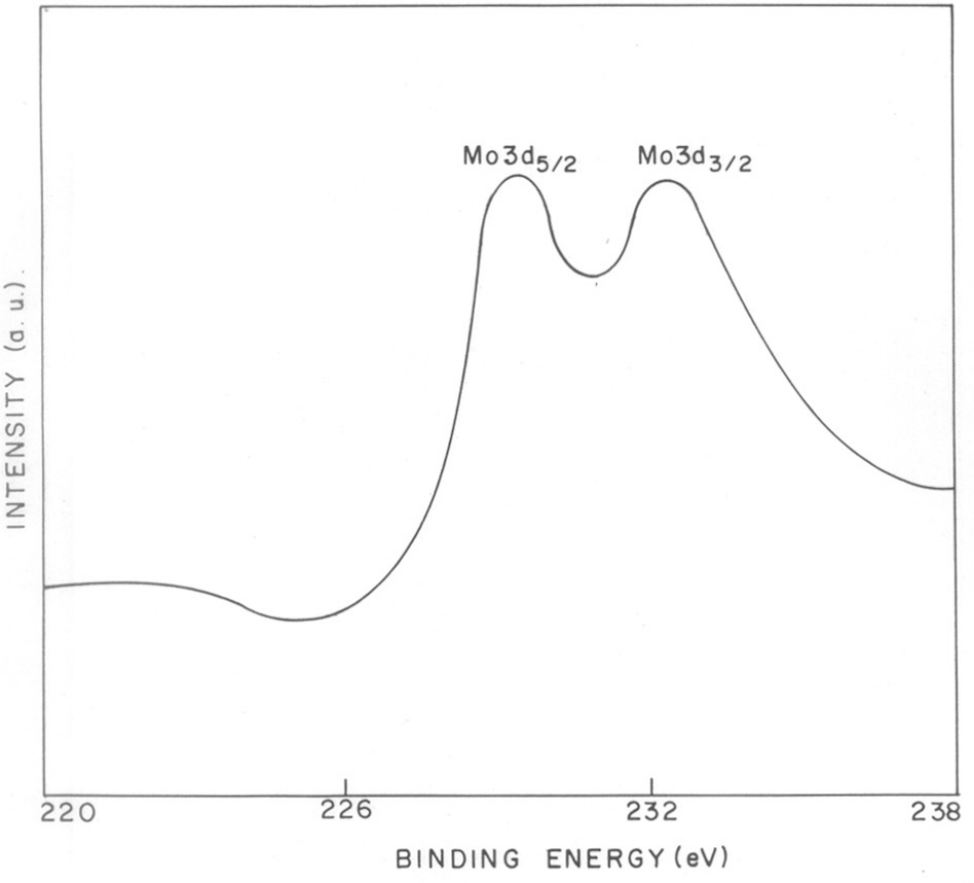

FIG. 4·18(b) XPS SPECTRUM OF PURE MoO_3 POWDER AFTER 2nd ETCHING FOR 5 MINUTES

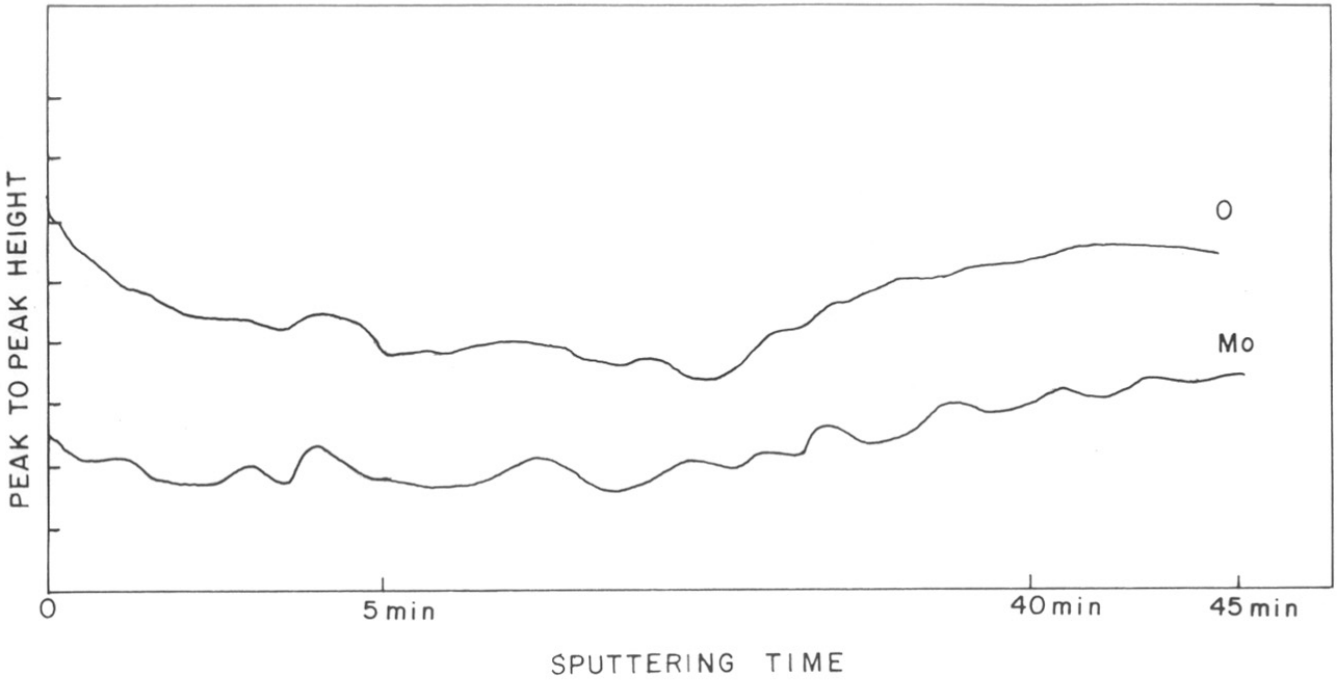

FIG. 4·19 AES DEPTH PROFILE OF SELECTIVE MOLYBDENUM–BLACK FILM.

the earlier studies, then AES profiling study can be explained as follows.

At the surface peak to peak height ratio for $\frac{O}{Mo}$ is equal to 2.8, which confirms the presence of MoO_3 as is seen by XPS study. But after etching, MoO_3 is converted to MoO_2, since $\frac{O}{Mo}$ ratio changes to 2 and remains constant upto the substrate. If the reduction is by electron beam or by argon ions, then where the presence of MoO_2 is indicated, we can presume that the film actually contains MoO_3 . This observation is then consistent with the earlier XPS depth profiling result, that the film has a MoO_3 composition throughout the bulk. This conclusion is also supported by the x-ray results on sample heated at 350°C, which shows the presence of Mo_4O_{11} .

4.7 Chemical Analysis

The molybdenum-black film was dissolved in conc. HCl and diluted to 250 °C. The Cu and Ni concentration was determined by atomic absorption spectroscopy and MoO_3 concentration was determined by gravimetric analysis. The volume fractions of Cu, Ni and MoO_3 were determined taking the respective bulk densities for Cu, Ni and MoO_3. The volume fractions obtained are given below.

The volume fraction of Cu = 0.32
Ni = 0.01
MoO_3 = 0.67

4.8 Optical Properties

For our films with optimized conditions the various features observed are as follows.

(1) In the visible part of the spectrum the reflectance is very low, i.e. the absorption is high, $\alpha \simeq 0.85$.

(2) IR reflectance is very high i.e. the emittance is low, $\epsilon \simeq 0.11$.

(3) The λ_{cutoff} is around 3.5 μm.

As seen from our studies of the film, the structure consists of a substrate i.e. nickel plated copper over which molybdenum trioxide film with sufficient thickness lies. In the bulk of the film, there are Cu and Ni particles in metallic form. It has also been shown that Cu and Ni concentration increases towards the substrate (vol. fractions of Cu=0.32, Ni=0.01, MoO_3 = 0.67). Such a compositional structure of the film is shown in Figure 4.20.

The high IR reflectance of the film can be easily explained if we assume that the high reflectance is due to metallic substrate. The observed IR reflectance of the substrate without film and with film are comparable taking into consideration the decrease in intensity of IR radiations according to Beer's law. The assumption, that the high IR reflectance is a contribution of the substrate is reasonable since MoO_3 having a band gap of 3.4-3.5 eV[163,164] is expected to be transparent for IR radiation. Furthermore, Cu and Ni particle size is smaller than the wavelength of

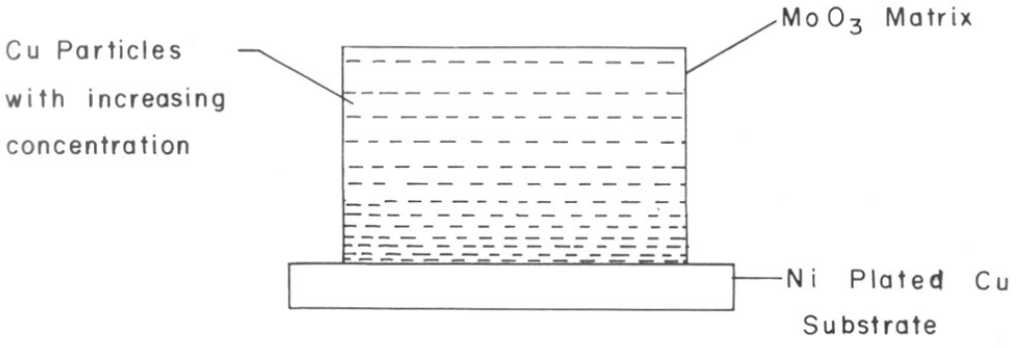

FIG. 4·20 COMPOSITIONAL STRUCTURE FOR SELECTIVE MOLYBDENUM-BLACK FILM.

the IR radiation considered and therefore would not contribute to the IR reflectance.

To explain the high absorption in the region 0.4 to 3.5 μm various possibilities are considered. It may be noted that band to band transition in MoO_3 would not explain the high ($\alpha \approx 0.85$), as only high energy photons can be involved in such transitions. In the region considered, the material will have very low absorption coefficient probably from band to impurity level transitions in MoO_3. In that case the morphology of the film should be such that the multiple reflections would increase α. But in the present case the α value ≈ 0.85 and therefore only morphological contribution is not expected to obtain such a high α value. In fact we feel that morphology would not be a major contribution for such a high α value in this region.

The characterization has shown that the films are non-homogeneous and have Ni and Cu concentration increasing towards the substrate in the MoO_3 matrix, therefore, we do not expect any interference inhanced absorption in our films. In fact, this is quite clear from the nature of reflectance curve for our film (Figure 4.3) . It may be also noted that the precise requirement for such absorption is not likely to be obtained through our method of preparation of these films.

The other possibility to explain high visible absorption can arise from the composite nature of the film

i.e. fine copper and nickel particles are dispersed in MoO_3 matrix resulting in resonance absorption which can be explained by using the Maxwell-Garnet theory. The requirements for the application of this theory are:

(1) the theory can be applied to the composite of metal particles dispersed in dielectrics,

(2) the critical volume fraction of the components requirement depending on the system,

(3) the metal particle is required to be spherical with particle size less than the radiations considered.

In this particular case, MoO_3 is known to be a dielectric (diaelectric constant $\simeq$ 6.13-6.32).[163] The Cu and Ni particles are spherical in shape and size is appropriate as is seen from SEM study. The volume fraction of Cu and Ni and MoO_3 as determined by chemical analysis are given below. (vol. fraction of Cu = 0.32, vol. fraction of Ni = 0.01 and vol. fraction of MoO_3 = 0.67). Another supporting evidence for application of Maxwell-Garnet theory is that, the metal particles (Cu and Ni) are dispersed in a diaelectric MoO_3.

Another interesting observation is that for the films deposited without Cu salt in the bath, the absorption in visible range is poor. Also, λ_{cutoff} is in the lower wavelength side, than observed in our films under optimized conditions. Such observations make us believe that, 'Cu' particles bring about the increase in the visible absorption and also the λ_{cutoff} shifts to the higher wavelength side.

The only alternative left is to consider the film as a cermet composition of Cu and Ni metal particles dispersed in MoO_3 matrix. Such cermets have been reported in the literature,[72,76,80,81,167] to increase the absorption in the visible as compared to absorption by dielectric without any additives.

To support our proposal we show the application of MG theory for the present case. We make it clear that this application of the theory is to show, how the extinction coefficient in the visible range increases for the cermets as compared to pure dielectric. For calculation, the volume fraction of metal copper is taken equal to 0.33 and volume fraction of MoO_3 equal to 0.67, since Ni volume fraction is very small $\simeq$ 0.01 as determined by chemical analysis.

Calculations have been done using the formula.[166]

$$\overline{n_i}^2 - \overline{k_i}^2 = \frac{ac + bd}{c^2 + d^2}$$

and

$$2\,\overline{n_i}\,\overline{k_i} = \frac{bc - ad}{c^2 + d^2}$$

where $\overline{n_i}$ and $\overline{k_i}$ are effective refractive index and extinction coefficient of composite respectively.

$$a = (n_i^2 - k_i^2)(1 + 2f) + 2n_o^2(1 - f)$$
$$b = 2n_i k_i (1 + 2f)$$
$$c = (n_i^2 - k_i^2)(1 - f) + n_o^2(2 + f)$$
$$d = 2n_i k_i (1 - f)$$

where 'f' is the volume fraction of metal in the medium of index n_o , n_i and k_i optical constants of the metal copper. The parameters used for calculations are given below, which have been taken from the literature.

Refractive indexes of MoO_3 at various wavelengths[167, 168] are tabulated in Table 4.6a. n_i and k_i of Cu[169,170] are tabulated in Table 4.6b. The calculated extinction coefficient of cermet (Cu/MoO_3) at different wavelengths are shown in Table 4.6c. It is clear from the Table 4.6c that $\bar{k}_i$ values, i.e. extinction coefficient of composite increases as compared to MoO_3. It is obvious that absorption coefficient $\alpha_i = \frac{4\ \bar{k}_i\ d}{\lambda}$ would change proportionately, where d is the thickness. If we compare these results with experimentally observed results in our films, one can appreciate the trend in the behaviour of the film matching with the cermet considered. We therefore, conclude that high absorption in our films can reasonably be explained by considering it as a cermet. The low emission in the thermal IR is decided by the substrate as film is transparent in IR as shown earlier.

4.8 Conclusions

(1) Solar selective molybdenum-black films are prepared successfully using cathodic electrolytic deposition techniques with $\alpha = 0.85$ and $\epsilon = 0.11$. The λ_{cutoff} lies at 3.5 μm. The films obtained were found to be well adherent to the substrate. The optical and thermal properties of the films are quite reproducible.

TABLE 4.6a

REFRACTIVE INDICES AT DIFFERENT WAVELENGTHS FOR Mo_3

λ (μm)	n_o	λ	n_o
0.45	4.0	0.95	2.38
0.5	3.3	1.00	2.38
0.6	2.8	1.5	2.38
0.7	2.5	2.00	2.38
0.85	2.38	2.5	2.38
0.9	2.38	3.00	2.38

TABLE 4.6b

REFRACTIVE INDEX AND EXTINCTION COEFFICIENT DATA FOR COPPER

λ	h_1	k_i
0.45	0.87	2.20
0.5	0.88	2.42
0.6	0.17	3.07
0.7	0.12	4.17
0.8	0.12	5.07
0.85	0.12	5.47
0.9	0.13	5.86
0.95	0.13	6.86
1.00	0.147	6.93
1.5	0.266	10.68
2.00	0.432	14.33
2.5	0.62	17.64
3.00	1.22	17.10

TABLE 4.6c

EFFECTIVE EXTENCTION ($\bar{k}_i$) COEFFICIENT FOR Mo-BLACK

λ	$\bar{\bar{k}}_i$
0.45	0.113
0.5	0.231
0.6	0.657
0.7	2.587
0.8	0.209
0.85	0.094
0.9	0.059
0.95	0.023
1.00	0.024
1.5	0.007
2.00	0.004
2.5	0.003
3.00	0.006

---

2. The absorption in this film is due to resonance absorption in the visible region and low emittance (ϵ) is because of the substrate, since the film is transparent in the IR region.

3. The molybdenum-black films are noncrystalline in nature and are not homogeneous, but contains nickel and copper particles embedded in MoO_3 matrix with increasing concentration towards the substrate.

4. The study also reveals that the morphology of the film changes with increasing the thickness.

5. Since the molybdenum-black film is a cermet, it can be used in concentrating type collectors, working at temperatures greater than 150°C.

.....

CHAPTER – V

SUMMARY

CHAPTER-V

SUMMARY

Copper-black - Electrolytic anodic oxidation process was successfully used for making solar selective copper-black films. The films obtained by this method were found to be quite uniform and well adherent to the substrate. Optical and thermal properties were found to be reproducible.

The study has shown that the time of anodization is a critical parameter which governs the optical and thermal properties of the film. The $\alpha \simeq 0.98$ and $\epsilon \simeq 0.2$ can be obtained at optimum time of anodization (t=60 sec). It was also seen from this study, that, $\lambda_{cut\ off}$ shifts towards the higher wavelength side on increasing the anodization time and shifts towards lower wavelengthside on lowering the anodization time. The values of α and ϵ of the selective copper-black film prepared by anodic oxidation process are such that the final device is likely to have a good conversion efficiency.

To explain the selectivity, the techniques were used such as X-ray, E.D. XPS, AES for the characterization of the film. The results obtained are as follows.

The x-ray and electron diffraction study have shown that the selective copper-black film is crystalline and consists of two phases namely cubic cuprous oxide(Cu_2O

and monoclinic cupric oxide (CuO) with crystallite size ranging from 100 A^{o} to 200 A^{o}. SEM studies on selective and non-selective copper-black films have shown that the morphology of the film changes as the thickness of the film is changed. The selective copper-black film has got structure with uniform distribution of particles of sizes ranging from 0.5 μm to 1 μm. The voids of size of the order of 0.5 μm are seen. The non-selective copper-black film has a distribution of varied particle sizes (> 3.5 μm) with more number of voids (size 1 μm to 10 μm).

XPS study on selective copper-black film gives information, that, the film contains cuprous oxide and/or copper and cupric oxide, but non-selective copper-black film contains only cupric oxide within the penetration depth of XPS.

XPS depth profiling study on selective copper-black film have shown that cupric oxide (CuO) layer is present only on the top. The layers below have possibly Cu_2O composition with oxygen concentration going down as one moves towards the substrate.

The XAES depth profiling study on selective copper-black film has confirmed that the film has cupric-oxide layer covering layers of non-stoichiometric cuprous oxide along the depth. This observation was supported by AES depth profiling study. A suitable model structure is proposed for the selective copper-black film making use of

different characterization results. This model explains the observed optical and thermal properties of the film.

The high absorption in this film is attributed to absorption by semiconducting cupric oxide (CuO) and cuprous oxide (Cu_2O) species along with graded structure and typical surface morphology of the film. The low emittance is due to the substrate copper, since the film is transparent in thermal IR region of spectrum.

Molybdenum-black - Electrolytic cathodic deposition process was successfully used for making solar selective molybdenum-black films. The films obtained by this method were found to be well adherent to the substrate. Optical and thermal properties were found to be reproducible.

The study has shown that the deposition time is critical parameter which governs the α and ϵ values. At optimum time of deposition (t = 60 seconds), α = 0.85 and ϵ = 0.11 can be obtained. It was also seen that the $\lambda_{cut\ off}$ shifts towards the higher wavelengthside on increasing time of deposition. The values of α and ϵ of the molybdenum-black film prepared by cathodic electro-deposition technique are comparable with reported values, prepared by other techniques. The selective molybdenum-black films can be deposited on different substrates by this method.

To explain the selectivity, following techniques were used for characterization of the film and results obtained are as follows.

The x-ray and electron diffraction studies have shown that the selective molybdenum-black films are non-crystalline in nature. Therefore, it was not possible to know the phases present as well as the chemical composition of the film. Elemental analysis of the selective molybdenum-black film on different substrates was carried out using EDAX technique. It indicated, the presence of molybdenum, nickel and copper in the film.

SEM studies on the molybdenum films were carried out to know the changes taking place in the morphology of the film with time of deposition. The study reveals that selective molybdenum film has a uniform distribution of particles ranging from 0.1 - 0.5 μm in size with few clusters and voids. The morphology of the thicker films shows a distribution of bigger particles (size > 1.5 μm) as compared to the particles in the selective film, with more clusters and voids.

XPS study on selective molybdenum-black film was carried out to know the oxidation state of molybdenum, copper and nickel, the presence of which is shown by EDAX technique. The study reveals that the film contains in the form of +6 oxidation state, while Cu and Ni are present in metallic form within the penetration depth of XPS.

To know the composition of the film along the thickness and uniformity of composition, XPS and AES depth profiling studies on the selective molybdenum-black film

were carried out. The study reveals that the film has MoO_3 composition throughout the bulk. The Cu and Ni are present in free state incorporated in MoO_3 matrix. Their concentration is increasing towards the substrate.

The chemical analysis of the selective molybdenum-black was done to know the volume fractions of MoO_3, Ni and Cu. The volume fractions obtained are given below:

$$\begin{aligned} Cu &= 0.32 \\ Ni &= 0.01 \\ MoO_3 &= 0.67 \end{aligned}$$

Finally a suitable model structure is proposed for the selective molybdenum-black film making use of different characterization results. This model explains the observed optical and thermal properties of the film.

The high absorption in this film is attributed to the composite nature of the film. The low emittance is due to the substrate since the film is transparent in IR region of spectrum.

The electrodeposition of selective blacks as reported in this thesis seem to be of practical use for the fabrication of solar thermal convertors, since (1) very good selectivity can be obtained, (2) large area film deposition is not a limitation, (3) good reproducibility, (4) easy monitoring of various properties required for good conversion.

REFERENCES

REFERENCES

1. H. Tabor, Trans. Conf. Use. Sol. Energy, Tucson, Arizona, Vol. II, Part I, Sect. A (1955), p. 32.

2. J.T. Gier and R.V. Dunkle, Trans. Conf. Use. Sol. Energy, Tucson, Arizona, Vol. II, Part I, Sect. A (1955) p. 41.

3. H. Tabor, Low Temperature Engineering Applications of Solar Energy, Ed. R.C. Jordan, ASHRAE, New York (1967)

4. B.O. Seraphin, in Topics in Applied Physics, Vol. 31 (Ed. B.O. Seraphin), Springer Verlag, Berlin (1979), p. 15.

5. B.O. Seraphin, in Physics of Thin Films, Vol. 10 (Eds. G. Hars and M.H. Francombe), Academic Press, New York (1979) p. 1

6. A.B. Meinel and M.P. Meinel, Applied Solar Energy, Addison Wesley, Reading, MA (1976)

7. B.O. Seraphin and A.B. Meinel, in Optical Properties of Solids - New Developments (Ed. B.O. Seraphin), North-Holland, Amsterdam (1976), p. 927.

8. M.M. Koltun, Selective Optical Surfaces for Solar Energy Converters, Allerton Press, Inc, New York, (1981).

9. O.P. Agnihotri and B.K. Gupta, Solar Selective Surfaces, John Wiley and Sons, New York (1981).

10. C.M. Lampert, Solar Energy Materials, Vol. 1 (1979), 319.

11. C.M. Lampert, Solar Energy Materials,Vol. 2, (1979), p. 1.

12. D.K. Pandya and K.L. Chopra, in Vacuum Surfaces - Thin Films (Eds. K.L. Chopra and T.C. Goel), Proc. Natnl. Vacuum, Symp. New Delhi, India, Vanity Books, 1981, p. 246.

13. P. Beucherie, Electric Power Systems Research, 3 (1981) 125

14. H. Tabor, Solar Energy Conversion - An Introductory Course, Waterloo, Ontario, Canada, 6-19 August , 1978, p. 253-86

15. J. Spitz, A. Aubert, J.M. Behaghel, S. Berthier, J. Lafit & J. Rivory, Appl. Phy. Rev. 14 (1979), 67

16. B.O. Seraphin, Fourth Course on Solar Energy Conversion, Miramase, Italy, September 6-24 (1977)

17. P.K.C. Pillai, R.C. Agarwal, Phys. Status Solidi, A Vol. 60, No. 1, 11-25 (1980)

18. T.S. Moss, Optical Properties of Semiconductors, Butlerworth, London (1959)

19. K.L. Chopra, Thin Film Phenomena, McGraw-Hill, New York (1969)

20. T.J. McMahon and S.N. Jasperson, Appl. Opt., 13 (1974), 2750

21. T.J. McMahon and D.S. Stierwalt, Proc. SPIE Conf. Opt. Sol. Energy Util Sandiego, Calif. 68 (1975), 169

22. B.K. Gupta, R. Thangaraj and O.P.Agnihotri, Solar Energy Materials (1979), 471

23. R.Messier, S.V. Krishnaswamy, L.R. Gibert and P. Swab, J. Appl. Phys. 51 (1980) 1611

24. P. Swab, S.V. Krishnaswamy and R. Messier, J. vac. Sci. Technol. 17 (1980) 362

25. L.F. Drummeter and G. Hass, in Physics of Thin Films, Vol. 2 (Eds, G. Hass and R.E. Thun), Academic Press, New York (1964), p. 305

26. R.E. Peterson and J.R. Ramsey, J. Vac. Sci. and Technol., 12 (1975) 471

27. H. Tabor, J. Harris, H. Wenberger and B. Doron, Further Studies on Selective Black Coatings, U.N. Conf. New Source of Energy, Rome, Italy (1961)

28. H.Y.B. Mar, R.J.H. Lin, Zimmer R.E., R.E. Peterson, and J.S. Goss, Tech. Rept. PB-252-383, Honeywell Corporation (1976)

29. A.B. Meinel, D.B. McKenny and W.T. Beauchamp, Air Stable Selective Surfaces for Solar Energy Collectors, Rept. NSF/RANN/SE/GE-41895/PR/74/7 (1975)

30. C.M. Horwitz, Optics Communications, 11 (1974) 210

31. J.H.A. Van Wakeren and J. Verhoeven, Institute voor Atoom en molcuul Fysica, Kruislaan, 407, Amsterdam (1975)

32. J.J. Cuomo, J.F. Ziegler and J.M. Woodall, Appl. Phys. Lett. 26 (1975) 557

33. D.P. Grimmer, K.C. Herr, W.J. McCroary, J. Vac. Sci. and Technol. 15 (1978) 59

34. G. Pellegrini, Solar Energy Materials, 3 (1980),391

35. H.G. Craighead, R. Bartynski, R.A. Buhrman, L. Wojcik and A.J. Siers, Solar Energy Materials, 1, (1979) 105

36. J.I. Gittleman, Appl. Phys. Lett. 28 (1975) 370

37. R.J.H. Lin and P.B. Zimmer, Honey Well Tech. Rept. 77, SRC, 55 (1977)

38. G. Giaquinta and N.A. Mancini, Intl. Symp. Workshop on Solar Energy, Cairo, Egypt (1978)

39. G.A. Niklasson, C.G. Grunquist and O. Hunderi, Appl. Opt. 20 (1981) 26

40. D.G. Booth and B.O. Seraphin, DOE Absorber Surfaces for Solar Receivers Conf., Boulder 24th Jan. 1979

41. H.Y.B. Mar, R.E. Peterson and P.B. Zimmer, Thin Solid Films, 39 (1976) 95

42. A. Donnodieu and B.O. Seraphin, J. Opt. Soc. Am., 68 (1978) 292

43. B.O. Seraphin and V.A. Wells, Int. Conf., The Sun in Mankind Service, Paris, France (1975)

44. P.M. Mattox, Sandia Laboratories, Albuquerque, NM SAND 75-0361 (1975)

45. P.M. Driver and P.G. McCormic Proc. Internat. Conf. ISES Meeting, New Delhi, India, Pergamon Press, New York, N.Y. (1978) p. 881

46. H.S. Potdar, N. Pavaskar, A. Mitra and A.P.B. Sinha, Solar Energy Materials, 4 (1981), 291

47. H.C. Hottel and T.A. Unger, Solar Energy, 3 (1959) 10

48. A. Aveline and I.R. Bonilla, Solar Energy Materials, 5 (1981) 211

49. R.B. Gillette, Solar Energy, 4 (1960), 24

50. G.B. Smith, A. Ignatiev and G. Zajac, J. Appl. Phys. 51 (1980) 4186

51. G.B. Smith and A. Ignatiev, Solar Energy Materials, 2 (1980), 461

52. W. Kruidhoff and Van der Leij, Solar Energy Materials, 2 (1979) 69

53. C. Chaudhary and H.K. Sehgal, Solar Energy, 28, (1982) 25

54. G. MacDonald, Thin Solid Films, 72 (1980) 83

55. P. Kokoropoulas, E. Salam and F. Daniels, Solar Energy, 3 (1959) 19

56. G.E. McDonald, NASA TMX-71730

57. M. Van der Leij, J. Electrochem. Soc. 125 (1978), 1361

58. C. Homhaul, O.T. Inal, C.E. Murr, A.E. Torma and I. Gundiler, Solar Energy Materials, 4 (1981), 309

59. M. Van der Leij, in Ref. 57, p. 7

60. S.B. Gadgil, R. Thangaraja, J.V. Iyer, A.K. Sharma, B.K. Gupta and O.P. Agnihotri, Solar Energy Materials, 5, (1981), 129

61. T.J. McMohan and S.N. Jasperson, Appl. Opt. 13 (1974) 2750

62. R. Marchini, and R. Gandy, J. Appl. Phys. 49 (1978), 390

63. D.M. Mattox and G.J. Kominaik, J. Vac. Sci. and Technol. 12 (1975), 182

64. B.K. Gupta, R. Thangaraj and O.P. Agnihotri, Solar Energy Materials, 1 (1979), 471

65. M.J. Peterson, F.H. Cocks, J. Mater. Sci. Vol.14, 2709 (1979)

66. K.J. Cathro, Solar Energy Materials, 5 (1981),317

67. P.K. Gogna and K.L. Chopra, Solar Energy, 23 (1979), 405

68. S.N. Kumar, L.K. Malhotra and K.L. Chopra, Solar Energy Materials, 3 (1980), 519

69. R.B. Pettit and R.R. Sowell, J. Vac. Sci. Technol., 13 (1976) 596

70. G.E. Garver, Solar Energy Materials, 1 (1979), 357

71. H.S. Potdar, R.I. Hegde, S. Badrinarayan and N. Pawaskar, Solar Energy Materials, 6 (1982) 183

72. H.G. Craighead, R. Bartynski and R. Buhrman, Solar Energy Materials, 1 (1979), 105

73. L.K. Thomas and E.E. Chain, Thin Solid Films, Vol. 105 (3), 203 (1983)

74. A. Anderson, O. Hunderi, C.G. Granquist, J. Appl. Physics, 51 (1980), 5544

75. C.M. Lampert and J. Washburn, Solar Energy Materials, 1 (1979) 81

76. J.C.C. Fan and S.A. Spura, Appl. Phy. Lett. 30 (1977), 511

77. B. Window, I.T. Ritchie and K.J. Cathro, Appl. Opt. 17 (1978) 2637

78. P.K. Gogna and K.L.Chopra, Thin Solid Films, 57, (1979) 299

79. J. Vaidyanathan, S.B. Gadgil, A.K. Sharma, B.K. Gupta and O.P. Agnihotri, Solar Energy Materials, 6 (1981) 113

80. D.R. McKenzie, Thin Solid Films, 62 (1979), 317

81.a J.C.C. Fan, P.M. Zavracky, Appl. Phy. Lett. 29 (1976) 478

b R.J. Blattner, C.A. Evans, Jr., A.J. Braundmeier,Jr., J. Vac. Sci. and Technol., 14(5), 1132 (1977)

82. G.B. Smith and A. Ignatiev, Solar Energy Materials, 4 (1981) 119

83. G.L. Harding, Solar Energy Materials, 7 (1982), 123

84. J.I. Gittleman, S.K. Sichel and Y. Aric, Solar Energy Materials, 1 (1979), 93

85. G.L. Harding, J. Vac. Sci. Technol. 15(1978), 65

86. G.L. Harding, J. Vac. Sci. Technol., 13 (1976), 1070

87. L.E. Flordal and R. Kivaisi, Vacuum, 27 (1977),399

88. R.N. Schmidt and K.C. Park,Appl. Opt. 4 (1965) 917

89. V.V. Li, A. Faizier, V.K. Gaziev and V.S. Trukhov, Appl. Sol. Energy, 13 (1977) 40

90. A.B. Meinel, D.B. McKenney, U.S. Dept. of Commerce, NTIS Report, NSF/RANN/SE/75/1

91. D.R. McKenzie R.C., McPhedran and L.M. Briggs, Solar Energy Materials, 7 (1982) 75-84

92. G.B. Pettit, J.J. Cuomo, T.H. Distefano and J.M. Woodalf, IBM Res. Rev. 22 (1978) 372

93. P. O'Neill, C. Doland and A. Ignatiev, Appl. Opt. 16 (1977) 2822

94. P.J. Martin, R.P. Netterfield and W.G. Sainty, Thin Solid Films, 87 (1981) 203

95. S. Lofving, Solar Energy Materials, 5 (1981) 103

96. D.R. McKenzie and J.J. Zybeít, Thin Solid Films, 85 (1981) 191

97. E. Valkonen and B. Karlsson, Solar Energy Mater. 7 (1982) 43-50

98. V. Chang, A. Cedeno and A. Rivas, Solar Energy Mater. 9 (1983) 91-100

99. D.R. McKenzie, N. Savvides, D.R. Mills, R.C. McPhedran, and L.C. Botten, Solar Energy Mater. 9, (1983) 113-126

100. S.N. Kumar, L.K. Malhotra and K.L. Chopra, Solar Energy Mater., Vol. 7 (1983) 439-452

101. G.A. Niklasson, C.G. Grunquist, Solar Energy Mater. 7 (1983) 501-510

102. E. Erben, A. Muehlratzer, B. Tihanyi and B. Cornils, Solar Energy Materials, 9 (1983) 281-292

103. A.D. Wilson and J.P. Holmes, Solar Energy Materials, 9 (1983) 347-363

104. G.L. Harding, Solar Energy Materials, Vol.7 (1982), 123-128

105. D. Maziere-Bezes and J. Valignat, Solar Energy Materials, 7 (1982) 203-211

106. L. Roux, J. Hanus, J.C. Francois and M. Sigrist, Solar Energy Mater. 7 (1982) 299-312

107. Marten Sikkens, Solar Energy Materials, 6 (1982), 403-413

108. Madhusudanam, Sehgal H.K., Solar Energy Convers, Manage. 1981, 21 (3) 199-204

109. H.R. Wilson, D.R. McKenzie and L.M. Briggs, Thin Solid Films, 91 (1982) 123-130

110. Randich I., Allred D., Thin Solid Films, 1981, 83(4), 393-8

111. Pillai, P.K.C., Agarwal R.C., Altern. Energy Sources, 1982, 4(1), 191-9

112. Agnihotri O.P., Gupta B.K., Agarwal P.K. and Bhatnagar V.P., Thin Solid Films, 1983, 109 (3) 993

113. Hosseini, R., Smith B.E., Critchley J.K., Surf. Technol. 1983, 20 (4), 321-30

114. Koltun M.M., Ry abova L.A., Agaev E.A., Ge-liote-khnika, 1982, 28

115. Parks, Jeanne M. Call, Patrick, Proc. Electro Chem. Soc. 1983, 83-I, 269-88

116. Pellegrini G., Braghera P., Quazzo F., Solar Energy Materials, 1982, 7 (3), 351-7

117. L.A. Lowenhein, Modern Electroplating, John Wiley and Sons, Inc, New York (1974)

118. A. Goswami and B.V. Rao, Ind. J. Pure Appl. Phys. 12 (1974) 21

119. D.K. Edwards, K.E. Nelson, R.D. Roddick and J.T. Gier, Report No. 60-93, Department of Engineering, University of California (Oct.1960)

120. S. Yamaguchi, J. Electrochem. Soc. 123 (10), 1586, (1976)

121. A. Roos, T. Chibuye, B. Karlsson, Solar Energy Materials, Vol. 7, No. 4, 453 and 467 (1983)

122. A. Scherer, O.T., Inal. & A.J. Singh, Solar Energy Materials, 9 (1983), 139-158

123. D.J. Close, Report ED7, Energy Section CSIR Organization, Melbourne, Australia (1962)

124. J.S. Halliday, Trans. Faraday, Soc. 50 (1954) 171

125. S.F. Bartram, Handbook of X-rays, ed. E.F. Kaelble (McGraw-Hill, 1967) Chapt. 17

126. D.M. Mattox, G.J. Kormiak, J. Vac. Sci. and Technol. 12 (1), 182, 1975

127. Parry Moon, J. Franklin Institute Vol. 230, 604 (1940)

128. S. Evans, J. Chem. Soc. Faraday Trans II, 71 (1975), 1044

129. D.C. Frost, A., Ishitani and C.A. McDowell, Mol. Phys. 24 (1972) 861

130. Tery L, Barr John J., Hackenergy, Applications of Surf. Sci. 10 (1982) 523-545

131. W.E. Swartz,Jr. and D.M. Hercules, Ana. Chem. 43, (1971), 1774

132.a G. Schon, Surf. Sci. 35 (1973) 96

b Paul E. Larson, J. of Electron Spectroscopy 4 (1974) 213-218

133. K.S. Kim and Nicholas Winograd, Surf. Sci. 43 (1974), 625-643

134. M.J. Dignam and D.B.Gibbs, Can. J. Chem. 48, 1242 (1970)

135. E. Muller,Z.Electrochem. 13, 133 (1907)

136. A.M. Shams, E.L. Din, et al. Electrochem. Acta. 9 (1964), 113

137. B. Miller, J. Electrochem. Soc. 116 (1969), 1675

138. N.A. Hampson, J.B. Lee and K.I. MacDonald, J. Electro Ana. Chem. 32 (1971) 165-173

139. Milgram A., Alvin A., J. Appl. Phys. 1983, 54 (2), 1053-7.

140. L.H. Kaplan and F.M. D'Heurle, J. Electrochem. Soc. 177 (1970) 693

141. H.S. Gurev, Proc. 140th National Meeting of Electrochem. Soc. (1971) p. 433

142. A.I. Derosa, D.B. Dove and R.E. Loehman, J. Vac. Sci. and Technol. 11 (1975), 455

143. J.J. Lander and L.H. Germer, Trans. MS AIME, 175 (1948) 648

144. G.E. Carver, D.D. Allerd and B.O. Seraphin, Proc. Soc. Photothermal Instrumentation Engineers, Vol.161/ IV, Optics Appl. to Solar Energy (1978)

145. G.E. Carver, Solar Energy Materials, 1 (1979) 357

146. T. Sugono, H. Chou, M. Yoshida and T. Nishi, Japn. J. Appl. Physics, 7 (1968) 1028

147. D.K. Seto, V.Y. Doo and S. Dash, Proc. 3rd Intern. Conf. CVD, Electrochem. Soc. (1971) p. 659

148. A.H. El-Hoshy, J. Electrochem. Soc. 118 (1971) 2028

149. H.S. Gurev, G.E. Carver and B.O. Seraphin, Solar Energy, Electrochem. Soc. (USA) 1976, p. 36

150. Y.S. Touloukian, Thermal radiative properties, Vol. 7 (Plenum Press, New York, 1970)

151. H.S. Gurev, Soc. Photo-optical Instrumentation Engineers, SPIE, Vol. 85, Optics in Solar Energy Utilization II, 1976

152. G.E. Carver, H.S. Gurev, and B.O. Seraphin, J. Electrochem. Soc. 125 (1978) 1138

153. I.E. Chain, G.E. Carver and B.O. Seraphin, Thin Solid Films, 72 (1980) 59

154. G.E. Carver, A. Divrechy, S. Karbal, J. Robin and Donnadien, Thin Solid Films, 94 (1982) 269-278

155. K.A. Gesheva, E.E. Chain and B.O. Seraphin, Solar Energy Mater. 3 (1980) 415

156. G.E. Carver, Thin Solid Films, 63 (1979) 169

157. R.A. Hoffman and R.O. Hull, Proc. Am. Electroplater's Soc. 1 (1939) 45

158. W.E. Swartz Jr. and D.M. Hercules, Anal. Chem. 43 (1971) 1774

159. S.O. Grim and L.J. Matienzo, Inorganic Chem. 14,, (1975) 1014

160. T.T. Lin and David Lichtman, J. Vac. Sci. and Technol. 15, 1689 (1978)

161. L.E. Firment and A. Ferretti, Surf. Sci. 129 (1983), 155-176

162. K.S. Kim, W.E. Baitinger, J.W. Amy and N. Winograd, J. Electro Spectrosc. Related Phenomena, 5 (1974), 351

163. A.A. Hanna and M.A. Khilla, Thermochemica Acta. 65, (1983) 311-320

164. R.B. Dzhanelidze et al., Soviet Phys. Solid State, Vol. 7, No. 8, 2082-3 (1966)

165. S. Sella and Tran, Khann Vien, Thin Solid Films, 90 (1982) 428

166. A.J. Sievers, Topics in Applied Physics, Vol. 31, page 111 (1979)

167. S.K. Deb, Proc. Roy. Soc.A,304, 211-231 (1968)

168. S.K. Deb and J.A. Choporian, J. Appl. Phys. Vol. 31, 13 (1966)

169. L.G. Schulz and F.R. Tangherlini, J. Opt. Soc. Am. 44, 362 (1954)
J. Opt. Soc. Am. 44, 357 (1954)

170. S. Roberts, Physical Review, 118, 1509 (1960)

171. Jacques C. Vedrine and Helene Praliques, Surface Science, 80 (1979) 101

LIST OF PUBLICATIONS

1. Solar selective copper-black layers by an anodic oxidation process, H.S. Potdar, N.R. Pavaskar, A. Mitra and A.P.B. Sinha, Solar Energy Materials, 4 (1981) 291-299.

2. Solar selective molybdenum-black films by cathodic electrodeposition, H.S. Potdar, R.I. Hegde, S. Badrinarayan and N.R. Pavaskar, Solar Energy Materials, 6 (1982) 183-190.

3. Patent - An Improved Device for Solar Thermal Conversion in which fluid is used as an absorber (applied), S.D. Sathaye, H.S. Potdar, H.S. Soni and A.P.B. Sinha